



University of Tennessee, Knoxville
**TRACE: Tennessee Research and Creative
Exchange**

[Doctoral Dissertations](#)

[Graduate School](#)

12-1989

The Influence of Environmental Factors on the Temperature of the Radiosonde Thermistor

James K. Luers

University of Tennessee - Knoxville

Follow this and additional works at: https://trace.tennessee.edu/utk_graddiss

 Part of the [Engineering Commons](#)

Recommended Citation

Luers, James K., "The Influence of Environmental Factors on the Temperature of the Radiosonde Thermistor. " PhD diss., University of Tennessee, 1989.
https://trace.tennessee.edu/utk_graddiss/1913

This Dissertation is brought to you for free and open access by the Graduate School at TRACE: Tennessee Research and Creative Exchange. It has been accepted for inclusion in Doctoral Dissertations by an authorized administrator of TRACE: Tennessee Research and Creative Exchange. For more information, please contact trace@utk.edu.

To the Graduate Council:

I am submitting herewith a dissertation written by James K. Luers entitled "The Influence of Environmental Factors on the Temperature of the Radiosonde Thermistor." I have examined the final electronic copy of this dissertation for form and content and recommend that it be accepted in partial fulfillment of the requirements for the degree of Doctor of Philosophy, with a major in Engineering Science.

Walter Frost, Major Professor

We have read this dissertation and recommend its acceptance:

Robert Turner, R. L. Young, K. R. Kimball, John E. Carothers

Accepted for the Council:

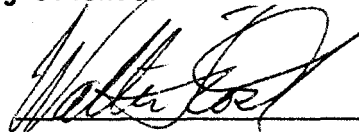
Carolyn R. Hodges

Vice Provost and Dean of the Graduate School

(Original signatures are on file with official student records.)

To the Graduate Council:

I am submitting herewith a dissertation written by James K. Luers entitled, "The Influence of Environmental Factors on the Temperature of the Radiosonde Thermistor". I have examined the final copy of this dissertation for form and content and recommend that it be accepted in partial fulfillment of the requirements for the degree of Doctor of Philosophy, with a major in Engineering Science.



Walter Frost, Major Professor

We have read this dissertation
and recommend its acceptance:

Robert E. Luers

R L Young

K R Kimble

John E. Caruthers

Accepted for the Council:



Vice Provost and
Dean of the Graduate School

**THE INFLUENCE OF ENVIRONMENTAL FACTORS ON THE TEMPERATURE
OF THE RADIOSONDE THERMISTOR**

**A Dissertation
In Partial Fulfillment of the
Requirements for the Degree of
Doctor of Philosophy
The University of Tennessee, Knoxville**

James K. Luers

December 1989

TO NICK ENGLER

For the loyal support he has given to me, the confidence he has instilled in me; and for the personal care and interest he has shown to me during his 22 years as my supervisor.

AND TO

MY MOTHER AND FATHER

For their constant love and support throughout my life, and for their belief that I could accomplish things far beyond my capabilities.

ACKNOWLEDGEMENT

The author expresses sincere appreciation to his advisor, Dr. Walter Frost. Without the total support he has shown to me throughout this endeavor, I would never have persevered. It is heartwarming to experience a professor taking a personal interest in ones life as Dr. Frost has done. Thank you, Dr. Frost, from the bottom of my heart.

The author also expresses his appreciation to Mr. Frank Schmidlin and Dr. Robert Turner. Mr. Schmidlin provided partial support for this dissertation and continually assisted me in providing and interpreting the experimental data. Dr. Turner first introduced me to the engineering sciences program at UTSI and encouraged me to apply. Without him, I'd still be dreaming about pursuing a PhD.

Sincere thanks also to my other committee members, Dr. Young, Dr. Kimball, and Dr. Carothers for the continued support they have shown, and encouragement they provided to me in pursuing my education.

Finally, I'd like to thank Ms. Martha Annes for the excellent typing of her first dissertation. The typing of a dissertation containing over 100 equations, was no menial task. She rates a solid gold star in scientific report production. Thanks, Martha.

ABSTRACT

A technique was developed to calculate the radiosonde temperature error as a function of altitude under different environmental conditions. The environmental conditions analyzed include the surface (or cloud) temperature, the atmospheric gaseous constituents, the aerosol and thermodynamic structure of the atmosphere, the solar elevation angle, the solar albedo, the rise rate of the balloon, and the atmospheric density.

The heat balance equations for the thermistor and lead wires were derived and a sensitivity analysis performed to establish the significance of each heating term. The Air Force LOWTRAN 6 code was used to model the solar and infrared irradiation of the thermistor in terms of the environmental parameters. LOWTRAN 6 output was then used to generate the radiation input to the heat balance equations of the thermistor and lead wires. The temperature error of the radiosonde was derived by solving these heat balance equations.

This technique for calculating the radiosonde temperature error was validated by comparing with data from flights of experimental radiosondes containing the Standard NWS radiosonde thermistor and three other thermistors with different radiative coatings. Each coating exhibited a different solar absorptance and infrared emission property which allowed the direct calculation of the radiosonde temperature error. The experimental measurements were compared with that predicted by the modeling technique. Comparisons were made between eight flights; four at night, three daylight, and one twilight, which

occurred during all seasons of the year and under various surface conditions. The comparisons showed good agreement. For the flights analyzed the temperature error at nighttime was small below 20 Km, and increased negatively above this altitude. At 30 Km the error generally exceeded -1° K. During the daytime the temperature error was positive and sometimes took on its maximum value as low as 20 Km. At altitudes near 30 Km and above the error often decreased due to influences of an increasing atmospheric temperature. Results from this study suggest that the radiosonde temperature error is likely to differ at different latitudes and solar elevation angles because of differing radiative fluxes to the thermistor and because of differing atmospheric temperature profiles.

TABLE OF CONTENTS

SECTION	PAGE
1.0 BACKGROUND	1
2.0 ACCURACY OF RADIOSONDE SYSTEM	6
2.1 Theoretical Studies	6
2.2 Experimental Studies	8
3.0 RESEARCH PROGRAM	12
3.1 Heat Balance Equation for Thermistor	13
3.1.1 Absorption of Radiation by the Thermistor	15
3.1.2 Radiation Emitted by the Thermistor	21
3.1.3 Heat Transfer to Thermistor by Convection	21
3.1.4 Heat Transfer by Electrical Current	24
3.1.5 Heat Transfer by Conduction from Lead Wires	24
3.1.6 Heat Balance Equation for Thermistor	25
3.2 Heat Balance Equation for Lead Wires	25
3.2.1 Absorption of Radiation by Lead Wires	26
3.2.2 Radiation Emitted by Lead Wires	28
3.2.3 Heat Transfer to Lead Wires by Convection	28
3.2.4 Heat Transfer by Electrical Current	29
3.2.5 Heat Transfer by Conduction Through Lead Wire	29
3.2.6 Heat Balance Equation for Lead Wires	29
3.3 Magnitude of Terms in Heat Balance Equation	30
3.4 Method of Solving Heat Balance Equations	32
3.5 Sensitivity of Parameters to Temperature Correction	36
3.5.1 Sensitivity Analysis Results	39
3.5.1.1 Nighttime Sensitivity Analysis	41

SECTION	PAGE
3.5.1.2 Daytime Sensitivity Analysis	49
3.5.1.3 Conclusions	55
3.6 Solar and Infrared Irradiation of Radiosonde Thermistor	58
3.6.1 Solar Radiation	58
3.6.1.1 Absorption of Solar Radiation	59
3.6.1.2 Scattering of Solar Radiation	61
3.6.1.3 Reflection of Solar Radiation	64
3.6.2 Non-Solar Radiation	68
3.6.3 The LOWTRAN 6 Atmospheric Propagation Program . .	70
3.6.3.1 Utilization of LOWTRAN 6 to Estimate Irradiance and Heating of the Radiosonde Thermistor	75
3.6.3.2 Sensitivity of Atmospheric Parameters to Radiation Absorbed by Thermistor . .	80
3.6.3.2.1 Nighttime Radiation	81
3.6.3.2.2 Daytime Radiation	85
3.7 Irradiation of the Thermistor From the Balloon and Radiosonde Instrument	89
4.0 RESULTS AND COMPARISONS WITH EXPERIMENTAL DATA	92
4.1 Comparison of Measurement with Simulation Results: Night Flights	94
4.2 Comparison of Measurements with Simulation Results: Day Flights	100
4.3 Conclusions	107
5.0 CONCLUSIONS AND RECOMMENDATIONS	109
REFERENCES	114
APPENDICES	120
Appendix 1: Average Presented Area and Fractional Percentage of Maximum Solar Irradiation of Thermistor . . .	121

SECTION	PAGE
Appendix 2: Order of Magnitude of Terms in Heat Balance Equation	124
Appendix 3: Solid Angle Increments of Sphere	128
Appendix 4: Influence of the Balloon on Radiosonde Temperature Error	130
A4.1 Irradiation of the Thermistor From the Balloon	130
A4.2 Exchange Factor Balloon to Thermistor	136
A4.3 Evaluation of Exchange Factor From Balloon to Thermistor	138
A4.4 Atmospheric Radiation Shielded by Balloon	139
A4.5 Influence of Balloon on Temperature of Thermistor	141
Appendix 5: Influence of the Radiosonde Instrument on the Radiosonde Temperature Error	145
A5.1 Irradiation of the Thermistor from the Radiosonde	145
A5.2 Exchange Factor for Side S1 with Thermistor	151
A5.3 Exchange Factor for Side S2 with Thermistor	159
A5.4 Atmospheric Radiation Shielded by the Radiosonde	161
A5.5 Influence of the Radiosonde on Thermistor Temperature	163
VITA	169

LIST OF TABLES

TABLE		PAGE
2.1	Values of Mean $\overline{\Delta T}$ in °K as Functions of Mean Afternoon-Daylight Solar Elevation Angle and Pressure Level (From McInturff and Finger, 1968)	10
3.1	Parameter Values Used in Order of Magnitude Analysis . .	32
3.2	Magnitude of Terms in Heat Balance Equations	33
3.3	Expressions for the Constants in Heat Balance Equations .	34
3.4	Sensitivity Analysis Parameters	38
3.5	Values of Sensitivity Analysis Variables	40
3.6	Estimates of Particles Smaller Than 20 μm Radius Emitted Into or Formed in the Atmosphere (10^6 Metric Tons/Year) (from Valley (1965))	62
3.7	Emissivity of Various Surfaces	69
A2.1	Typical and Extreme Value of Variables Used in Order of Magnitude Analysis	125

LIST OF FIGURES

FIGURE		PAGE
3.1	Thermistor geometry and heat transfer processes	14
3.2	Coordinate system for defining angular distribution of radiation	17
3.3	Azimuthal direction of thermistor relative to incoming radiation (2-dimensional view)	19
3.4	Absorptivity of standard radiosonde coating for $0.25 \leq \lambda \leq 2.5$ microns (Schmidlin, et al. (1986))	22
3.5	Lead wire geometry	27
3.6	Variation in temperature error with amount of infrared radiation absorbed by the thermistor at different air temperatures	42
3.7	Variation in temperature error of thermistor with altitude (Nu) and air temperature	43
3.8	Variation in thermistor temperature error with changes in the emissivity of the thermistor (solid line) and of the lead wires (dashed line)	44
3.9	Variation in the thermistor temperature error with changes in the radius and length of the thermistor and the radius of the lead wires (nighttime)	45
3.10	Variation in the thermistor temperature error, ΔT , with the amount of solar radiation absorbed by the thermistor at different air temperatures	50
3.11	Variation in thermistor temperature error with altitude (Nu) and temperature	53
3.12	Variation in thermistor temperature error with changes in the emissivity of the thermistor and lead wires	54
3.13	Variation in the thermistor temperature error with changes in the radius and length of the thermistor and radius of the lead wires	56
3.14	Spectral distribution curves related to the sun; shaded areas indicate absorption, at sea level, due to the atmosphere constituents shown (Valley, 1965)	60

FIGURE		PAGE
3.15	Variation in reflectance as a function of cloud thickness parameter h/L for different solar zenith angles (Valley, 1965)	63
3.16	Spectral reflectance for water surfaces (Valley, 1965) .	65
3.17	Spectral reflectance for snow and bare soils (Valley, 1965)	66
3.18	Spectral reflectance for vegative formation (Valley, 1965)	67
3.19	Comparison of the near infrared solar spectrum with laboratory spectra of various atmospheric gases (Valley, 1965)	71
3.20	Atmospheric Profiles Available in LOWTRAN 6	73
3.21	LOWTRAN Input: Aerosol profiles, solar elevation, lower boundary properties	76
3.22	Method of calculating radiation absorbed by thermistor .	77
3.23	Baseline Input Parameters for LOWTRAN 6	82
3.24	Nighttime radiation absorbed by thermistor under different environmental conditions	83
3.25	Direct solar radiation absorbed by thermistor versus altitude and solar elevation angle. The absorbed radiation is an average value over one revolution of the thermistor	87
4.1	Temperature error profile: Nighttime Flight, 17 Feb 83, 01:51 Z	95
4.2	Temperature error profile: Nighttime Flight, 8 Mar 83, 23:07 Z	96
4.3	Temperature error profile: Nighttime Flight, 13 Sept 83, 23:17 Z	97
4.4	Temperature error profile: Nighttime Flight, 23 June 87, 23:33 Z	98
4.5	Temperature error profile: Daytime Flight, 26 Feb 87, 15:33 Z	101
4.6	Temperature error profile: Daytime Flight, 19 June 87, 15:01 Z	102

FIGURE		PAGE
4.7	Temperature error profile: Daytime Flight, 23 June 87, 15:47 Z	103
4.8	Temperature error profile: Twilight Flight, 5 Mar 87, 21:54 Z	104
A1.1	Geometry describing irradiation of the thermistor	122
A1.2	Average percent of maximum irradiation of thermistor versus elevation angle	123
A4.1	Geometry of balloon and thermistor	131
A4.2	Geometry for reflections off balloon	134
A4.3	Solid angle defining thermistor view of balloon	140
A5.1	Idealized geometry of the radiosonde	146
A5.2	Geometry for calculating radiant power irradiating S2	150
A5.3	Geometry for thermistor view of side S1	152
A5.4	Geometry applicable to configuration # 2 (Kreith, 1962)	154
A5.5	Application of configuration # 2 geometry to thermistor → S1 exchange factor	155
A5.6	Geometry of thermistor view of side S2	156
A5.7	Application of configuration # 2 geometry to thermistor → S2 exchange factor	157
A5.8	Solid angle defining thermistor view of side S1	158
A5.9	Solid angle geometry for thermistor view of side S2	162
A5.10	Side S2 boundaries of solid angle versus approximation	164

LIST OF SYMBOLS

A_p	= Presented area of thermistor in specified direction, cm^2
b	= Width of radiosonde, cm
C	= Specific heat of thermistor, $\text{cal/g } ^\circ\text{K}$
C_p	= Specific heat of air, $\text{cal/g } ^\circ\text{K}$
C_w	= Specific heat of lead wires, $\text{cal/g } ^\circ\text{K}$
E	= Radiosonde battery voltage, volts
$F_{X \rightarrow Y}$	= Exchange factor from surface X to surface Y
h	= Height of radiosonde, Km
h_c	= Heat transfer coefficient for cylinder in laminar cross flow, $\text{cal/sec cm}^2 \text{ } ^\circ\text{K}$
I	= Electrical current, amps
$I()$	= Intensity of radiation striking the thermistor, cal/sec steradian
I^*	= Intensity of radiation propagating through the atmosphere
I_b	= Intensity of radiation striking the thermistor from direction of balloon
I_0	= Solar constant, cal/sec cm^2
I_{rs}	= Intensity of radiation striking the thermistor from direction of radiosonde instrument
J_1, J_2, J_3	= Constants
k	= Thermal conductivity of air $\text{cal/sec cm } ^\circ\text{K}$
K_1, K_2, K_3	= Constants
k_w	= Thermal conductivity of lead wire, $\text{cal/sec cm } ^\circ\text{K}$
l	= Length of thermistor, cm
m	= Mass of thermistor, g
Nu	= Nusselt number
q	= Heating rate, cal/sec

\hat{q}	= Heating rate per steradian, cal/sec steradian
q'	= Heating rate per unit length of wire, cal/sec cm
R	= Electrical resistance of thermistor
Re	= Reynolds number
R_f	= Electrical resistance of fixed resistor in radiosonde circuitry, ohms
R_t	= Total resistance of circuit containing thermistor, ohms
R_w	= Electrical resistance of lead wire per unit length, ohms
r	= Radius of thermistor, cm
r_b	= Radius of balloon, m
r_w	= Radius of lead wire, cm
S	= Tether length, m
t	= Time, sec
T	= Temperature of thermistor, °K
T_b	= Temperature of balloon, °K
T_c	= Cloud temperature, °K
T_E	= Equivalent blackbody temperature, °K
T_{S_i}	= Temperature of side S_i , °K
T_{surf}	= Surface temperature of the ground, °K
T_w	= Temperature of lead wire, °K
T_∞	= Free stream ambient temperature, °K
w	= Length of radiosonde, cm
\dot{z}	= Vertical ascent rate of balloon (thermistor), m/sec
Z_E	= Solar elevation angle, deg
α	= Absorptivity of thermistor
ΔT	= $T - T_\infty$, °K

ϵ	= Emissivity of thermistor
η	= Index of refraction of air
θ	= Elevation angle, deg
ρ_b	= Reflectivity of balloon
ρ_w	= Density of lead wires, g/cm ³
σ	= Stephen Bolzman constant, cal/sec cm ² °K ⁴
ϕ	= Azimuth angle, deg
Ω	= Solid angle designation
λ	= Wavelength, microns
q_{eb}	= Diffuse radiation emitted by balloon, cal/sec
q_{db}	= Diffuse radiation reflected from balloon and absorbed by thermistor
q_b	= Total heating rate of thermistor from balloon radiation
q_{sb}	= Reflected direct solar radiation from balloon absorbed by thermistor
q_{sdb}	= Reflected diffuse solar radiation from balloon absorbed by thermistor
q_{abs}	= Total radiation absorbed by thermistor for given environment
$q_{sh/b}$	= Radiation shielded by balloon from absorption by thermistor
q_{eS1}	= Radiation emitted by Side S1 and absorbed by thermistor
q_{sdS1}	= Reflected diffuse solar radiation from S1 absorbed by thermistor
$F_{\downarrow}(\lambda)$	= Total downwelling radiant power at wavelength λ , cal/sec cm ²
q_{dS1}	= Diffuse radiation reflected from S1 and absorbed by thermistor
q_{S1}	= Total radiation absorbed by thermistor from Side S1 for given environment
q_{S2}	= Direct solar power irradiating S2 when perpendicular to sun

- \bar{q}_{s2} = Average direct solar power irradiating S2 over one revolution
- \bar{q}_{sS2} = Average reflected direct solar power irradiating S2 and absorbed by thermistor
- $q_d(\phi_0, \lambda)$ = Diffuse power irradiating S2 at λ and ϕ_0
- $\bar{q}_d(\lambda)$ = Average diffuse power irradiating S2 at λ during one revolution
- \bar{q}_{dS2} = Average diffuse power reflected from S2 and absorbed by thermistor
- q_{S2} = Total heating rate of thermistor from radiation from Side S2
- q_{RS} = Total heating rate of thermistor from radiation from radiosonde
- $q_{Sh/RS}$ = Radiation shielded by radiosonde from absorption by thermistor
- $q_{Sh/S1}$ = Radiation shielded by Side S1 from absorption by thermistor
- q_{sS1} = Reflected direct solar radiation from Side S1 absorbed by thermistor
- q_{sdS2} = Diffuse solar radiation reflected from S2 absorbed by thermistor
- \bar{q}_d = Average diffuse solar power irradiating S2 during one revolution

1.0 BACKGROUND

The United States standard radiosonde (rawinsonde) instrument provides synoptic measurements of pressure, temperature, relative humidity and wind on a nationwide basis. These measurements are generally available between the earth's surface and 10 millibars (about 30 Km). At the present time, temperature data are reported as actually measured; i.e., transmitted without corrections or adjustments of any kind. It has been established by both experimental and theoretical studies that a bias exists in the temperature measurements from both day and night radiosonde flights at the upper altitude range (20-30 Km) of the instrument. This temperature error (bias) primarily occurs because of the influence of solar and infrared radiation on the radiosonde thermistor.

In an early study, Johnson and McInturff (1968): 1) suggested that daytime reported temperatures can exceed nighttime temperatures by 2° K at high altitudes. Weather analysis charts produced from radiosonde data are known to show discontinuities in the temperature and geopotential fields caused by this day/night temperature bias. These discontinuities, on nationwide weather maps, can be directly linked with those radiosonde observations that were in sunlight versus darkness at the observation time. In terms of magnitude, a radiosonde temperature bias of 1° K produces a geopotential height error exceeding 50 meters at 100 mb (16 Km) and 500 meters at 10 mb (30 Km). This problem is further compounded at worldwide weather analysis centers where observations from different countries using different instruments, having different errors, must be merged into a useful

product. So critical is the problem of discontinuities in temperature and geopotential fields that numerous international radiosonde intercomparison series have been conducted to improve the compatibility and accuracy of radiosonde observations (Nash and Schmidlin (1987)).

Radiosonde temperature bias errors are also important for other reasons. Satellite temperature retrieval requires the use of zonal averaged radiosonde temperature data as input to the regression equation used in deriving satellite temperatures. Significant satellite temperature errors can be attributed to a bias in the zonal mean radiosonde data.

Rocketsonde density and pressure data also require a radiosonde observation at the tie-on (overlap) point for use as the initial value to begin the upward integration of rocketsonde temperature data versus height. Historically, temperature discrepancies between the two sensors in the overlap region (of several degrees Kelvin) have not been satisfactorily explained. When the error is in the radiosonde temperature, a significant bias in the integrated rocketsonde profiles of pressure and density result. This temperature discrepancy in the overlap region varies from flight to flight and may be due to changes in the radiosonde temperature error with environmental conditions.

The objective of the research effort presented herein is to develop a technique for estimating the temperature error of the radiosonde thermistor at altitudes between 10 and 30 Km as a function of the environmental conditions that control the radiation budget to the thermistor. The technique is then validated by comparing the estimated temperature errors with experimentally measured error profiles obtained at Wallops Island, Virginia using especially designed multi-thermistor

radiosondes.

Sections 1.0 and 2.0 of this report provide background information about the radiosonde temperature errors. Section 3.0 states the research problem and outlines the steps that are followed in deriving and validating the technique for estimating the radiosonde temperature error. The remainder of Section 3.0 and Section 4.0 describe the research that was performed and the results that were achieved.

The radiosonde system consists of an expandable balloon, a radiosonde instrument that provides measurements of atmospheric temperature, pressure, and relative humidity and a ground meteorological device (GMD) receiving station. Tracking of the transmitted signal by the GMD ground station provides a vertical profile of the wind field. Regular observations at over 100 U.S. weather stations, made at 0:00 Zulu hours and 12:00 Zulu hours are transmitted to the National Weather Service data bank at Suiteland, Maryland where that information is combined with satellite and other worldwide data to serve as the basic measurements utilized in prognostic weather forecasting models. The radiosonde system has remained relatively unchanged since the days of World War II.

The radiosonde instrument contains a rod thermistor to measure temperature, a humidity sensitive carbon element to measure relative humidity, and an aneroid cell to measure atmospheric pressure. Present day National Weather Service radiosondes are manufactured by VIZ. The length of the rod thermistor is approximately 4 cm (Friedman, VIZ^{*}); its diameter, 0.12 cm. The electrical resistance of the thermistor is

* Manufacturers Brochure Technical Publication 730919;
VIZ Manufacturing Company, 335 E. Price St., Philadelphia, PA 10144

calibrated as a function of temperature over the range from 200° K to 310° K. The temperature sensitive thermistor is coated with a white ceramic coating that provides high solar reflectivity. The reflective coating on the rod thermistor is specifically designed to minimize the absorption of solar radiation so that the thermistor temperature is an accurate approximation to the true atmospheric air temperature. The assumption that the thermistor temperature equals the air temperature is, in fact, inherent in all data routinely used by the National Weather Service. No correction to thermistor temperature are presently applied to remove radiation effects from the ambient air temperature measurement.

The humidity element consists of a carbon element which absorbs water vapor. The resistance of the element is influenced by the amount of water vapor absorbed and can be related to the relative humidity of the surrounding environment. The humidity element provides the moisture profile and allows one to deduce the altitudes associated with a cloud deck. After exiting a cloud layer, however, the humidity element must release moisture by evaporation before regaining its humidity measurement capability.

The aneroid cell consists of a sealed expandable capsule whose expansion characteristics are calibrated as a function of pressure. To each aneroid cell is attached an arm which mechanically moves over a pressure index scale controlling the electric circuitry. The aneroid cell expands as the external atmospheric pressure decreases, causing the mechanical arm to switch contacts in a manner that can be identified relative to the pressure calibration index. The geopotential height is derived from the simultaneous solution of the

hydrostatic equation and ideal gas law. A vertical profile of the horizontal wind field is derived from smoothing and differentiating the position measurements of the instrument as obtained from the angular and range measurements from the GMD ground station.

2.0 ACCURACY OF THE RADIOSONDE SYSTEM

Extensive theoretical and empirical evaluations of the accuracy of the radiosonde system have been made in the past (e.g.; Hodge and Harmantas (1965), Schmidlin (1969), Nestler (1983)). Over 50 references relative to radiosonde accuracy have been cited since 1960 (Lenhard (1970, 1973)). For the most part, experimental and theoretical results are in good agreement concerning the accuracy of the system so that today a general consensus exists concerning radiosonde accuracies (Schmidlin (1987a), Schmidlin and Finger (1987), Nash and Schmidlin (1987)). In lieu of discussing all of the studies germane to a radiosonde accuracy assessment, the discussion will be limited to reviewing a few classic studies that thoroughly quantify the problem that will be investigated. The problem addressed in this research is primarily related to the temperature measurement capability of the radiosonde thermistor. Pressure, relative humidity and height error assessments are not of major significance to the problem addressed herein. Consequently, the present state of knowledge concerning theoretical and experimental measurements of radiosonde temperature accuracy will be reviewed and then a technique will be derived for further evaluating radiosonde temperature errors as a function of environmental conditions. The technique will be validated by comparison with experimental data.

2.1 Theoretical Studies

Theoretical studies of the accuracy of U.S. radiosonde temperature measurements have been performed by Badgley (1957), Ney, et al. (1960), Ballard and Rubio (1968), Williams and Acheson (1976), and Luers

(1980). Similar theoretical analyses of the Chinese sonde (Bingxun (1987)), and of the Australian radiosonde which uses the same thermistor as the U.S. sonde have been made by Pearson (1967) and Talbott (1971). The methodologies utilized in these analyses are consistent with or a simplification of Ballard and Rubio's heat transfer analysis. Ballard and Rubio derive a steady-state heat transfer equation for the thermistor. This heat transfer equation takes into account the convective heat transfer between the thermistor and the environment, radiation absorbed and emitted by the thermistor, and the heat conduction through the lead wires into the thermistor resulting from the lead wires possessing a different steady-state temperature than that of the thermistor. Ballard and Rubio also solved a time dependent form of the heat transfer equation to determine the time constant of the radiosonde thermistor. By assuming average values of both direct and reflected solar radiation impinging on the thermistor and average values of long-wave radiation from the ground and sky, they were able to solve the heat transfer equation analytically for the temperature correction and determine the contribution due to each term. The largest correction was found to be due to the solar irradiation of the thermistor which under their assumed solar radiation budget amounted to $\approx 1.5^\circ$ K at 30 Km with larger values above and decreasing values at lower altitudes. The magnitude of this correction largely exceeds the random component of thermistor error which is less than $\pm 0.5^\circ$ K. The next most significant correction term was the conduction from the lead wire term. The magnitude of this term was $\approx \pm 0.3^\circ$ K. In comparing their results

to experimental measurements by Daniels (1968) utilizing two thermistors having different radiative coatings, Ballard and Rubio concluded that discrepancies between their results and experimental measurements could be explained by either a variation in their assumption of solar irradiation of the thermistor or by a small variation of the absorption coefficient of the thermistor.

Comparable analyses performed by Bingxun (1987) for the Chinese sonde and Talbott (1971) for the Australian sonde made similar assumptions and provided comparable results. All of the above studies conclude that the major source of error in radiosonde thermistor temperatures, particularly at high altitudes, is due to the radiative heating of the thermistor due to solar radiation and, to a lesser degree, conduction through the lead wires. Because both the short-wave (Powell (1986)) and long-wave irradiation (Coombes and Harrison (1986)) of the thermistor and lead wires can vary considerably with environmental changes of cloud cover, solar zenith angle, ground temperature, water vapor, ozone, carbon dioxide and aerosols, temperature errors calculated by Ballard and Rubio (1968) and others using average values can be expected to be in considerable error when non-average environmental conditions exist. No theoretical studies exists concerning the change in the radiative temperature correction with changes in the environment.

2.2 Experimental Studies

Several experimental studies have been performed which qualitatively verify the theoretical calculations discussed above. McInturff and Finger (1968) compared differences between day and

nighttime radiosonde measurements at the same location and at the same altitude as a function of solar zenith angle. Over 1,000 observations were used in their statistical analysis. Table 2.1 from McInturff and Finger (1968) summarizes the average temperature differences observed vs. pressure level and solar elevation angle. McInturff attributes these differences to solar radiation errors present in the daytime flights but absent from the nighttime flights. However, no conclusion can be drawn concerning whether the daytime temperatures are too high (warm) as a result of solar irradiation of the thermistor or the nighttime temperatures are too low (cold) because of the long-wave emissions from the thermistor, or some combination of the two. Nevertheless, the differences observed in their study are consistent with the magnitude of solar radiation errors predicted by Ballard and Rubio (1968). Follow-on studies by Johnson and McInturff (1978), and McInturff, et al. (1979) contained an enlarged data base and produced some refinement in their earlier estimates. Considerable scatter, however, exists in their data indicating that different magnitude temperature errors exist for the same solar angle and pressure level. Such scatter could result from varying environmental conditions that on a daily basis produce differing temperature errors.

Schmidlin, Huffman, and Luers (1986) developed a multi-sensor radiosonde system that allowed the direct measurement of the radiative temperature error for the standard radiosonde thermistor. The technique consisted of coating three thermistors with paints having different emission and absorption properties both in the short-wave and the infrared regions of the electromagnetic spectrum. A black paint with solar absorptivity, spectrally weighted over the solar spectrum

Table 2.1 Values of Mean $\overline{\Delta T}$ in °K as Functions of Mean Afternoon-Daylight Solar Elevation Angle and Pressure Level
(From McInturff and Finger, 1968)

Solar Elevation Angle (Degrees)	Pressure Level (mb)				
	<u>100</u>	<u>50</u>	<u>30</u>	<u>20</u>	<u>10</u>
-5°	0.2	0.5	0.7	0.8	1.3
0°	0.4	0.8	1.0	1.3	2.0
10°	0.8	1.1	1.5	2.0	2.7
20°	0.9	1.3	1.8	2.2	3.0
30°	1.0	1.3	1.9	2.3	3.1
40°	1.0	1.3	1.9	2.3	3.1
50°	1.0	1.3	1.9	2.2	2.9
60°	1.0	1.3	1.8	2.1	2.7

0.25 $\leq \lambda \leq$ 2.5 μ of $\alpha = 0.94$ and longwave emissivity of $\epsilon = 0.86$ over the wavelengths 2.5 $\leq \lambda <$ 20 μ was combined with an aluminum painted thermistor with $\alpha = 0.31$ and $\epsilon = 0.22$ and the standard radiosonde thermistor whose solar absorptivity and long-wave emissivity properties were measured to be $\alpha = 0.12$ and $\epsilon = 0.86$. Because of their different coatings the temperature difference between thermistors varied throughout a flight. This allowed the heat transfer equation for each thermistor to be solved simultaneously for: a) the ambient air temperature; b) the solar flux impinging upon each thermistor; and c) longwave irradiation of the thermistors. The accuracy by which the

temperature error (i.e.; temperature error = temperature of the standard thermistor - air temperature) can be measured by this technique was shown by the authors to be within $\pm 0.5^\circ$ K.

Over 80 experimental flights have already been made with these multi-thermistor radiosonde systems (Schmidlin (1987b)). Daytime temperature errors of up to $+2.5^\circ$ K at 30 Km have been measured, as well as nighttime temperature errors as large as -2.0° K. Considerable variation from flight to flight occurs. Variation of the temperature error with solar zenith angle has been found to be significant but this parameter alone does not adequately explain the variability of the temperature error. Environmental factors such as cloud cover and ground temperature are believed to account for much of the remaining variability that is seen in the experimental flights (McMillin, et al. (1988)). Fortunately the environmental conditions prevalent at each flight time were recorded for the experimental data set. The cloud cover, cloud type, ground temperature, launch time and solar zenith angle are thus available for analysis. Profiles of ozone and water vapor could also be obtained for the geographic area representative of the experimental flight data if needed. A representative subset of the 80 launches of multi-thermistor radiosonde under known environmental conditions forms the data set for testing a simulation technique for estimating the radiosonde temperature error as a function of environmental conditions. The development and validation of this technique is the major thrust of the work described in this dissertation.

3.0 RESEARCH PROGRAM

The objective of the research proposed herein is to derive and validate a technique to determine the sensitivity of the radiosonde temperature error to variations in the natural environment. The approach is as follows. A complete derivation of the heat balance equation for the radiosonde thermistor is developed. Input to the heat balance equation requires the modeling of radiative fluxes that irradiate the thermistor as a function of environmental parameters. The significant environmental parameters included are cloud cover, solar zenith angle, ground temperature, cloud top temperature, and the vertical profiles of aerosols, ozone, water vapor and carbon dioxide (Morcrette and Geleyn (1985)). The LOWTRAN 6 atmospheric radiance and transmission model (Kneizys et al. (1983)) is used to model the radiative fluxes on the thermistor as a function of the environmental parameters. A sensitivity analysis is then performed to assess the relative and absolute influence of each environmental parameter on the heating rate of the thermistor.

The radiosonde temperature error is then calculated for various environmental conditions by solving the thermistor heat balance equations using the appropriate upward and downward radiative fluxes generated from the LOWTRAN 6 model, and other necessary input parameters. Non-environmental input parameters used in the heat balance equation, such as the thermistor and lead wire dimensions and the absorptivity and emissivity of the thermistor coating are also varied in the simulations to assess the influence of each parameter on the temperature error. Finally, to validate the technique, the

environmental conditions representative of several of the 80 experimental flights are input into the LOWTRAN 6 program to derive the atmospheric irradiation of the thermistor. The radiation values are then used in the heat balance equation to solve for the temperature error so that a comparison can be made between the simulated errors and those actually measured by the experimental flights. The following sections describe in detail the approach pursued in performing each of these tasks and the results.

3.1 Heat Balance Equation for Thermistor

The temperature of the thermistor (as shown in Figure 3.1) is influenced by the absorption of radiation from the surroundings, by the emissions of radiation from the thermistor, by the convective transfer of heat between the thermistor and the environment, by the electrical heating of the thermistor as a result of the current used to measure the thermistor resistance, and by the conduction of heat through the lead wires to the thermistor. Equation 3.1 describes the time rate of change of the thermistor temperature as a function of these heat transfer processes.

$$mC \frac{dT}{dt} = q_{abs} - q_{emit} + q_{conv} + q_{elec} + q_{cond} \quad (3.1)$$

In deriving the heat transfer equations we assume that the temperature of the thermistor is uniform. The thermistor is calibrated at fixed uniform temperatures versus resistance so that by measuring thermistor resistance, the corresponding temperature of the thermistor is known. It will also be assumed, based upon experimental measurements, that the thermistor coating emits as a gray body. That is, its emissivity is independent of wavelength. For absorption and emission calculations,

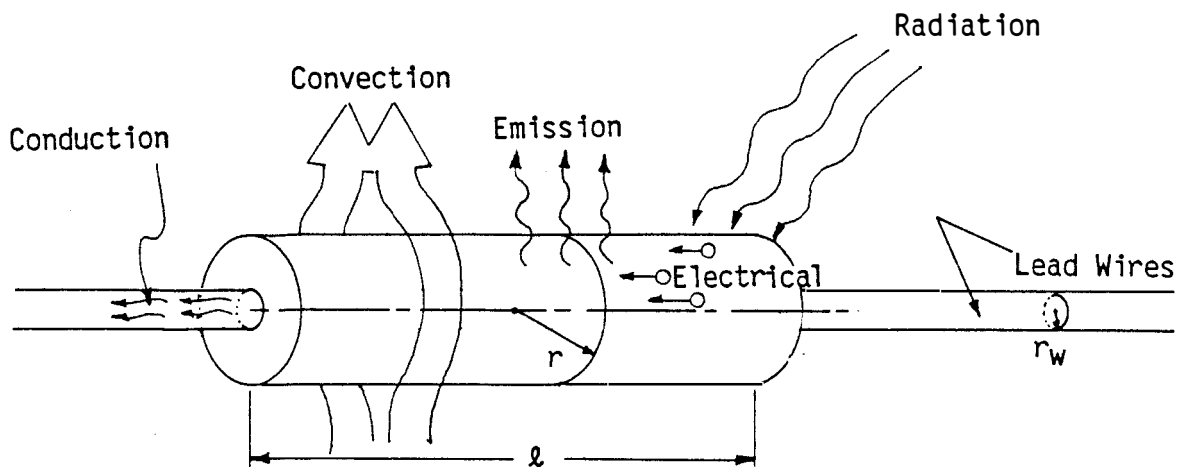


Figure 3.1 Thermistor geometry and heat transfer processes.

emissivity

the wavelength region is divided into a shortwave $0.25 \leq \lambda \leq 2.5 \mu$, and a longwave region $2.5 < \lambda \leq 40\mu$. The thermal energy irradiating the thermistor in the shortwave region can be restricted to the sun as its source. The longwave region, also referred to as the infrared region (although classically infrared radiation extends to shorter wavelengths) includes as sources all non-solar radiation emitting at temperatures occurring on the earth and in the atmosphere. This range of wavelength classification was defined to conform with the measurement capabilities of instruments used in measuring the absorption properties of thermistor coatings. A Beckman DK-2 scanning Spectrophotometer provided spectral measurements of absorptivity (reflectivity) over the shortwave (solar) range to $0.25 \leq \lambda \leq 2.5\mu$ while a Gier Dunkle Infrared Reflectometer was used to measure a single value of longwave emissivity integrated over the infrared wavelength region from 2.5 to 20μ . Thus for this report the terms shortwave and solar refer interchangeably to the wavelength region from 0.25 to 2.5μ , while the terms longwave and infrared refer to the region from 2.5 to 40μ .

The thermistor is assumed to be of cylindrical shape with length l and radius r as shown in Figure 3.1. It is attached on the end by two lead wires serving as electrical conductors through the thermistor. Each lead wire is of radius r_w . With these assumptions and definitions, it is now possible to describe each of the heat transfer terms in detail.

3.1.1 Absorption of Radiation by the Thermistor (Q_{abs})

To facilitate modeling of the radiation impinging on the thermistor the absorption term of the heat transfer equation will be written in

terms of the angular variation of radiant flux relative to a plane parallel earth. The angular distribution of radiant intensity will be defined in terms of θ where, $0 \leq \theta \leq \pi$ and ϕ where $0 < \phi \leq 2\pi$. The elevation angle θ and azimuth angle ϕ are defined in relation to the direction from which the thermistor receives radiation as shown in Figure 3.2. For upward propagating radiation, $\cos\theta < 0$ and for downward propagating radiation, $\cos\theta > 0$. The coordinate system is defined so that the X-Y plane is parallel to the earth with the thermistor axis lying in this plane. It is assumed that the thermistor remains in the X-Y plane (parallel to the earth) as it ascends and rotates through the atmosphere. The X-axis is oriented in the direction of the projection of the line between the sun and the thermistor on the X-Y plane. With this definition, axial symmetry about the X-axis can be assumed for incoming solar radiation.

The total radiation striking the thermistor could be derived by integrating the hemispheric irradiance for all points on the thermistor. However, by assuming a uniform temperature for the thermistor and uniform absorption properties, this integration can be simplified.

Consider radiation from the direction θ, ϕ of intensity $I(\theta, \phi, \lambda)$ striking the thermistor (see Figure 3.2). Assuming the intensity irradiating the thermistor from the direction (θ, ϕ) does not vary along the length of the thermistor and that the thermistor is a diffuse absorbing surface then, the rate of heat transfer per steradian is:

$$\hat{q} = A_p(\theta, \phi') \int_{\lambda} \alpha(\lambda) I(\theta, \phi, \lambda) d\lambda \quad (3.2)$$

where ϕ' is the azimuthal angle of the thermistor relative to the

Geometry Used in Defining Intensity

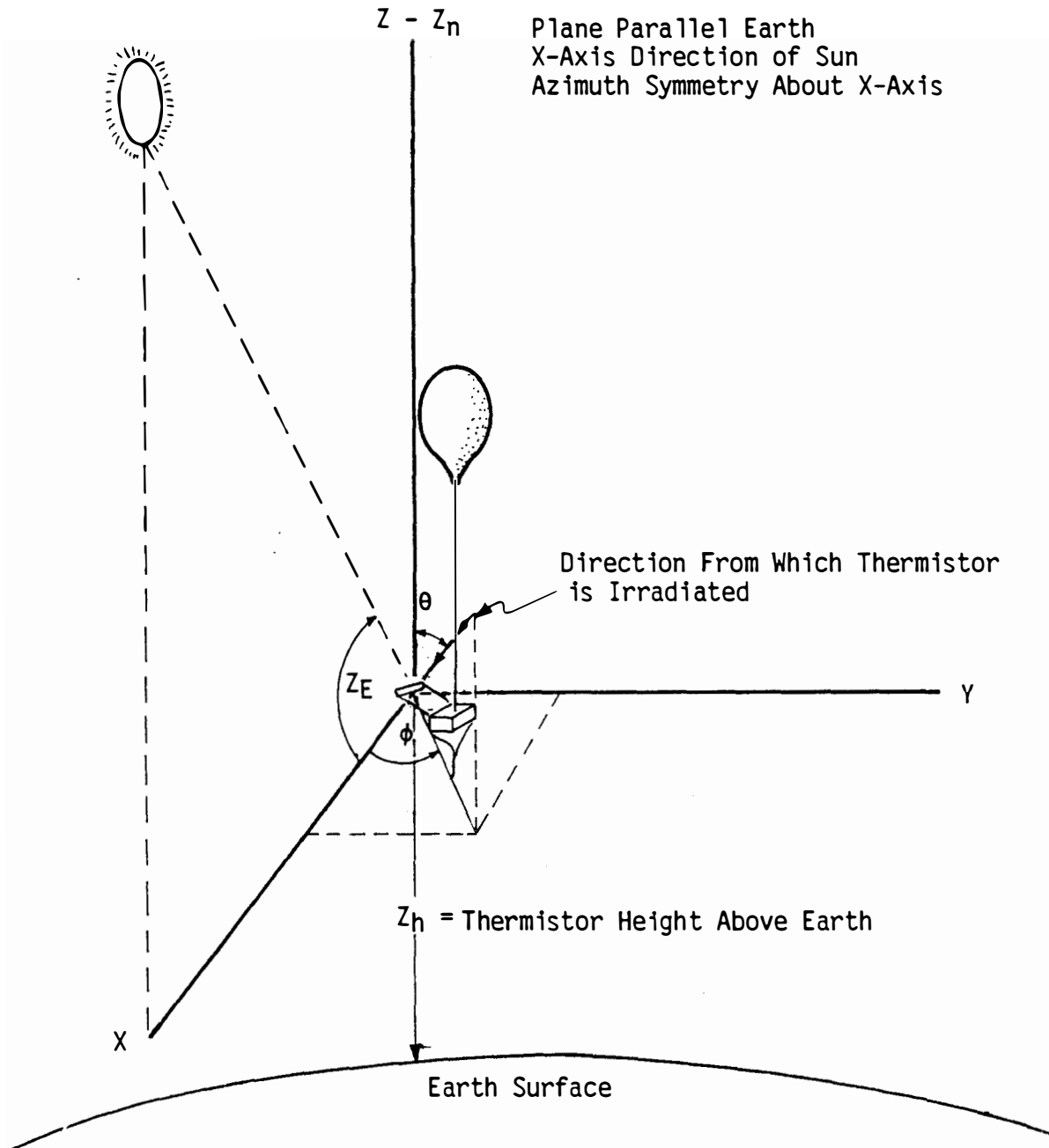


Figure 3.2 Coordinate system for defining angular distribution of radiation.

azimuthal direction of incoming radiation as shown in Figure 3.3, $A_p(\theta, \phi')$ is the projected area of a thermistor in the direction of the incoming radiation and $\alpha(\lambda)$ is the absorption coefficient of (all points on) the thermistor. $I(\theta, \phi, \lambda)$ is the intensity of radiation of wavelength λ from the pencil of radiation $d\Omega$ in the direction (θ, ϕ) . As the balloon and thermistor rotate in the atmosphere, the projected area of the thermistor in a fixed direction (θ, ϕ) varies. Assuming the thermistor rotates at a rate faster than the time constant of the thermistor, it is appropriate to calculate an average heating rate per revolution. The average rate of heat transfer from the (θ, ϕ) direction during one revolution is:

$$\bar{q} = \bar{A}_p(\theta) \int_{\lambda} \alpha(\lambda) I(\theta, \phi, \lambda) d\lambda \quad (3.3)$$

where $\bar{A}_p(\theta)$ is the average presented area of the thermistor, given by:

$$\bar{A}_p(\theta) = \frac{1}{2\pi} \int_0^{2\pi} A_p(\theta, \phi') d\phi' \quad (3.4)$$

Integrating this average thermistor heating rate over all incoming directions gives the total heating rate of the thermistor as:

$$q_{abs} = \int_{\Omega} \bar{q} d\Omega = \int_{\phi=0}^{2\pi} \int_{\theta=0}^{\pi} \bar{A}_p(\theta) \int_{\lambda} \alpha(\lambda) I(\theta, \phi, \lambda) d\lambda \sin \theta d\theta d\phi \quad (3.5)$$

where $\bar{A}_p(\theta)$ is given by Equation 3.4 and numerically evaluated in Appendix 1. The bar symbol has been dropped from q_{abs} for convenience.

Equation 3.5 is the basic equation for calculating the radiation absorbed by the thermistor. The intensity $I(\theta, \phi, \lambda)$ defines the angular distribution of radiation irradiating the thermistor. This irradiation of the thermistor comes from the direct impingement of upward and downward propagating atmospheric radiation, as well as from radiant

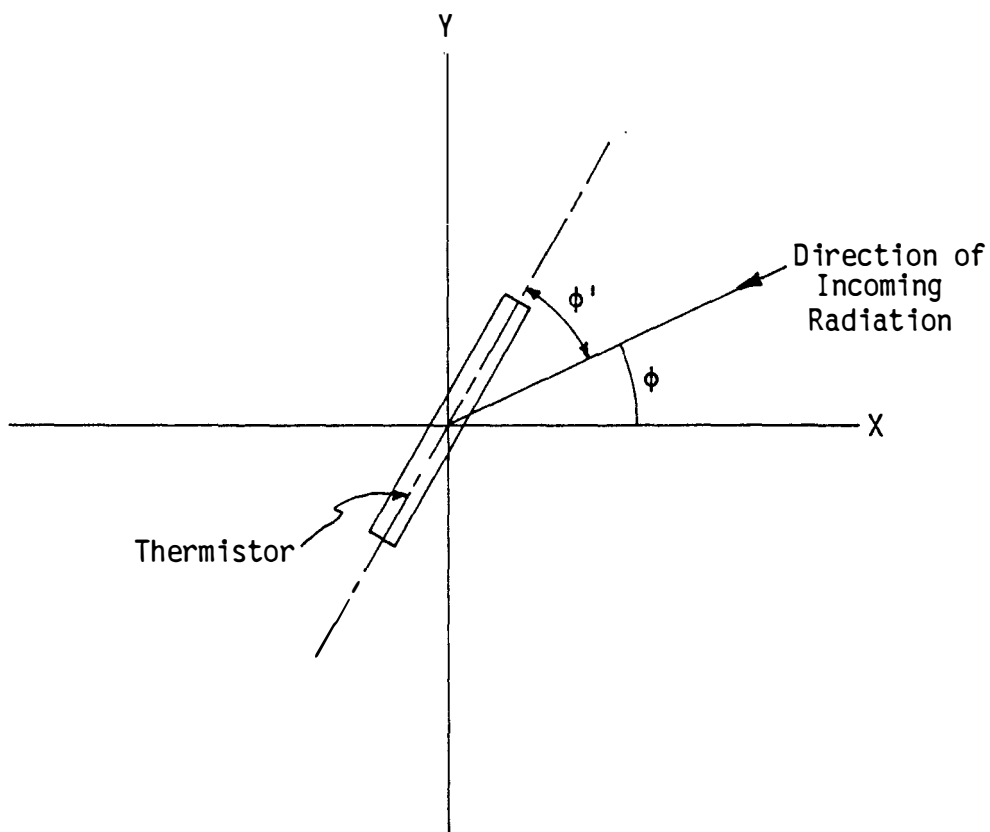


Figure 3.3 Azimuthal direction of thermistor relative to incoming radiation (2-dimensional view).

exchange between the thermistor and the radiosonde balloon and instrument package. In terms of components, the intensity $I(\theta, \phi, \lambda)$ irradiating the thermistor can be written as:

$$I(\theta, \phi, \lambda) = \begin{cases} I_b(\theta, \phi, \lambda); & \theta, \phi \in \Omega_b \\ I_{rs}(\theta, \phi, \lambda); & \theta, \phi \in \Omega_{rs} \\ I^*(\theta, \phi, \lambda); & \theta, \phi \notin \Omega_b, \Omega_{rs} \end{cases} \quad (3.6)$$

where $I_b(\theta, \phi, \lambda)$ is the intensity irradiating the thermistor from the solid angle Ω_b consisting of lines of sight (rays) from the thermistor that intersect the balloon, and $I_{rs}(\theta, \phi, \lambda)$ is the intensity arriving from the solid angle Ω_{rs} defined by lines of sight from the thermistor that intersect the radiosonde instrument. In the remaining directions the radiation arriving at the thermistor comes directly from the radiation propagating through the atmosphere. Thus $I^*(\theta, \phi, \lambda)$ is the radiant intensity that is modeled, in layers, as the upward and downward propagating atmospheric radiation. An atmospheric radiation model LOWTRAN 6 is used to derive the angular distribution of the atmospheric radiation, in all directions, versus altitude as a function of environmental conditions. These environmental conditions include surface temperature, cloud cover, aerosol content, solar zenith angle, surface reflection characteristics, gaseous constituents, etc.

Equation 3.6 can be analyzed by calculating the magnitude of each of the three terms to establish the significance of the first two. This is done in Appendices 4 and 5 and summarized in Sections 3.7. The expression $I^*(\theta, \phi, \lambda)$ is derived from modeling the upward and downward propagation of atmospheric radiation using the LOWTRAN 6 model. Section 3.6.3 describes this model. Other parameters needed in the calculation of Equation 3.5 include the absorptivity, $\alpha(\lambda)$ of the thermistor as a function of wavelength. This is known from laboratory

measurements. Figure 3.4 from Schmidlin, et al. (1986) shows the absorptivity between 0.25 and 2.5 microns as a function of wavelength for the coating used on the standard radiosonde thermistor. The emissivity is an integrated value for the infrared region from 2.5 to 40 microns (Schmidlin, et al. (1986)). The influence of temperature on absorptivity is assumed negligible over the range of temperatures experienced by the thermistor. With this information, Equation 3.5 can be numerically integrated to give the rate of heat transfer to the thermistor due to absorbed radiation. Simplification, however, will be made before performing the integration.

3.1.2 Radiation Emitted by the Thermistor (q_{emis})

Assuming the thermistor to act as a gray body and having a uniform temperature T and emissivity ϵ , the total emittance over the entire surface area of the cylindrical thermistor is given by Equation 3.7.

$$q_{emis} = 2\pi(rL + r^2 - r_w^2) \sigma T^4 \epsilon \eta \quad (3.7)$$

where η is the index of refraction of air and σ the Stephan Boltzman constant. The term containing r_w^2 is small compared to other terms and is ignored in further analysis. Assuming η is approximately 1 and the thermistor dimensions are known, q_{emis} is expressed as a function of only one unknown, the thermistor temperature, for substituting into (Equation 3.1) the heat balance equations.

3.1.3 Heat Transfer to Thermistor by Convection (q_{conv})

The thermistor ascends through the air at a vertical velocity considerably greater in magnitude than the horizontal velocity of the thermistor relative to the air. Thus, for the purpose of determining a heat transfer coefficient, the airflow over the cylinder can be considered as crossflow. The end plates of the cylinder account for

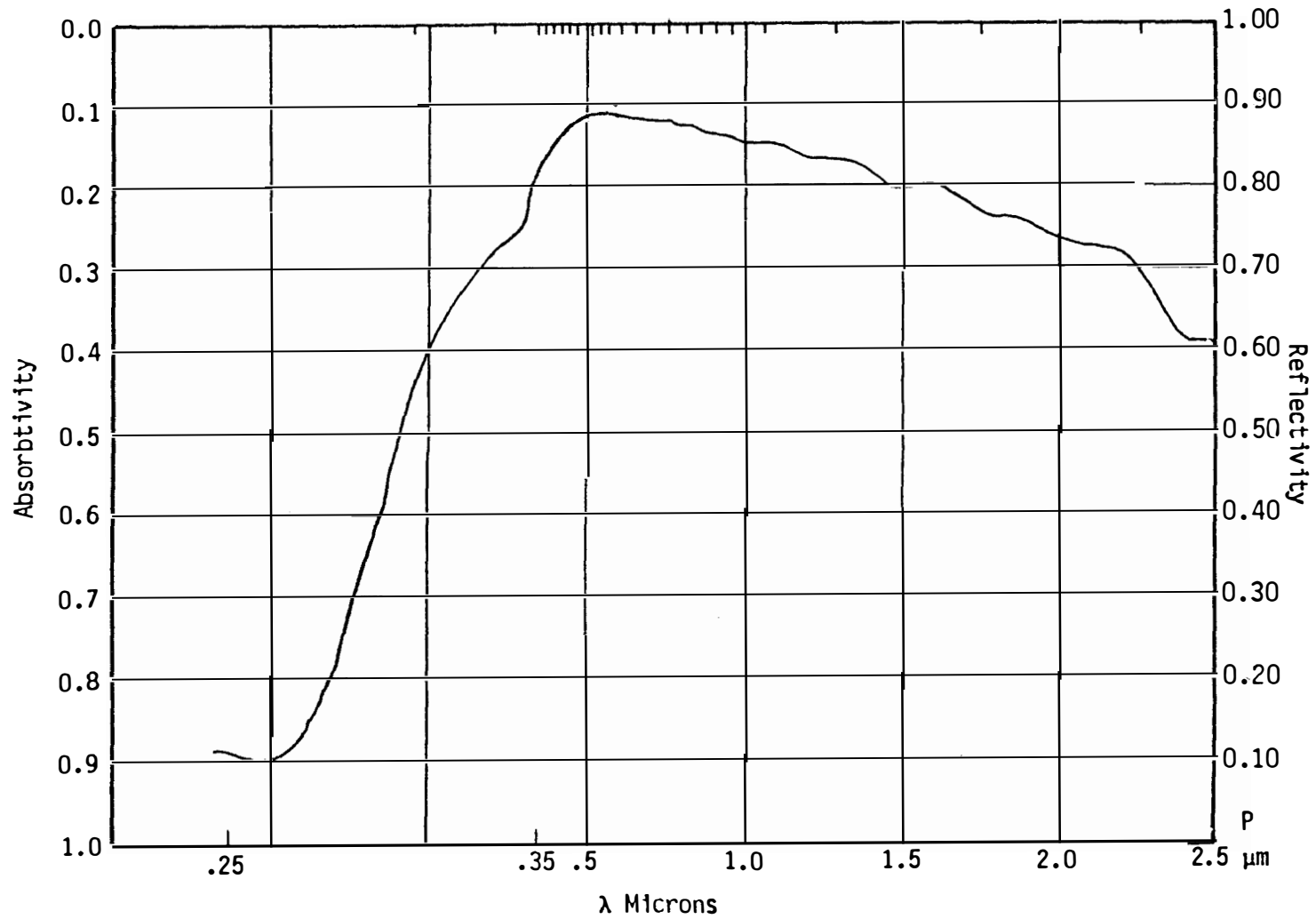


Figure 3.4 Absorptivity of standard radiosonde coating for $0.25 \leq \lambda \leq 2.5$ microns (Schmidlin, et al. (1986)).

less than 2% of the total area of the thermistor and thus the convective transfer through the end plates can be ignored.

If the ambient temperature is denoted by T_∞ , and the convective heat transfer coefficient by h_C , then the heating rate of the thermistor (Kays and Crawford (1980)) resulting from convection can be written as:

$$q_{\text{conv}} = - 2\pi r l h_C (T - T_\infty) \quad (3.8)$$

To determine the airflow regime over the thermistor, the Reynolds number must be calculated. For a nominal balloon rise rate of 5 m/sec the Reynolds number, based upon the diameter of the cylindrical thermistor, varies from about 400 at the surface to 5 at 30 Km. Thus, laminar flow is evident. The heat transfer coefficient for laminar cross flow is given in terms of Nusselt number as (Fand and Reswani (1972)):

$$Nu = 0.184 + 0.324 Re^{0.5} + 0.291 Re^m \quad (3.9)$$

$$\text{where } m = 0.247 + 0.0407 Re^{-0.168}$$

This equation shows a good fit with experimental data for Reynolds numbers 10^{-2} to 10^5 . The Nusselt number is related to the heat transfer coefficient by $h_C = \frac{kNu}{2r}$ where k is the thermal conductivity of air. The thermal conductivity is evaluated as a function of temperature using Equation 3.10 obtained from the U.S. Standard Atmosphere Supplements (1966).

$$k = \frac{6.325 \times 10^{-7} T_\infty^{3/2}}{T_\infty + 245.4 \times 10^{-(12/T)}} \quad (3.10)$$

All variables in Equation 3.8, other than the unknown T can be evaluated and thus Equation 3.8 can be substituted into Equation 3.1.

3.1.4 Heat Transfer by Electrical Current (q_{elect})

Heat is added to the thermistor as a result of the electric current passing through the thermistor that is used to measure the thermistor's resistance. The heating rate is given by:

$$q_{\text{elect}} = I^2 R \quad (3.11)$$

where I is the current passing through the thermistor of resistance R . The current is calculated from the known battery voltage of the radiosonde ($E = 18$ volts) and the total resistance R_t of the circuit as:

$$I = E/R_t \quad (3.12)$$

The total resistance of the circuit includes contributions from the thermistor, the wiring, and a fixed resistor. The thermistor resistance varies with temperature from approximately 12,000 ohms at 310° K to 3,500,000 ohms at 200° K. The fixed resistor has a resistance of $R_f = 1,000,000$ ohms. The resistance of the wires can be considered negligible. Rewriting Equation 3.11 in terms of the circuit resistances gives:

$$q_{\text{elect}} = \frac{E^2 R}{(R_f + R)^2} \quad (3.13)$$

Equation 3.13 can be evaluated directly as a function of thermistor temperature using the thermistor calibration curve to relate temperature to resistance. However, the magnitude of the electrical heating term will be shown in Section 3.3 to be negligible throughout the entire temperature range experienced by the thermistor.

3.1.5 Heat Transfer by Conduction from Lead Wires (q_{cond})

The heating rate of the thermistor due to conduction through the lead wires is given by (Arpaci (1966)):

$$q_{\text{cond}} = 2\pi r_w^2 k_w \left. \frac{\partial T_w}{\partial \ell} \right|_{\ell=0} \quad (3.14)$$

The temperature gradient of the wire at its interface with the thermistor ($l=0$) must be determined to evaluate the conduction term. All other parameters in Equation 3.14 have known or measured values. To determine the temperature gradient in the lead wires requires developing the heat balance equation for the wires. This equation is developed in a manner similar to that for the thermistor without assuming, however, that the lead wire temperature is uniform. Section 3.2 develops the heat balance equation for the lead wires.

3.1.6 Heat Balance Equation for Thermistor

Substituting into Equation 3.1 the expressions for each of the heating sources yields the following expression for the time rate of change of the thermistor temperature.

$$mC \frac{\partial T}{\partial t} = q_{abs} - 2\pi(r_l + r^2) \sigma T^4 \epsilon \eta - 2\pi r l h_c (T - T_\infty) + 2\pi r_w^2 k_w \left. \frac{\partial T_w}{\partial l} \right|_{l=0} \quad (3.15)$$

where q_{abs} is given by Equation 3.5. Equation 3.15 cannot be solved directly for the thermistor temperature because, as previously mentioned, the gradient of the lead wire temperature needed to evaluate the last term must be expressed in terms of T . To achieve this, an additional heat balance equation must be derived for the heat transfer processes occurring in the lead wires. The following section derives this heat balance equation. After this derivation, the solution of the heat balance equation for the lead wire will allow the evaluation of the temperature gradient at the thermistor/wire interface which, in turn, will permit the solution of Equation 3.15.

3.2 Heat Balance Equation for Lead Wires

A control volume approach is used to derive the heat balance

equation for the lead wires. The temperature of the wire is assumed to be uniform radially but varying with length. For a control volume of length $d\ell$ the time rate of change of the temperature of the control volume can be expressed as the sum of heat fluxes resulting from radiation absorbed at the surface of the wire, the radiant energy emitted by the wire, the convective heat transfer resulting from the air motion over the wire, the electrical heating of the wire due to the current passing through the lead wire, and the conductive transfer of heat along the length of the wire. Figure 3.5 shows a sketch of the geometry of the lead wire control volume.

3.2.1 Absorption of Radiation by Lead Wires (q'_{wabs})

An expression for the absorption of radiation by the lead wires is derived analogous to that for the thermistor. Consider radiation from the direction (θ, ϕ) of intensity $I(\theta, \phi, \lambda)$ striking an element of the lead wire of length $d\ell$. The rate of heat exchange to the wire of length $d\ell$ from radiation arriving in the direction (θ, ϕ) per steradian is:

$$d\hat{q}_w(\theta, \phi) = dA_{pw}(\theta, \phi') \int_{\lambda} \alpha_w(\lambda) I(\theta, \phi, \lambda) d\lambda$$

where $dA_{pw}(\theta, \phi')$ is the projected area of the element of wire of length $d\ell$ in the (θ, ϕ) direction, and ϕ' is as defined in Figure 3.3. The average rate of radiant heat transfer to the element $d\ell$ over one revolution of the sensor, from the direction (θ, ϕ) per unit solid angle is:

$$\overline{d\hat{q}_w}(\theta, \phi) = d\overline{A}_{pw}(\theta) \int_{\lambda} \alpha_w(\lambda) I(\theta, \phi, \lambda) d\lambda$$

where from Appendix 1 $d\overline{A}_{pw}(\theta)$ can be written as:

$$d\overline{A}_{pw}(\theta) = 2r_w d\ell \overline{F}_r(\theta)$$

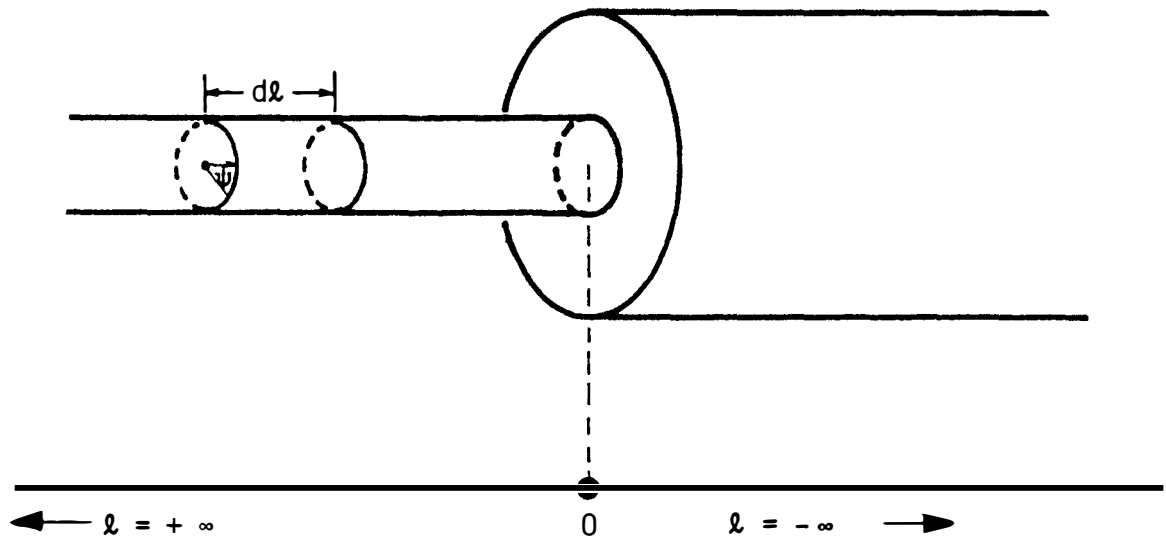


Figure 3.5 Lead wire geometry.

and $\bar{F}_r(\theta)$ is the average percent of the length of an element of wire projected at an elevation angle θ , during one revolution.

Integrating this rate of heat transfer over all directions of incoming radiation provides the total radiant heat transfer rate of the wire of length $d\ell$ as:

$$\bar{q}'_{wabs} d\ell = 2r_w d\ell \bar{F}_r(\theta) \int_{\lambda} \int_{\Omega} \alpha_w(\lambda) I(\theta, \phi, \lambda) d\Omega d\lambda \quad (3.16)$$

The above equation is analogous to that derived for the absorption by the surface of the rod thermistor. This equation is evaluated in the same manner as Equation 3.5 for the thermistor.

3.2.2 Radiation Emitted by Lead Wires (q_{wemis})

Because the temperature of a lead wire varies with length over the distance $d\ell$, the value of T_w at the midpoint of the control volume will be assumed for calculating the emitted radiation. Assuming a gray body, the power emitted (Sparrow and Cess (1978)) is given by:

$$dq_{wemis} = 2\pi r_w \epsilon_w \sigma T_w^4(\ell) \eta^2 d\ell \quad (3.17)$$

The value for all parameters in the above equation are known except for the wire temperature which is considered the unknown.

3.2.3 Heat Transfer to Lead Wires by Convection (q_{wconv})

The heat convection term for the lead wire control volume is given by:

$$dq_{wconv} = 2\pi r_w h_{cw} (T_w(\ell) - T_{\infty}) d\ell \quad (3.18)$$

The heat transfer coefficient is assumed to be that of a cylinder in laminar crossflow as given by Equation 3.9. The air temperature T_{∞} is assumed as a given. Thus, the only unknown in the above equation is the temperature of the wire.

3.2.4 Heat Transfer by Electrical Current ($q_{w\text{elect}}$)

The equation for electrical heating of the lead wires is:

$$dq_{w\text{elect}} = I^2 R_w d\ell \quad (3.19)$$

The current, I , passing through the lead wires depends upon the battery voltage and the resistance of the circuit and has been given by Equation 3.12. The electrical resistance of the lead wire per unit length, R_w , is a function of the wire temperature but can be considered to have an approximate magnitude 0.0035 ohms per cm throughout the temperature range of interest. The calculation of the magnitude of Equation 3.19 will show the electrical heating term for the lead wires to be negligible (see Section 3.3).

3.2.5 Heat Transfer by Conduction Through Lead Wire ($q_{w\text{cond}}$)

The net conduction of thermal energy into the control volume is the difference between the heat flowing into one end of the control volume by conduction and that flowing out the other end. For a wire of radius r_w the heat conduction into the segment $d\ell$ is given by $q_{in} = -\pi r_w^2 k_w \frac{\partial T_w}{\partial \ell}$ and that out of the segment as $q_{out} = -\pi r_w^2 k_w \frac{\partial T_w}{\partial \ell} + \frac{\partial}{\partial \ell} (-\pi r_w^2 k_w \frac{\partial T_w}{\partial \ell}) d\ell$ so that the net conduction into the control volume is:

$$dq_{w\text{cond}} = +\pi r_w^2 k_w \frac{\partial^2 T_w}{\partial \ell^2} d\ell \quad (3.20)$$

The only unknown variable in calculating the right side of Equation 3.20 is the wire temperature T_w .

3.2.6 Heat Balance Equation for Lead Wires

By summing all of the heat transfer terms for a lead wire, the heat balance equation becomes:

$$\begin{aligned} \pi r_w^2 \rho_w c_w \frac{\partial T_w}{\partial t} = & q_{w\text{abs}} - 2\pi r_w \epsilon_w \sigma T_w^4 \eta^2 - 2\pi r_w h_{cw} (T_w - T_\infty) \\ & + \pi r_w^2 k_w \frac{\partial^2 T_w}{\partial \ell^2} + I^2 R_w \end{aligned} \quad (3.21)$$

The spatial boundary conditions for solving this second-order differential equation are $T_w = T$ at $z = 0$ and $\frac{\partial T_w}{\partial z} = 0$ at $z = +\infty$ where z is the distance along the wire from the thermistor/lead wire junction. The unknown in solving Equation 3.21 is the wire temperature as a function of length and time. Because the wire temperature is a very slowly changing function of time, as the balloon ascends through the atmosphere, the time variation can be neglected and Equation 3.21 becomes an ordinary differential equation. The ambient temperature is assumed to be given. The absorption term is not a function of the wire temperature and can be considered a constant for solving the equation at a given altitude. Equation 3.21 is a second-order, non-homogeneous non-linear differential equation that does not possess a closed form analytic solution, but can be integrated once (as shown in Section 3.4) and $\frac{dT_w}{dz}$ evaluated at $z = 0$. This gradient of the wire temperature at the thermistor/lead wire junction is then substituted into Equation 3.15 for evaluating the temperature of the thermistor. Equation 3.15, in its steady-state form, is an algebraic equation solved iteratively for the thermistor temperature. The solution method is further described in Section 3.4.

3.3 Magnitude of Terms in Heat Balance Equation

Prior to attempting the solution of the heat balance equations of the thermistor and lead wire, an estimate has been made of the magnitude of each term in each equation. Direct calculation of every term was not possible because of the unknown value of various derivatives and integrals. However, using appropriate assumptions, order of magnitude estimates (or maximum value estimates) could be established.

The assumptions include simplifying the absorption term to consist of separate solar and infrared components. Maximum solar absorption was assumed to occur at a high solar zenith with 50% albedo. To estimate infrared absorption, an equivalent black body temperature for upwelling and downwelling atmospheric radiation was assumed (Gergen (1957)) and the thermistor absorption due to this blackbody temperature calculated. An equivalent black body atmospheric temperature for upwelling (downwelling) radiation is defined to be the temperature assumed by a perfect blackbody flat surface, oriented parallel to the earth, with upper (lower) surface insulated and lower (upper) surface in radiative equilibrium with the atmosphere.

Appendix 2 describes the calculation of the magnitude of each term in the heat balance equations. The parameter values used as input to the calculations are shown in Table 3.1. The resulting order of magnitude estimates are shown in Table 3.2. Note that the units for the thermistor heat balance equation are cal/sec which differs from the lead wire units of cal/sec per cm of length of the lead wires. From this order of magnitude analysis we can conclude that: a) the electrical heating of the thermistor and lead wires is at least two orders of magnitude smaller than the other terms and can be ignored; b) the lead wire conduction term can be very significant if the temperature gradient in the lead wire at the thermistor junction is greater than 0.1° K/cm ; and c) by assuming an atmospheric temperature gradient of $1^\circ \text{ K per } 100 \text{ m}$ the magnitude of the time rate of change term, with a balloon rise rate of 5 m/sec ($\frac{dT}{dt} \approx 0.05^\circ/\text{sec}$) is approximately 8.4×10^{-4} which is smaller than the other significant terms. Thus, assuming a steady state solution $\left[\frac{dT}{dt} = 0 \right]$ is not unrealistic.

Table 3.1 Parameter Values Used in Order of Magnitude Analysis

Symbol	Parameter Value
m	0.12g
C	0.14 cal/g °K
r	0.06 cm
ℓ	4.0 cm
h _C	4 X 10 ⁻³ cal/sec cm ² °K (surface) 6.8 X 10 ⁻⁴ cal/sec cm ² °K (30 Km)
T - T _∞	3° K
z	5 m/sec
ε	0.86
σ	1.354 X 10 ⁻¹² cal/sec cm ² °K ⁴
η	1.0
E	18 volts
R	12,000 (310° K) to 3,500,000 (200° K) ohms
R _f	1,000,000 ohms
c _w	0.093 cal/g °K (copper)
ρ _w	8.9 g/cm ³ (copper)
r _w	0.0125 cm
k _w	0.92 cal/sec cm °K
ε _w	0.06 (tin coating)
R _w	.0035 ohms/cm
h _{Cw}	1.92 X 10 ⁻² cal/sec cm ² °K (surface) 3.26 X 10 ⁻³ cal/sec cm ² °K (30 Km)
T	300° K (max) 200° K (min)
α	0.15 (standard coating)
α _w	0.08 (tin coating)
I ₀	333.5 X 10 ⁻⁴ cal/sec cm ² (solar power)

3.4 Method of Solving Heat Balance Equations

Restricting the heat balance Equations 3.15 and 3.21 to those terms which are significant results in the following equations to be solved for the thermistor temperature T and wire temperature T_w:

$$0 = q_{abs} - 2\pi (r\ell + r^2) \sigma T^4 \epsilon - 2\pi r\ell h_C (T - T_\infty) + 2\pi r_w^2 k_w \left. \frac{dT_w}{d\ell} \right|_{\ell=0} \quad (3.22)$$

(thermistor heat balance, q_{abs} given by Equation 3.5)

Table 3.2 Magnitude of Terms in Heat Balance Equations

Term	Thermistor Heat Balance	Lead Wire Heat Balance	Comments
Time rate of change $mC \frac{dT}{dt}$	cal/sec $1.68 \times 10^{-2} \frac{dT}{dt}$	cal/sec cm $4.1 \times 10^{-4} \frac{dT}{dt}$	
Absorption: Solar	2.88×10^{-3}	8.0×10^{-5}	$Z_E=80^\circ$, Albedo=50% $T_E=250^\circ K$
Longwave	2.21×10^{-3}	0.53×10^{-5}	
Emission	1.44×10^{-2}	3.34×10^{-5}	$T=300^\circ K$
Convection: Walls	3.08×10^{-3}	7.68×10^{-4}	Can ignore end plates
Electrical Heating	1.3×10^{-5} (max) 9.1×10^{-7} (min)	2.16×10^{-11} (max) 2.09×10^{-14} (min)	Assumes 1,000,000 ohms fixed resistance
Conduction	$2.1 \times 10^{-2} \frac{dT_w}{d\ell} \Big _{\ell=0}$	$4.5 \times 10^{-4} \frac{d^2 T_w}{d\ell^2}$	

$$0 = q'_{wabs} - 2\pi r_w \epsilon_w \sigma T_w^4 - 2\pi r_w h_{C_w}(T_w - T_\infty) + \pi r_w^2 k_w \frac{d^2 T_w}{d\ell^2} \quad (3.23)$$

(lead wire heat balance, q'_{wabs} given by Equation 3.16).

Equations 3.22 and 3.23 are solved simultaneously at various altitudes that represent the path of an ascending radiosonde balloon from the surface to 30 Km. An atmospheric temperature and density profile are assumed as input. Reviewing the terms in Equation 3.22 and 3.23, q_{abs} and q'_{wabs} can be calculated independent of both the air temperature and the unknown thermistor temperature provided the

thermistor absorptivity is not a function of thermistor temperature and that the irradiation of the thermistor from above and below is not dependent upon the local air temperature -- both valid assumptions. Sections 3.6, 3.7, and 3.8 discuss the calculation of the q_{abs} and q_{wabs} terms for different environmental conditions. The emissivities, ϵ and ϵ_w , in the emission terms are also assumed to be independent of the unknown thermistor and wire temperatures. The heat transfer coefficient in the convective heating terms is a function of Reynolds number and is also independent of the thermistor and wire temperatures. The thermal conductivity of the lead wire, k_w , in the conduction terms can be considered independent of the wire temperature within the range of temperatures experienced by the lead wires.

With the above assumptions, all of which are reasonable, the form of Equations 3.22 and 3.23 can be written as:

$$K_1 + K_2 T + K_3 T^4 = - \left. \frac{dT_w}{d\ell} \right|_{\ell=0} \quad (3.24)$$

and

$$\frac{d^2 T_w}{d\ell^2} = J_1 + J_2 T_w + J_3 T_w^4 \quad (3.25)$$

where K_i and J_i are given in Table 3.3.

Table 3.3 Expressions for the Constants in Heat Balance Equations

$$J_1 = \frac{q_{wabs} + 2\pi r_w h_{cw} T_\infty}{\pi r_w^2 k_w}$$

$$K_1 = \frac{q_{abs} + 2\pi r \ell h_c T_\infty}{2\pi r_w^2 k_w}$$

$$J_2 = - \frac{2h_{cw}}{r_w k_w}$$

$$K_2 = - \frac{r \ell h_c}{r_w^2 k_w}$$

$$J_3 = - \frac{2\epsilon_w \sigma}{r_w k_w}$$

$$K_3 = - \frac{(r \ell + r^2) \sigma \epsilon}{r_w^2 k_w}$$

The boundary conditions are that the thermistor and wire temperature are equal at the interface:

$$T_w = T \text{ at } \ell = 0$$

and that the wire temperature approaches a constant at large distances from the interface. This follows from the fact that all heat transfer processes affecting the wire, except conduction through the wire, are independent of wire length; the heat conduction through the wire decreases with increased distance from the thermistor. Thus,

$$T_w = \text{const at } \ell = + \infty$$

and

$$\frac{dT_w}{d\ell} = \frac{d^2T_w}{d\ell^2} = 0 \text{ at } \ell = + \infty$$

Multiplying Equation 3.25 by $2 \frac{dT_w}{d\ell}$ and integrating gives:

$$\left[\frac{dT_w}{d\ell} \right]^2 = 2 \int (J_1 + J_2 T_w + J_3 T_w^4) dT_w \quad (3.26)$$

or

$$\frac{dT_w}{d\ell} = \pm \left[2 \left(J_1 T_w + J_2 \frac{T_w^2}{2} + J_3 \frac{T_w^5}{5} + D \right) \right]^{1/2} \quad (3.27)$$

The constant D is evaluated from the boundary condition that the temperature gradient in the wire goes to zero at large distances from the thermistor, that is:

$$\frac{dT_w}{d\ell} = 0 \text{ as } \ell \rightarrow \infty$$

The temperature of the wire at $\ell = \infty$ is designated $T_{w,\infty}$. Likewise, substituting $\frac{d^2T_w}{d\ell^2} = 0$ as $\ell \rightarrow \infty$ into Equation 3.25 gives the wire temperature at $\ell = \infty$ as a solution to the equation:

$$J_1 + J_2 T_{w,\infty} + J_3 T_{w,\infty}^4 = 0 \quad (3.28)$$

Resubstituting the value of D into Equation 3.27 gives:

$$\frac{dT_W}{d\ell} = \pm \left[2J_1(T_W - T_{W,\infty}) + J_2(T_W^2 - T_{W,\infty}^2) + 2 \frac{J_3}{5} (T_W^5 - T_{W,\infty}^5) \right]^{1/2} \quad (3.29)$$

where $T_{W,\infty}$ is evaluated by solving Equation 3.28.

Evaluating Equation 3.29 at the wire/thermistor junction ($\ell=0$) gives:

$$\frac{dT_W}{d\ell} \Big|_{\ell=0} = \pm \left[2J_1(T - T_{W,\infty}) + J_2(T^2 - T_{W,\infty}^2) + \frac{2J_3}{5} (T^5 - T_{W,\infty}^5) \right]^{1/2} \quad (3.30)$$

The two solutions of the above equation reflect the heat flow into or out of the thermistor depending whether the thermistor or wire temperature is larger. Equation 3.30 is substituted into Equation 3.24 to give the equation for the thermistor temperature:

$$K_1 + K_2T + K_3T^4 \pm \left[2J_1(T - T_{W,\infty}) + J_2(T^2 - T_{W,\infty}^2) + \frac{2J_3}{5} (T^5 - T_{W,\infty}^5) \right]^{1/2} = 0 \quad (3.31)$$

The above equation is a function of one unknown, T , since the wire temperature $T_{W,\infty}$ is calculated from Equation 3.28. Based on quasi-steady state assumptions, the constants J_1 , J_2 , J_3 , K_1 , K_2 , K_3 , are evaluated at each altitude for which a solution for the thermistor temperature is desired. Equation 3.31 is an algebraic equation solved iteratively for T using the air temperature as the initial guess of T . Convergence was achieved by interval having until $|T_i - T_{i-1}| \leq 0.001^\circ \text{ K}$.

3.5 Sensitivity of Parameters to Temperature Correction

Solving the heat balance equations for the thermistor temperature allows the determination of the radiosonde temperature error ($\Delta T = T - T_\infty$) which is defined as the thermistor temperature minus the air temperature. For routine National Weather Service radiosonde observation, the thermistor temperature is assumed to be the air temperature. Thus ΔT can be thought of as the temperature error in the

NWS measurement.

A primary purpose of this study is to provide an understanding of how the temperature error, ΔT , changes under different environmental conditions. This is achieved by calculating ΔT under a representative set of input conditions and then varying each parameter to establish the sensitivity of ΔT to changes in that parameter. Sensitivity analysis parameters include environmental variables, spatial variables and instrumentation variables. Table 3.4 shows a list of sensitivity analysis variables and the heat transfer terms in which they play a role. Sensitivity analysis variables for the absorption term include α and all of the environmental parameters which relate to the various radiant intensities, I^* , I , I_b and I_{rs} (see Equation 3.6). The radiation absorption term requires the most extensive modeling. The radiative fluxes absorbed by the thermistor from the environment are modeled in wavelength bands over a wide range of environmental parameters. Section 3.6 describes the modeling of these radiative fluxes. The heating of the thermistor by absorbed radiation depends upon the absorptivity of the thermistor and the absorptivity of the lead wires. These absorptivity values are obtained from laboratory measurements as a function of wavelength. Wavelengths of interest can be restricted to $0.25 \leq \lambda \leq 40$ microns since over 95% of the solar and earth emitted radiation is concentrated in this region (Valley (1965)).

When the expression for \bar{A}_p from Appendix 1 is substituted into Equation 3.5, q_{abs} is seen to be the product of the cross-sectional area of the thermistor, the thermal energy per unit area irradiating the thermistor and the absorptivity of the thermistor, integrated over all wavelengths. All of the above are varied as sensitivity analysis

Table 3.4 Sensitivity Analysis Parameters

Parameter	Heat Transfer Term
I^* , I , I_b , I_{rs}	q_{abs} , q_{wabs}
$\alpha(\lambda)$	q_{abs}
$\alpha_w(\lambda)$	q_{wabs}
ϵ	q_{emis}
ϵ_w	q_{wemis}
r , ℓ	q_{emis} , q_{elect} , q_{cond} , q_{conv}
r_w	q_{wcond}
h_c , T_∞	q_{conv}

parameters. In this section, however, the sensitivity of ΔT to the magnitude of thermal energy irradiating the thermistor is analyzed without specifying what environmental parameters effect the magnitude. The relationship between the magnitude of thermal energy and environmental parameters is considered in Section 3.6.3.2 and then related to ΔT throughout the computations carried out in this section.

The thermistor emission term contains r , ℓ , and ϵ , all of which are varied as sensitivity analysis parameters. The convective transfer term for the thermistor requires an expression for the heat transfer coefficient for a cylinder in crossflow. A Reynolds number of less than 400 throughout the flight assures laminar flow. The heat transfer coefficient, or Nusselt number, is expressed as a function of Reynolds

number which, in turn, relates to the diameter of the thermistor and the velocity of the air over the thermistor (or balloon rise rate). The rise rate variability was investigated and found not to have a major influence on Nusselt number and thus not included as a sensitivity analysis variable. The thermistor radius is considered as a sensitivity analysis variable. The heat conduction from the lead wires into the thermistor is believed to be a significant term and requires an accurate determination of the temperature gradient at the interface with the thermistor. Solution for the gradient requires, in turn, solving the heat balance equation for the lead wires as previously described. The only additional sensitivity analysis parameters derived from the lead wire equation are the absorptivity, α_w , and emissivity, ϵ_w , of the lead wires and the radius, r_w , of the lead wires.

The parameters listed in Table 3.4 have been varied over a representative range of values shown in Table 3.5 to establish the influence of each parameter on the radiosonde temperature error. The variability of the radiant intensity parameters I^* , I , etc. is established in a later section. A range of values of total radiation absorbed by the thermistor and lead wire, as defined in Table 3.5, serves as input for the sensitivity analysis.

3.5.1 Sensitivity Analysis Results

The heat balance equations for the lead wires (Equation 3.22) and thermistor (Equation 3.23) are solved for the steady-state thermistor temperature over the range of parametric values as discussed in the previous section. The range of values span those commonly encountered at a mid-latitude geographic location (such as Wallops Island, VA)

Table 3.5 Values of Sensitivity Analysis Variables

Variable	Baseline Value	Range
q_{abs}	3.61×10^{-3} cal/sec	$1.3 \times 10^{-3} \leq q_{abs} \leq 6 \times 10^{-3}$
q'_{wabs}	$\frac{q_{abs}}{\ell} \frac{r_w}{r} \frac{\epsilon_w^*}{\epsilon}$	
Nu	1.7 (30 Km)	$1.7 \leq Nu \leq 8.0$ (6 Km)
T	220°K	$194^\circ \leq T \leq 274^\circ$
ϵ	0.86	$0.2 \leq \epsilon \leq 1.0$
ϵ_w	0.06	$0.02 \leq \epsilon_w \leq 0.86$
r	0.06 cm	$0.02 \leq r \leq 0.10$
r_w	0.0125 cm	$0.006 \leq r_w \leq 0.02$
ℓ	4.0 cm	$4.0 \leq \ell \leq 16.0$

* q'_{wabs} scales with q_{abs} according to this relationship

during both day and night flight conditions. The parameters that were varied in this analysis are: the radiation absorbed by the thermistor (q_{abs}) and lead wire (q_{wabs}), the air temperature (T_∞), the Nusselt number (Nu), the emissivity of the thermistor (ϵ) and lead wires (ϵ_w), the radius of the thermistor (r) and lead wire (r_w), and the length of the thermistor (ℓ). The absorbed radiation is divided into day versus night flights. For night flights, the absorbed radiation is restricted to the infrared band from $2.5 \leq \lambda \leq 40 \mu$ with a constant emissivity (absorptivity) assumed over the band. For day flights, the solar and infrared components are combined by addition. The solar radiation

absorbed by the thermistor and lead wire are wavelength dependent through $\alpha(\lambda)$ and $\alpha_w(\lambda)$. A range of values of absorbed radiation that are utilized in this sensitivity analysis reflect mid-latitude environmental conditions and the wavelength dependent absorption properties of the standard NWS radiosonde (see Figure 3.4). The Nusselt number is varied to account for the altitude, or change in density, effect on the temperature error ΔT . The convective heat transfer coefficient is the only variable in the heat balance equations that is influenced by a change in density or altitude. (Note however, the radiation terms are expected to vary somewhat with altitude. This is analyzed in Section 3.6).

3.5.1.1 Nighttime Sensitivity Analysis

A set of baseline values were chosen which are physically representative of those expected for a nominal flight condition. These baseline values and a range of variation for each parameter are shown in Table 3.5 and served as input for solving the heat balance equations. Figures 3.6 through 3.9 show results from parameter variations under nighttime conditions with no solar input. All variables held constant in Figures 3.6 and 3.9 are fixed at their baseline values.

Influence of Absorbed Radiation

Figure 3.6 is a plot of the temperature error versus absorption for two selected temperature values with two additional calculations that extend the range of temperatures. This figure shows significant variation in the temperature error with changes in absorbed radiation. Environmental changes due to cloud cover and earth surface temperature could account for perhaps a 50% change in the infrared radiation

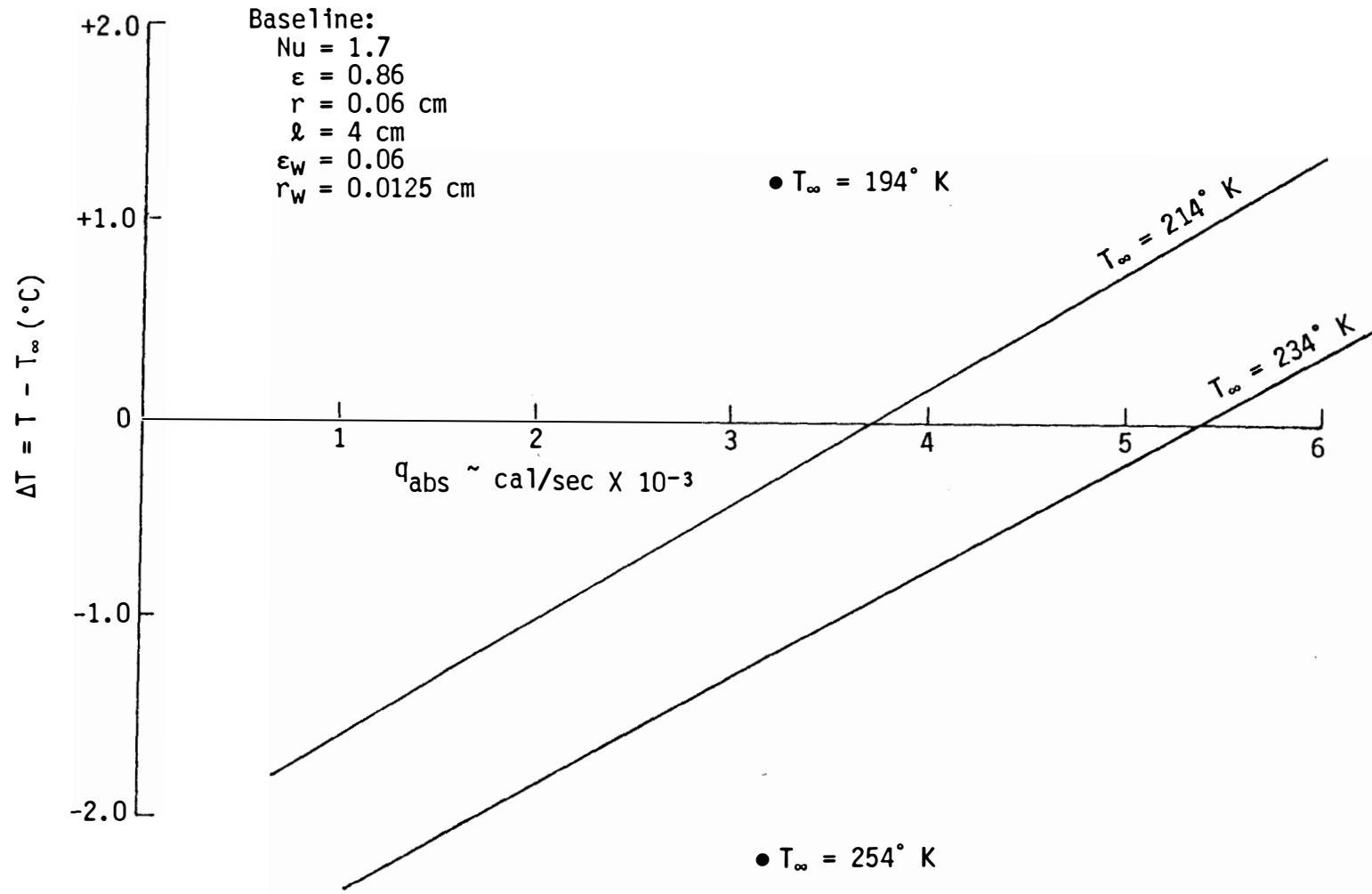


Figure 3.6 Variation in temperature error with amount of infrared radiation absorbed by the thermistor at different air temperatures.

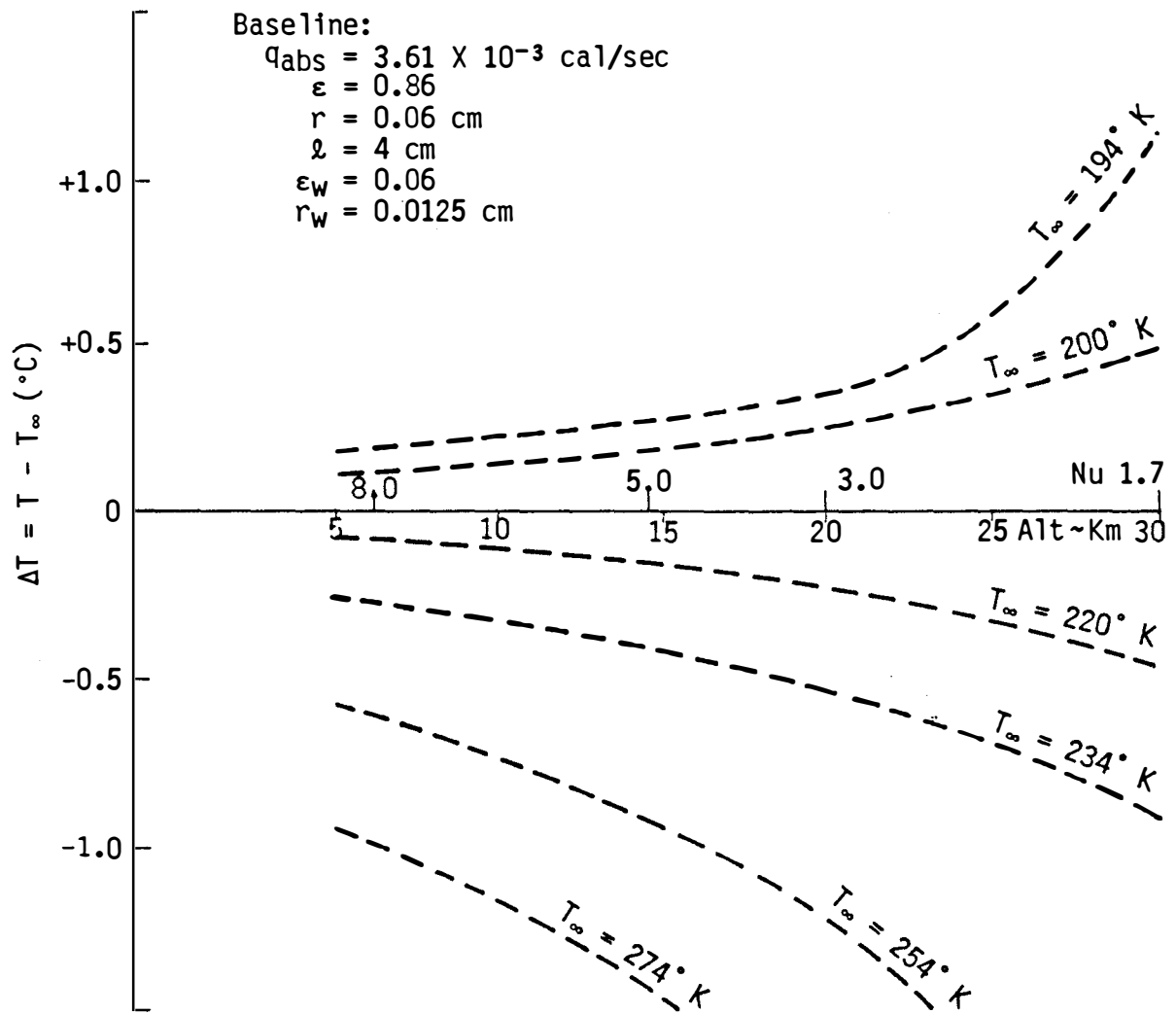


Figure 3.7 Variation in temperature error of thermistor with altitude (Nu) and air temperature.

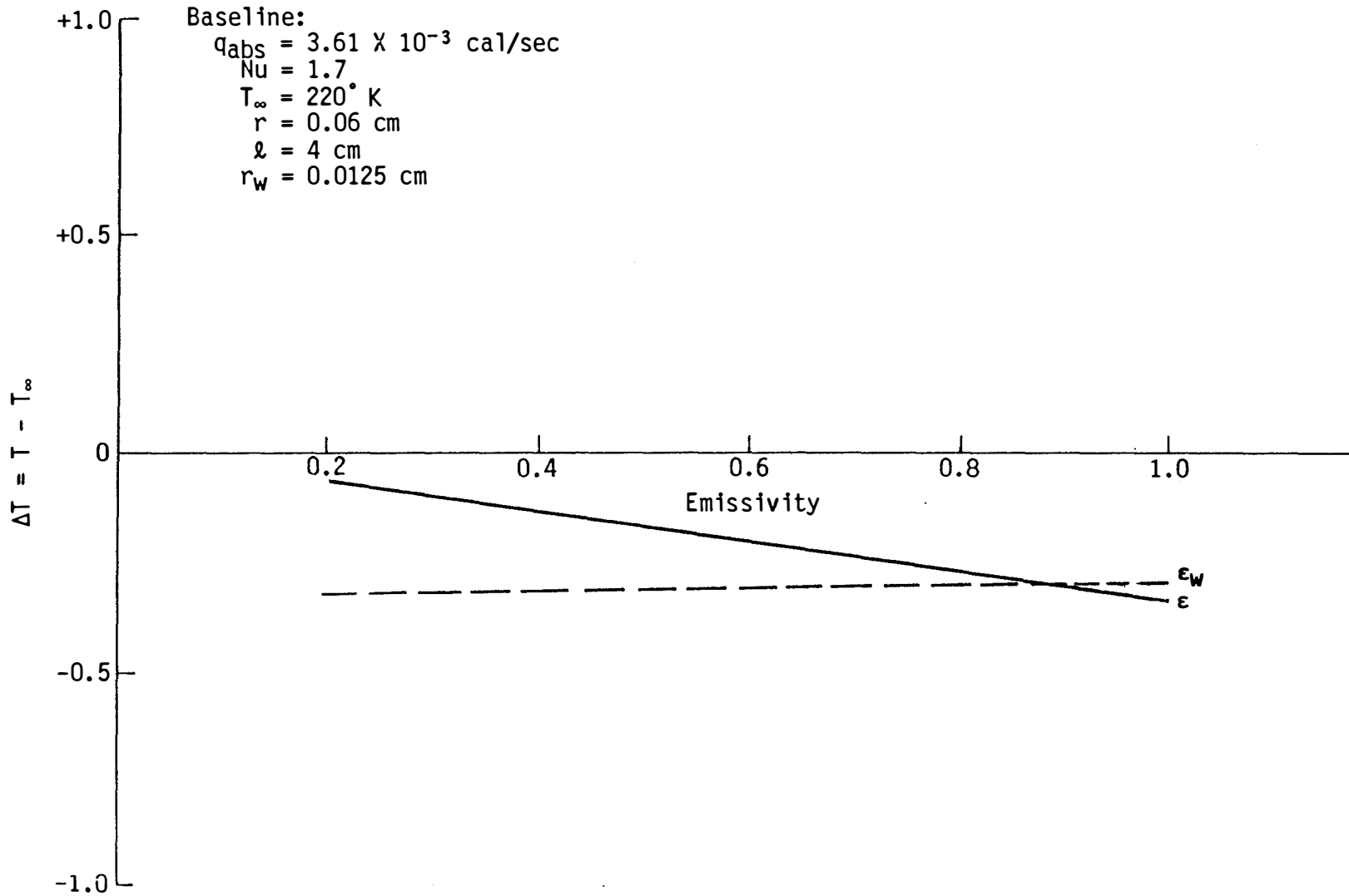


Figure 3.8 Variation in thermistor temperature error with changes in the emissivity of the thermistor (solid line) and of the lead wires (dashed line).

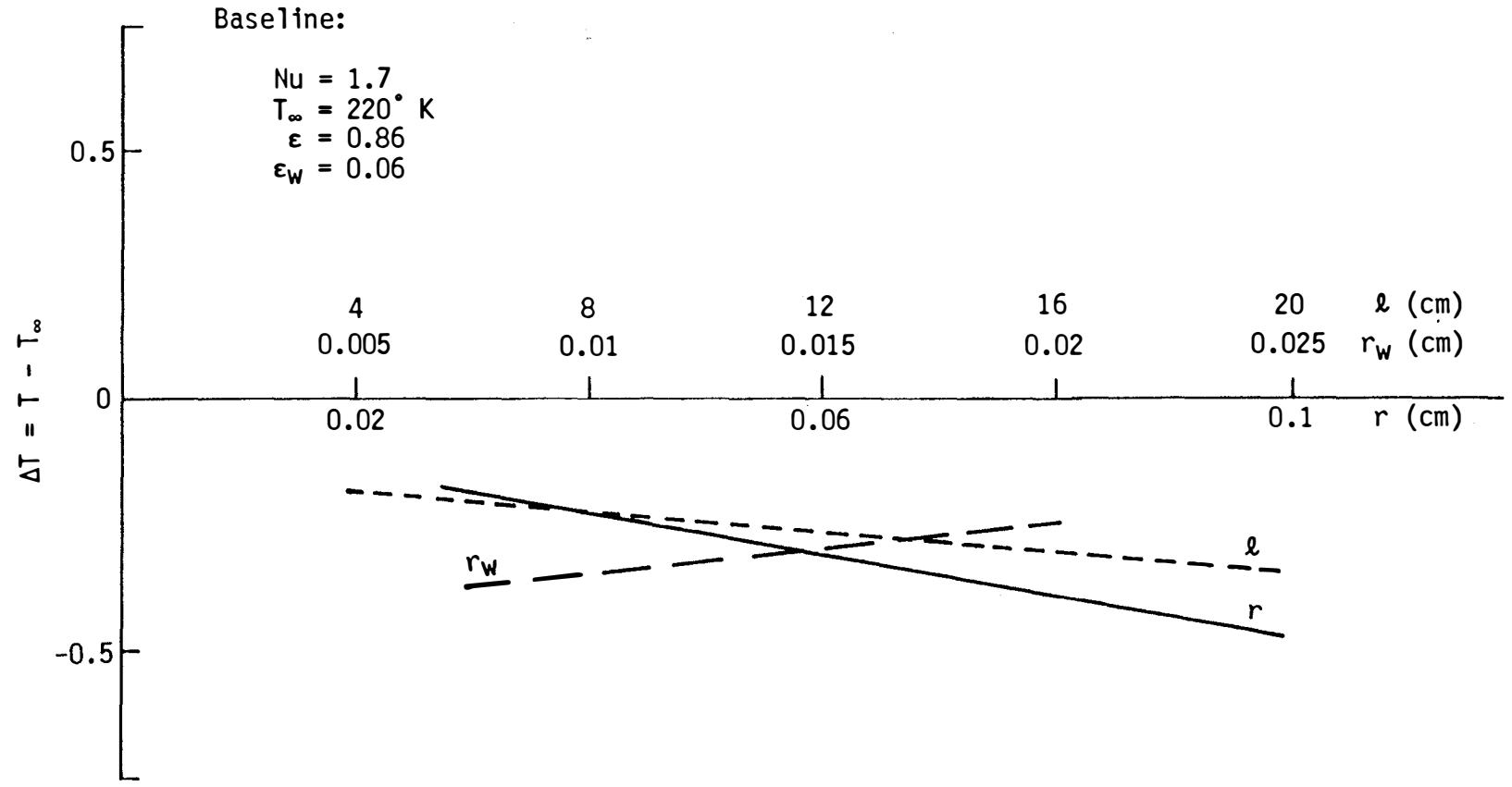


Figure 3.9 Variation in the thermistor temperature error with changes in the radius and length of the thermistor and the radius of the lead wires (nighttime).

(Wenkert (1985)) which, from the baseline value of 3.6×10^{-3} cal/sec. would, in turn, change the temperature error by as much as 1° K. In general, Figure 3.6 shows, for an altitude of 30 Km, a temperature error change of approximately 0.7° K for each change in absorbed infrared radiation of 1×10^{-3} cal/sec. Figure 3.6 also shows a large variation in the temperature error with air temperature as seen by the individual data points shown. This occurs because the absorption of infrared radiation by the thermistor and lead wires can be considered independent of temperature while the energy emitted is proportional to the fourth power of the thermistor temperature which, although not exact, is close to the air temperature. Thus, as the temperature of the atmosphere at a particular altitude (in this case 30 Km) changes with season or geographic location, the emission then changes and produces a very significant change in the radiosonde temperature error.

Influence of Altitude

The variation of temperature error with altitude is shown in Figure 3.7 for various air temperatures. The temperature error increases with increasing altitude (decreasing Nu) at all air temperatures. This occurs because the heat transfer by convection increases with increased air density (decreasing altitude) while the absorbed radiation, emitted radiation, and conduction heat transfer processes are not dependent on atmospheric density or altitude. The rate of change of the temperature error with altitude is more significant when the temperature error itself is large. This is believed to be due to the fact that as ΔT increases the emission term which varies as the fourth power of temperature predominate over the convective influence which varies to the first power.

Influence of Air Temperature

The variation of the thermistor temperature error with air temperature at a given altitude is very significant. Even at low altitudes, significant temperature errors may occur under extreme maxima or minimum air temperature conditions.

Influence of Emissivity

In the sensitivity analysis of emissivity, the irradiation of the thermistor (rather than the amount absorbed by the thermistor), was held constant at the value associated with the baseline conditions while the emissivity of the thermistor and lead wires were independently varied. Since the amount of absorbed infrared radiation is directly proportional to the emissivity, as is the amount emitted, a change in emissivity proportionally changes the magnitude of these two terms. A change in the temperature error occurs, however, because the convective and conduction terms must compensate to make the steady-state heat balance equation equal to zero. Thus, a change in the thermistor temperature results. Figure 3.8 shows the change in thermistor temperature error as a function of changes in ϵ and ϵ_w . The emissivity of the wire is seen to exert no real influence on the temperature of the thermistor. The emissivity of the thermistor has a moderate influence on ΔT . However, for the standard rawinsonde thermistor ($\epsilon = 0.86$) any small deviations from this value would introduce a negligible change into the thermistor temperature error.

Influence of Radius and Length

A review of the heat transfer equation for the thermistor and lead wires shows that the absorption, convection and emission terms are directly proportional to the radius. In essence, however, the heat

transfer coefficient in the convective terms is a nonlinear function of radius so that the convective terms do not actually vary in direct proportion to the radius. Thus, changes in radius of the thermistor or wire will not effect all terms proportionally. In the sensitivity analysis of radius and length the atmospheric radiation was held fixed at the value corresponding to that baseline condition while the amount absorbed by the thermistor varied in proportion to its length and radius. Figure 3.9 shows the variations in the thermistor temperature error resulting from a two-fold increase and decrease in the radius of the thermistor and lead wires. Results from this figure show for the thermistor error, a maximum change in ΔT of $\pm 0.15^\circ$ K over this range. A physical examination of several thermistors reveals minimal variation in radius -- far less than the factor of two tolerances calculated. Thus, thermistor non-uniformities in diameter contribute negligibly to the radiosonde temperature error. Variation in the radius of the lead wires shows a change in ΔT of less than 0.1° K over the same range. The manufacturing tolerance of the radius of the lead wire is percentage wise better than the thermistor. Thus, this factor does not significantly influence the radiosonde temperature error.

The length of the thermistor appears only in the thermistor (not lead wire) heat balance equation. The absorption, convection and emission terms of the heat balance equation are directly proportional to the length l . The conduction through the ends of the cylindrical thermistor is, however, independent of thermistor lengths. Thus, variations in the thermistor temperature error due to the length of the thermistor reflect the rate of thermal energy that can be transported by conduction through the lead wires. Figure 3.9 shows the variation

in ΔT for a variation of thermistor length from 4 to 16 cm. Only a 0.2° K increase in the temperature error occurs over this extreme change in thermistor lengths. Thus, for practical application, the length of the thermistor is independent of the radiosonde temperature error.

3.5.1.2 Daytime Sensitivity Analysis

To establish the variation of ΔT for daytime conditions an additional absorption term for the solar radiation impinging on the thermistor and lead wires was included in the heat balance equations. The total absorbed radiation was the sum of two components, an infrared radiation component for $2.5 \leq \lambda \leq 40\mu$ and the solar component in the wavelength range from $0.25 \leq \lambda < 2.5\mu$. The baseline value for the infrared used in the nighttime calculations was retained for the day sensitivity analysis. No variations in the infrared radiation was introduced into the daytime calculations. For the solar component, a baseline value of 3.2×10^{-3} cal/sec for absorption by the thermistor was utilized. The absorption by the wires took on a directly related value consistent with its dimensions and absorptivity. The baseline values for the other parameters and their range of variability were the same as those introduced into the nighttime analysis (see Table 3.5).

Influence of Absorbed Radiation

Figure 3.10 shows significant change in the temperature error with both the amount of absorbed solar radiation and with air temperature. The amount of absorbed solar radiation depends upon environmental factors such as cloud cover, solar angle and aerosol content, as well as the absorptivity of the thermistor. The standard NWS radiosonde has a coating which is specifically utilized because of its low

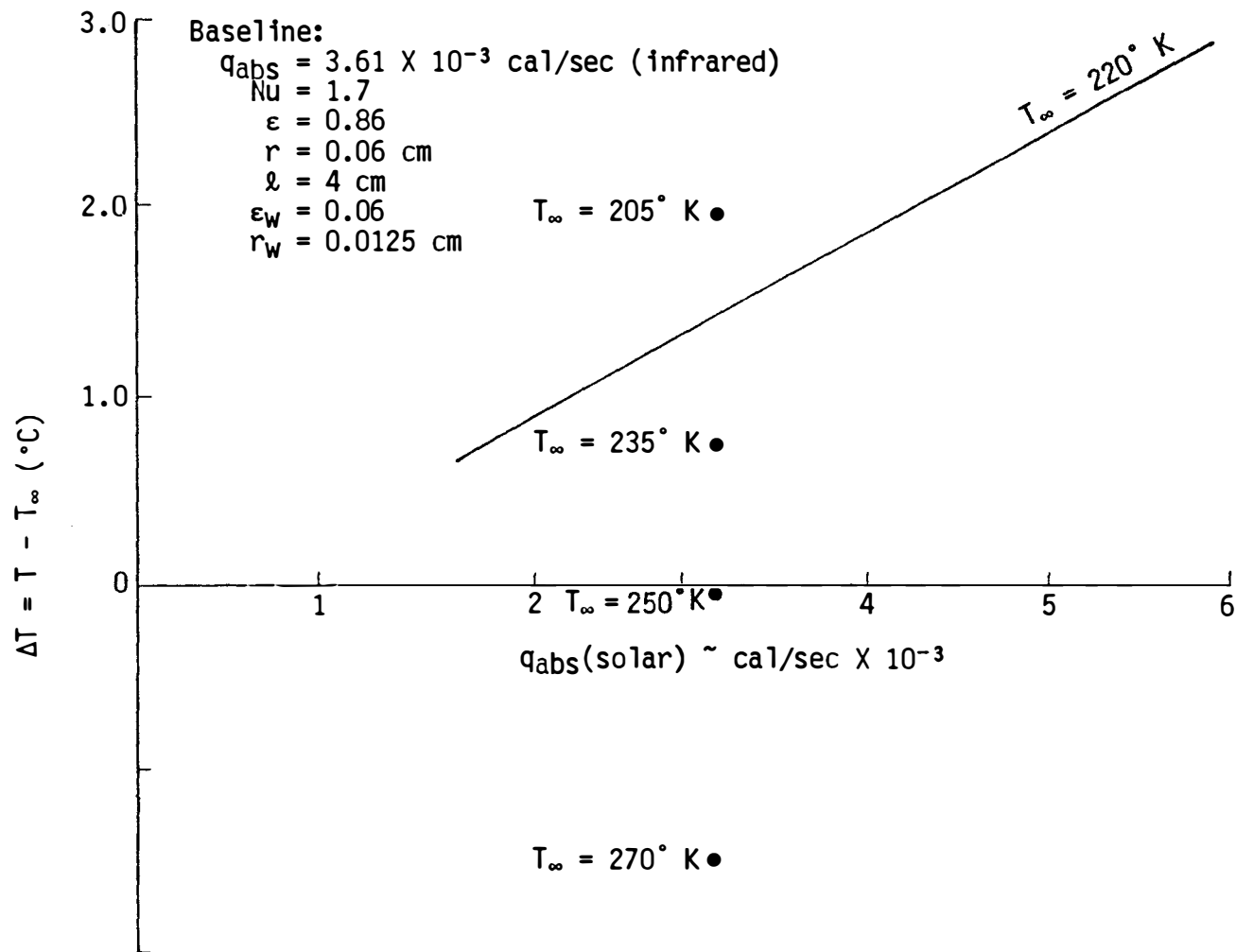


Figure 3.10 Variation in the thermistor temperature error, ΔT , with the amount of solar radiation absorbed by the thermistor at different air temperatures.

absorptivity of solar wavelength radiation. Since the absorbed radiation is directly proportional to absorptivity, thermistors with a highly absorbent coating would increase the amount of absorbed solar radiation by a factor of 5 or even more. According to Figure 3.10, the resulting temperature error would increase by many degrees. As a note of interest, experimental daytime flights using black paint coated thermistors have verified a 5°-10° K increase in the thermistor temperature over that obtained with the standard radiosonde thermistor. For daytime flights, as for nighttime, a change in absorbed radiation at an altitude of 30 Km of 1×10^{-3} cal/sec produces a change of about 0.7° K in the temperature error.

Influence of Solar Angle

The solar zenith angle affects the average amount of radiation impinging on the cylindrical thermistor during a 360° thermistor rotation. The average thermistor irradiation as a function of elevation angle is derived in Appendix 1. Applying this derivation to the solar elevation shows that a 35% decrease in maximum irradiation occurs when going from a solar elevation angle of 90° to 0° (also see Talbot (1972)). A 35% decrease relative to the baseline value of absorbed solar radiation will result in (Figure 3.10) a decrease in ΔT of 0.7° K. This value is consistent with that experimentally derived by MacInturff and Finger (Table 2.1) utilizing day/night temperature differences at varying daytime solar angles.

Influence of Air Temperature

The variation in ΔT with air temperature reflects the ability or inability of the thermistor to dissipate the solar and infrared energy through emission and convection. At very high temperatures, the

infrared energy emitted from the thermistor may even exceed the combined solar and infrared absorption producing a negative temperature error. It must be kept in mind, however, that Figure 3.10 assumes a baseline value of absorbed infrared radiation. Variations from the baseline value move the family of curves in Figure 3.10 upward or downward as appropriate.

Influence of Altitude

Figure 3.11 shows a moderate variation in ΔT with altitude. As with the nighttime case, increased convection decreases the magnitude of ΔT at the lower altitudes. An altitude increase from 15 Km to 30 Km can increase the temperature error by 50%. In general, more variation during a flight would be expected due to changes in the atmospheric temperature profile than due to the influence of altitude or Nusselt number.

Influence of Emissivity

The influence of the emissivity was assessed by holding fixed the radiant energy impinging upon the thermistor at the value corresponding to the baseline conditions, while varying the amount of infrared radiation absorbed and emitted through the emissivity of the thermistor and lead wires. The influence of emissivity on ΔT is depicted in Figure 3.12. As was observed with the nighttime case, the wire emissivity has no measurable influence on the thermistor temperature error. The variation in ΔT with the thermistor emissivity is minimal. The variability in the emissivity of the standard NWS radiosonde thus is not a source of appreciable error.

Influence of Radius and Length

The variation in ΔT due to changes in dimension of the thermistor

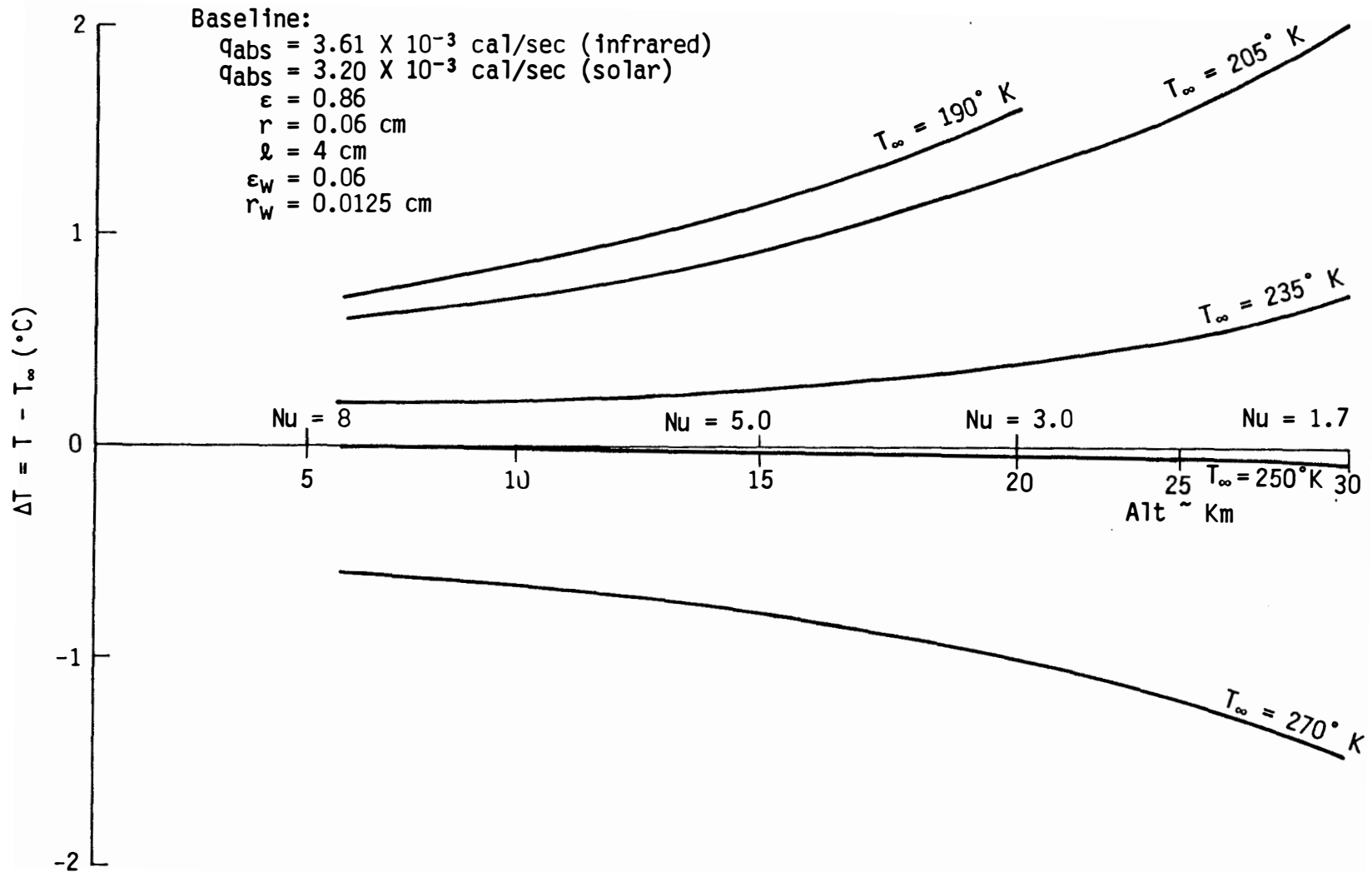


Figure 3.11 Variation in thermistor temperature error with altitude (Nu) and temperature.

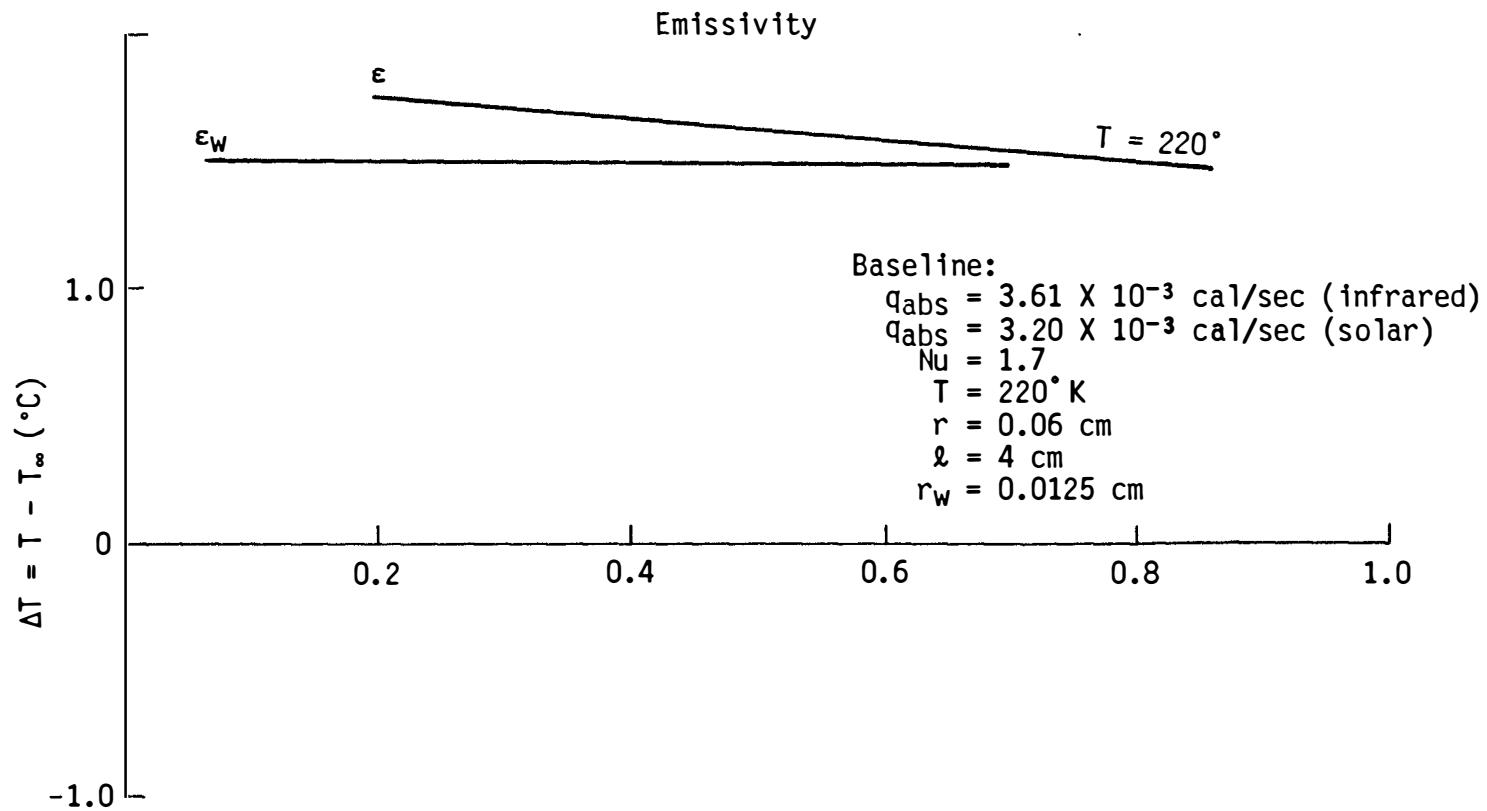


Figure 3.12 Variation in thermistor temperature error with changes in the emissivity of the thermistor and lead wires.

and lead wires were assessed by holding fixed the thermal energy per unit area impinging on the thermistor at the rate associated with the baseline conditions. Changes in thermistor dimensions produced the results shown in Figure 3.13. This figure, which includes the influence of solar radiation, shows a temperature error somewhat larger than for the corresponding nighttime case. This increased magnitude is partially due to the fact that the temperature error itself is of a larger magnitude. Thus, the various terms contribute proportionally more to the temperature error. Nevertheless, from this figure the contribution to ΔT from errors in the dimensions of the thermistor and lead wire would be expected to be less than 0.1°K at 30 Km altitude even when ΔT is large.

3.5.1.3 Conclusions

Results from the sensitivity analysis have provided important information concerning those parameters that significantly influence the radiosonde temperature error. Results were obtained for both daytime and nighttime atmospheric radiation conditions and are summarized as follows.

Nighttime Radiation

- 1) Environmental changes in the infrared radiation budget which can occur due to cloud cover, surface temperature, aerosols and gases can significantly affect the radiosonde temperature error. A 50% change in the radiation budget (which is not unreasonable as shown in Section 3.6) can cause a 1° change in the temperature error.
- 2) The air temperature greatly influences ΔT because the thermistor temperature, which controls the rate of energy dissipated through emissions, remains within a few degrees of the air temperature. A

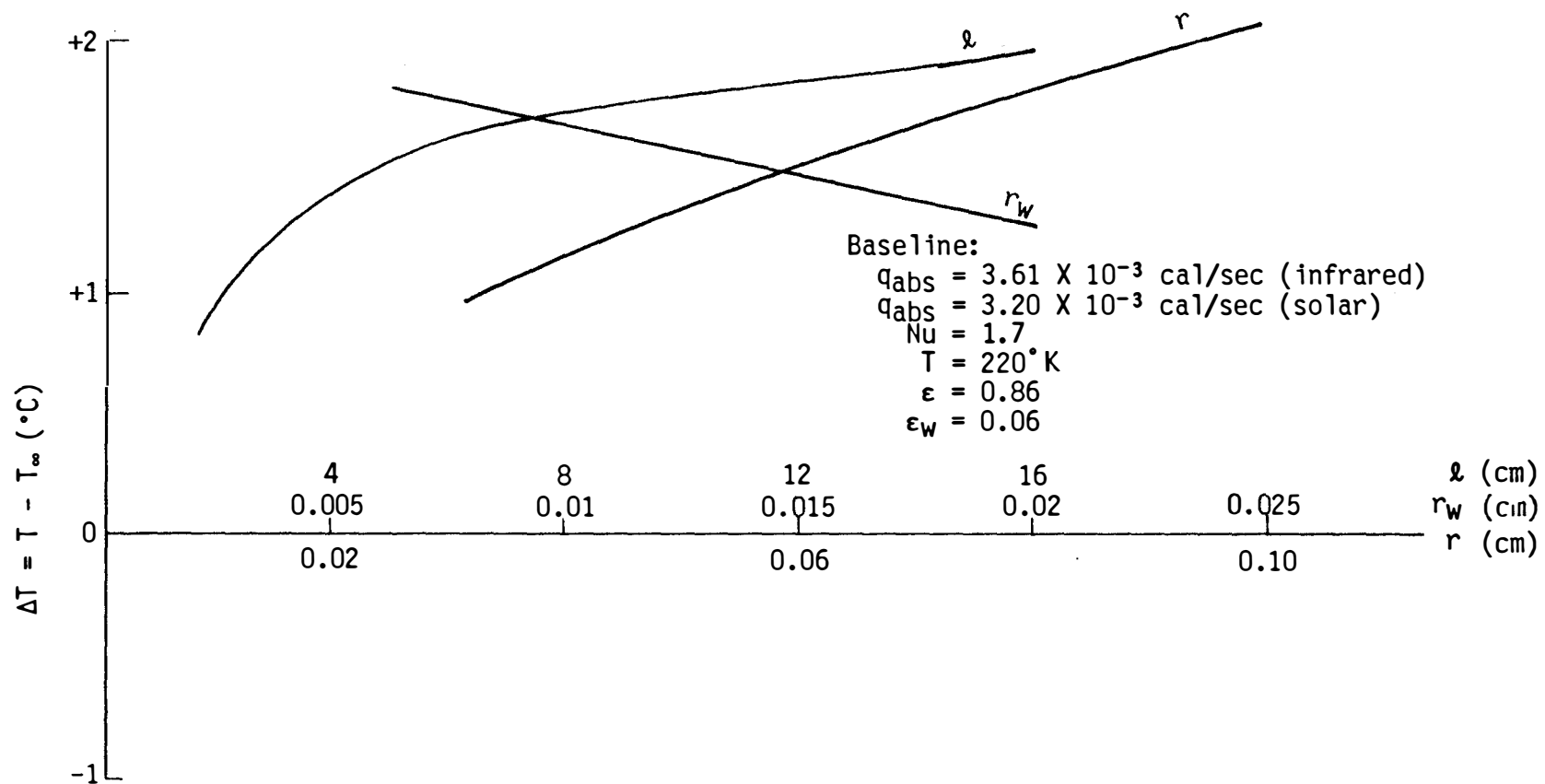


Figure 3.13 Variation in the thermistor temperature error with changes in the radius and length of the thermistor and radius of the lead wires.

change in T_{∞} by 20° K at 30 Km can produce a change in ΔT of 1° K or more.

- 3) The temperature error increases with increased altitude due to a lessening influence of convection. For this reason the temperature error may significantly increase in magnitude between 15 Km and 30 Km.
- 4) Changes in the emissivities of the thermistor and lead wires from their nominal values due to manufacturing processes has no significant influence on ΔT .
- 5) Variation in the dimension of the thermistor and lead wires from their manufacturing specifications does not contribute significantly to the error in ΔT .

Daytime Radiation

Results from varying sensitivity parameters under daytime solar environmental conditions are similar to the nighttime results.

- 1) Environmental changes in the solar radiation budget significantly affect the thermistor temperature error (ΔT). A 50% change in solar irradiation can produce a change in ΔT of 1° K or more.
- 2) Changes in solar elevation angle from 90° to 0° results in a 35% decrease in solar heating of the thermistor. This, in turn, can cause a decrease in ΔT of $\approx 0.7^{\circ}$ K at 30 Km. These results are consistent with the experimental results shown in Table 2.1.
- 3) Changes in air temperature significantly affect ΔT . A 20° K change in T_{∞} at 30 Km produces a change in ΔT of somewhat less than 1° K.
- 4) An increase in altitude produces a larger ΔT because of the lessening influence of convection. An altitude increase from 15 to 30 Km results in increasing ΔT to approximately 1.5 times its 15

Km value.

- 5) The thermistor temperature error is not significantly influenced by variations in the emissivity of the thermistor and lead wires from their nominal values under solar radiation conditions.
- 6) The thermistor temperature error shows some sensitive to changes in the radius of the thermistor and lead wires, and the length of the thermistor. However, the variability of these parameters from their nominal values is not sufficient to cause a change in ΔT of more than 0.1° K .

3.6 Solar and Infrared Irradiation of Radiosonde Thermistor

As previously defined in Section 3.1.1 $I^*(\theta, \phi, \lambda)$ is the radiant intensity of the atmosphere at a given altitude, at wavelength λ in the direction specified by elevation angle, θ , and azimuth, ϕ . The intensity $I^*(\theta, \phi, \lambda)$ includes contributions from solar radiation, both direct and reflected, long-wave emissions from the ground, the clouds, the atmosphere and terrestrial and background radiation from the sky. A model will be utilized that calculates the upward and downward fluxes of atmospheric radiative intensities at altitude levels from the surface to 30 Km -- the maximum height of the radiosonde sensing altitude. The model will utilize environmental input parameters that can be varied so as to vary the radiative fluxes within the range of values experienced in the natural environment. The following sections discuss each of the sources of radiation and the parameters that significantly effect the intensity of radiation between the surface and 30 Km.

3.6.1 Solar Radiation

The spectral distribution of solar irradiation impinging on the top

(≈ 100 Km) of the atmosphere is shown in Figure 3.14. The spectral energy distribution can be approximated to a reasonable degree as that produced by a black body emitting at a temperature of 5900° K. The solar constant is defined to be the total irradiance of the sun, per unit area, in the direction perpendicular to the sun at a distance of one astronomical unit outside of the earth's atmosphere. One astronomical unit is the mean distance between the earth and the sun. At this distance, the sun subtends an arc of 32 minutes or 0.00931 radians. The solar constant is approximately 1396 ± 27 watts per square meter (333.5 cal/sec m^2). Variations in the solar constant seldom exceeds 2% at any time, and over averages of a number of days are considerably less than 1% (Valley 1965). Because of the earth's elliptical orbit around the sun its distance from the sun varies, being the closest in early January and farthest in early July. This variation in distance accounts for a maximum of solar flux impinging upon the top of the atmosphere of approximately 1438 w/ m^2 in January and a minimum to 1345 w/ m^2 in early July.

Over 99% of the total radiant power of the electromagnetic spectrum of the sun is contained between the wavelengths of 0.22 microns and 11 microns. The solar spectrum peaks at a wavelength of 0.48 microns. To reasonably model the intensity of solar radiation, it is sufficient to restrict the wavelengths of interest to $0.25 \leq \lambda \leq 2.5$ microns. Over 96% of the total solar irradiance is contained within this range. Once the solar radiation enters the earth's atmosphere, it is depleted and defused by absorption, scattering and reflections.

3.6.1.1 Absorption of Solar Radiation

Gaseous absorption of solar radiation only becomes significant at

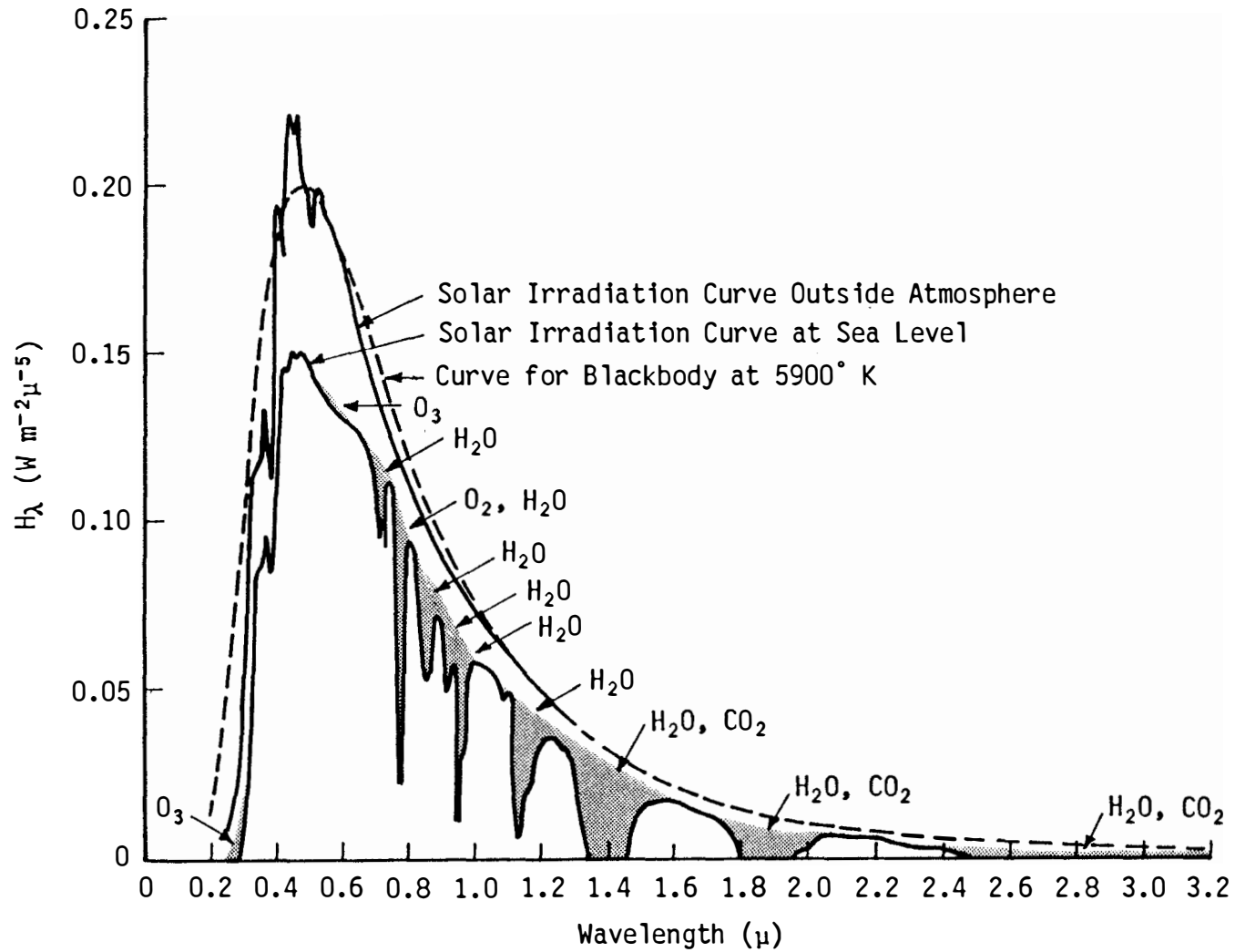


Figure 3.14 Spectral distribution curves related to the sun; shaded areas indicate absorption, at sea level, due to the atmosphere constituents shown (Valley, 1965).

wavelengths greater than 0.7 microns as shown in Figure 3.14. Between 0.7 and 3 microns water vapor, carbon dioxide and oxygen are significant absorbers. Ozone is an efficient absorber below 0.3 microns where the more dangerous ultra-violet rays exist. However, the energy content in the solar spectrum below 0.3 microns makes ozone absorption an insignificant factor in the total irradiation of the radiosonde thermistor.

3.6.1.2 Scattering of Solar Radiation

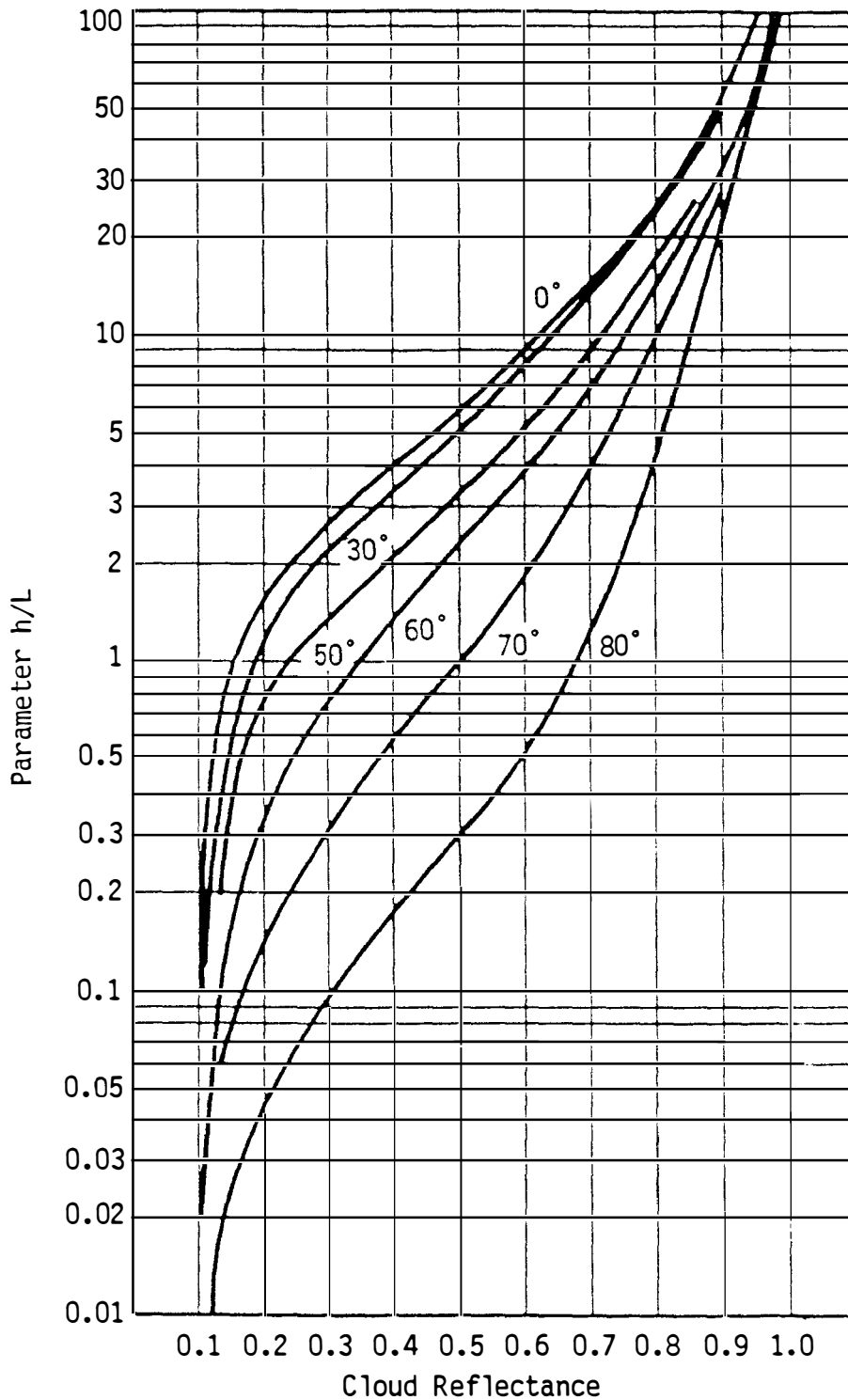
Scattering of solar radiation occurs due to the presence of both air molecules and aerosols (Whitney and Malchow (1977)). Table 3.6 shows an estimate of the annual man-made and natural aerosols entering the atmosphere on a worldwide basis. The loss in radiative intensity at the surface of the earth due to scattering is shown in Figure 3.14 as the difference between the sea level curve and the outside of the atmosphere curve with the shaded area due to absorption. Two types of scattering occur, Rayleigh scattering and Mie scattering. The scattering functions differ considerably between Rayleigh and Mie scattering. The size parameter $\alpha = \frac{2\pi r^*}{\lambda}$ where r^* is the radius of an assumed spherical particle, determines the type of scattering. For Rayleigh scattering the size parameter is less than 1 indicating the scatters are of a dimension smaller than the wavelength of the radiation. Air molecules are a significant source of Rayleigh scattering. For Mie scattering, the size parameter takes on a value in excess of 2. Aerosols, dust, and cloud particles are major sources of Mie scattering. For solar radiation, at wavelength less than 0.4 microns and at altitudes above the earth's aerosol contaminated regions, Rayleigh scattering generally predominates. At altitudes less

Table 3.6 Estimates of Particles Smaller Than 20 μm Radius Emitted Into or Formed in the Atmosphere (10^6 Metric Tons/Year) (From Valley (1965))

Natural	
Soil and rock debris*	100 - 500
Forest fires and slash-burning debris*	3 - 150
Sea salt	300
Volcanic debris	25 - 150
Particles formed from gaseous emissions:	
Sulfate from H_2S	130 - 200
Ammonium salts from NH_3	80 - 270
Nitrate from NO_x	60 - 430
Hydrocarbons from plant exudations	75 - 200
Subtotal	773 - 2200
Man-made	
Particles (direct emissions)	10 - 90
Particles formed from gaseous emissions:	
Sulfate from SO_2	130 - 200
Nitrate from NO_x	30 - 35
Hydrocarbons	15 - 90
Subtotal	185 - 415
Total	958 - 2615

than a few kilometers in the aerosol layer, Mie scattering predominates. Severe Mie scattering occurs with clouds. Because cloud size droplets are in the range of a few microns to 30-40 microns, they scatter solar radiation as large particles relative to solar wavelength. Because of their thickness, clouds can reflect by scattering up to nearly 100% of incoming solar radiation (see Figure 3.15).

The modeling of Rayleigh and Mie scattering requires the choice of appropriate scattering functions which describe the probability density distribution of the reflection angle relative to the direction of incoming radiation. In addition to determining the appropriate



h: Cloud Thickness
 L: Mean Free Path Length of a Light Ray

Figure 3.15 Variation in reflectance as a function of cloud thickness parameter h/L for different solar zenith angles (Valley, 1965).

scattering functions, the number and size of scattering particles must be known. For molecular scattering, the atmospheric density and composition provide this information. For Mie scattering aerosol number, density and a characteristic dimension must be known. This information allows the definition of a scattering coefficient for Rayleigh and Mie scattering as a function of wavelength. Scattering coefficients for Rayleigh and Mie scattering, specified in terms of these parameters, are utilized in the LOWTRAN 6 code.

3.6.1.3 Reflection of Solar Radiation

Solar radiation impinging upon a radiosonde thermistor may come along a direct path from the sun with part of it being absorbed or scattered by the intervening atmosphere. Other radiation may reach the thermistor as a result of scattering off of aerosol particles or molecules. Still other radiation may be reflected off of the earth's surface or clouds to the thermistor. This third type requires further discussion. The probability of a ray reflection can be close to 0 or as high as nearly 1, depending upon the type of surface on the earth. The probability of reflection depends upon the nature of the surface and the wavelength of the radiation. A water surface is generally a poor reflector (Figure 3.16) over most (solar) wavelengths between 0.4 and 0.85 microns reflecting 15% or less of the incoming radiation. Snow reflects between 60% and 80% of radiation in this spectral band (Choudhury and Chang (1981)) depending upon the age and density of the snow (Figure 3.17). Bare soil reflects less than 25% over most wavelengths as also shown in Figure 3.17. Vegetation covered ground reflects less than 20% for $\lambda < 0.6 \mu$ while reflecting up to 50% or more as the wavelength increases (Figure 3.18).

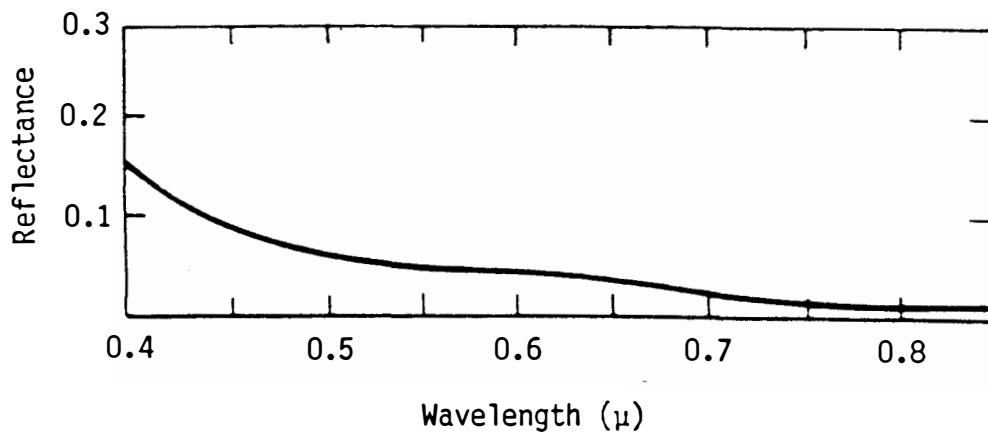


Figure 3.16 Spectral reflectance for water surfaces (Valley, 1965).

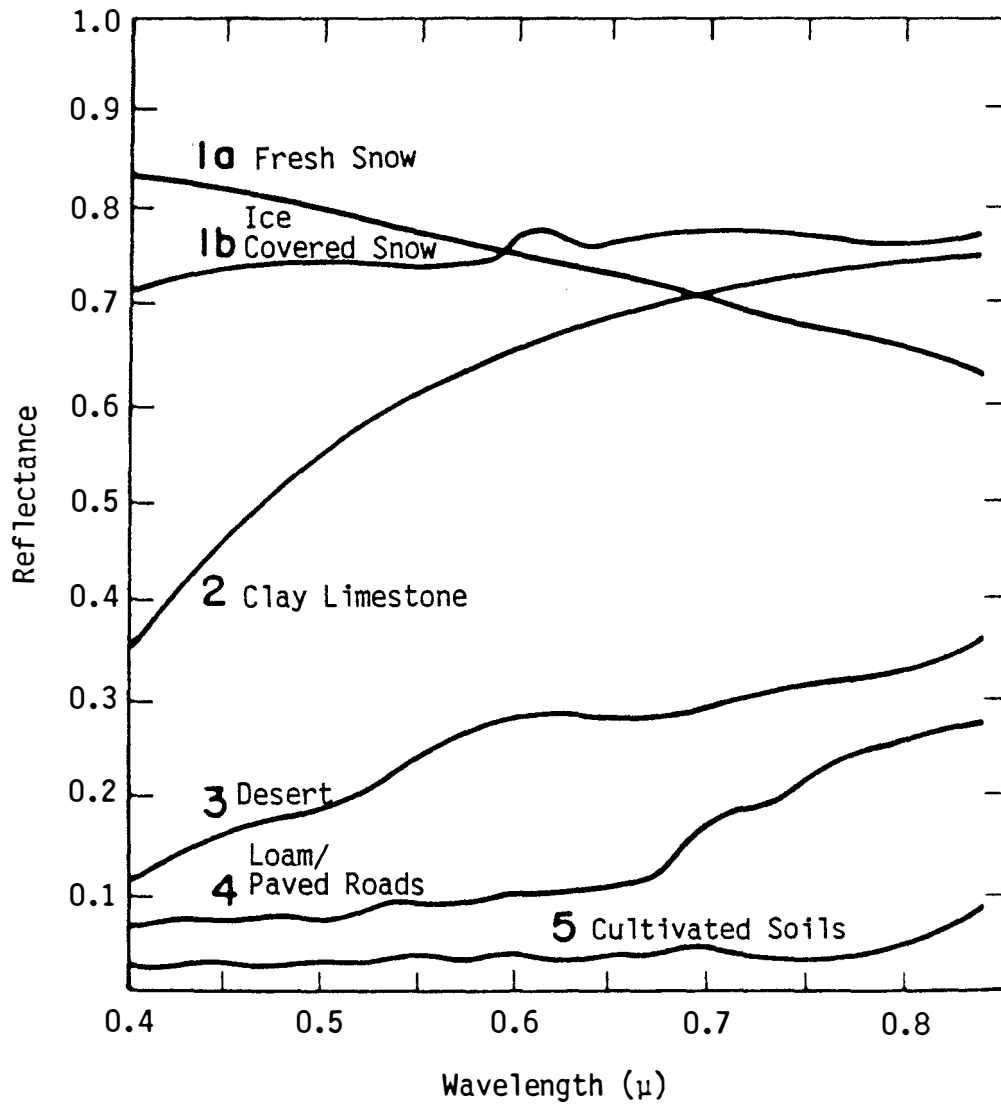


Figure 3.17 Spectral reflectance for snow and bare soils (Valley, 1965).

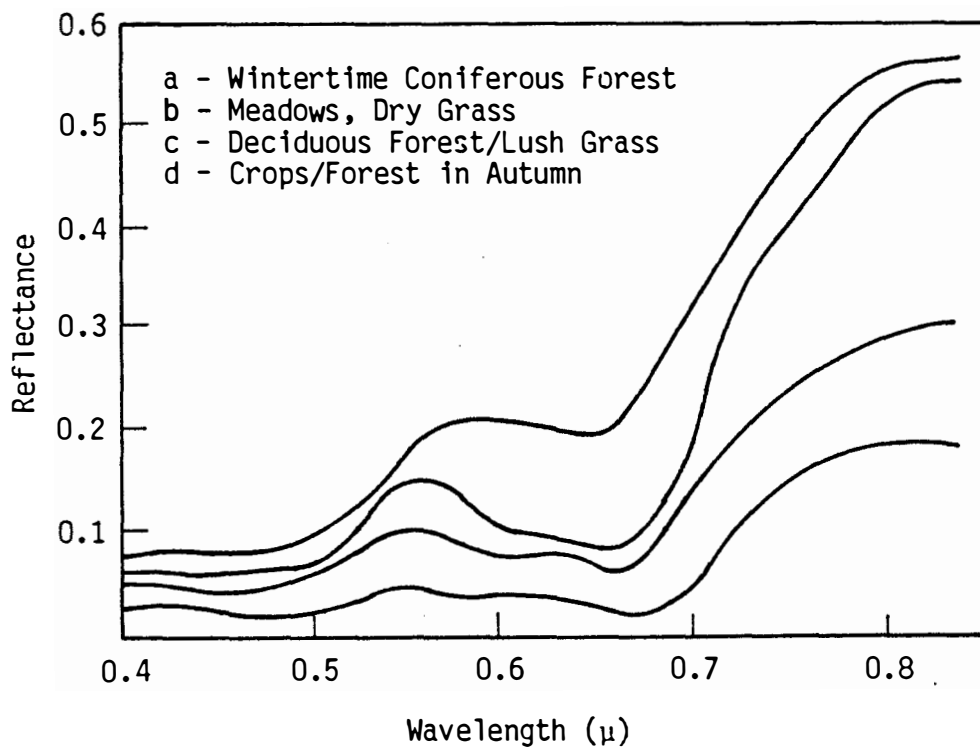


Figure 3.18 Spectral reflectance for vegative formation (Valley, 1965).

In summary, to model the solar radiant intensity of the atmosphere, the following environmental conditions which occur nonuniformly in nature must be considered. These conditions are specified in the input to the LOWTRAN 6 code.

- (a) The amount of water vapor and carbon dioxide in the atmosphere because of their absorption properties for wavelengths between 0.7 and 3.0 microns.
- (b) The number density and size distribution of both man-made and natural aerosols, including clouds because of their predominate role in Mie scattering. For Rayleigh scattering the atmosphere composition is considered invariant so that the size parameter for the molecules is constant. However, the variation in atmospheric density with altitude must be included to account for the variation in the number density of scatterers.
- (c) Surface properties of the ground, because of the range of reflection coefficients for different types of surfaces.

3.6.2 Non-Solar Radiation

In addition to the direct, scattered, and reflected solar radiation, radiation from other sources is also present in the atmosphere. At nighttime these radiation sources predominate. The major sources of non-solar radiation are emissions from the earth's surface, emissions from clouds, and emissions from gaseous constituents of the atmosphere especially carbon dioxide and water vapor. The radiation from the non-gaseous sources have a spectrum that peaks in the infrared region and is closely related to the temperature of the emitting substance. The non-gaseous sources, including the ground surface and cloud particles, can be considered as gray body emitters

that emit as a continuous spectrum depending only on the temperature and emissivity of the surface or cloud particles. The temperature range for an emitting surface may vary from 200° K for tropical clouds, and very cold arctic ice fields to 310° K for desert sands. The emissivity values for various surfaces is shown in Table 3.7 (Sutherland and Bartholic (1977), and Valley (1965)). Experimental measurements indicate that dense clouds emit as black bodies at the cloud top temperature with an emissivity approximately equal to 1. Cirrus clouds, which often do not provide an optically dense path, also emit at the temperature of the cloud top, but will also allow radiation from the surface to penetrate through the cloud region providing a combination of radiative fluxes from two surfaces.

Table 3.7 Emissivity of Various Surfaces

Surface	Emissivity
Water	$\epsilon = 0.96$
Bare Ground	$\epsilon = 0.93$
Vegetation	$\epsilon = 0.98$
Ice	$\epsilon = 0.97$
Snow	$\epsilon = 0.82$
Clouds	$\epsilon = 0.95-1.00$

Diatomic atmospheric gases absorb and emit in narrow spectral bands, dictated by their vibrational and rotational modes of quantum energy transfer. Gases, in general, emit and absorb energy at the same wavelengths. Figure 3.19 shows the spectral absorption of energy for various atmospheric gases as a function of wavelength from 1 to 15 microns. Of over-riding significance are the water vapor absorption bands, especially the bands centered around 1.9, 2.7 and 6.3 microns; the carbon dioxide absorption bands at 2.7, 4.3 and 15.0 microns; and to a lesser degree, the ozone absorption at 9.5 microns. Nitrogen and oxygen, the main gaseous constituents of the atmosphere, are transparent to radiation over the entire spectral range of interest.

The atmosphere both emits radiation over the various spectral bands, as well as absorbs radiation from the ground and clouds over the same spectral bands. The cumulative effect of emission and absorption over a spectral band depends upon the temperature of the emitting gaseous constituent, as well as the intensity and wavelength of radiation being absorbed by the gas.

In summary, the total nonsolar irradiation of a thermistor from the ground surface, clouds, and atmospheric gases requires the utilization of a model which simulates the radiative interaction of the various layers of the atmosphere taking into account scattering, absorption, and gaseous emissions.

3.6.3 The LOWTRAN 6 Atmospheric Propagation Program

The LOWTRAN 6 atmospheric transmission and radiance model is the 1983 derivative of a series of models developed by the Air Force Geophysics Laboratory (Kneizys, et al. (1983)). LOWTRAN 6 calculates atmospheric transmission and radiance in intervals of 20 cm^{-1}

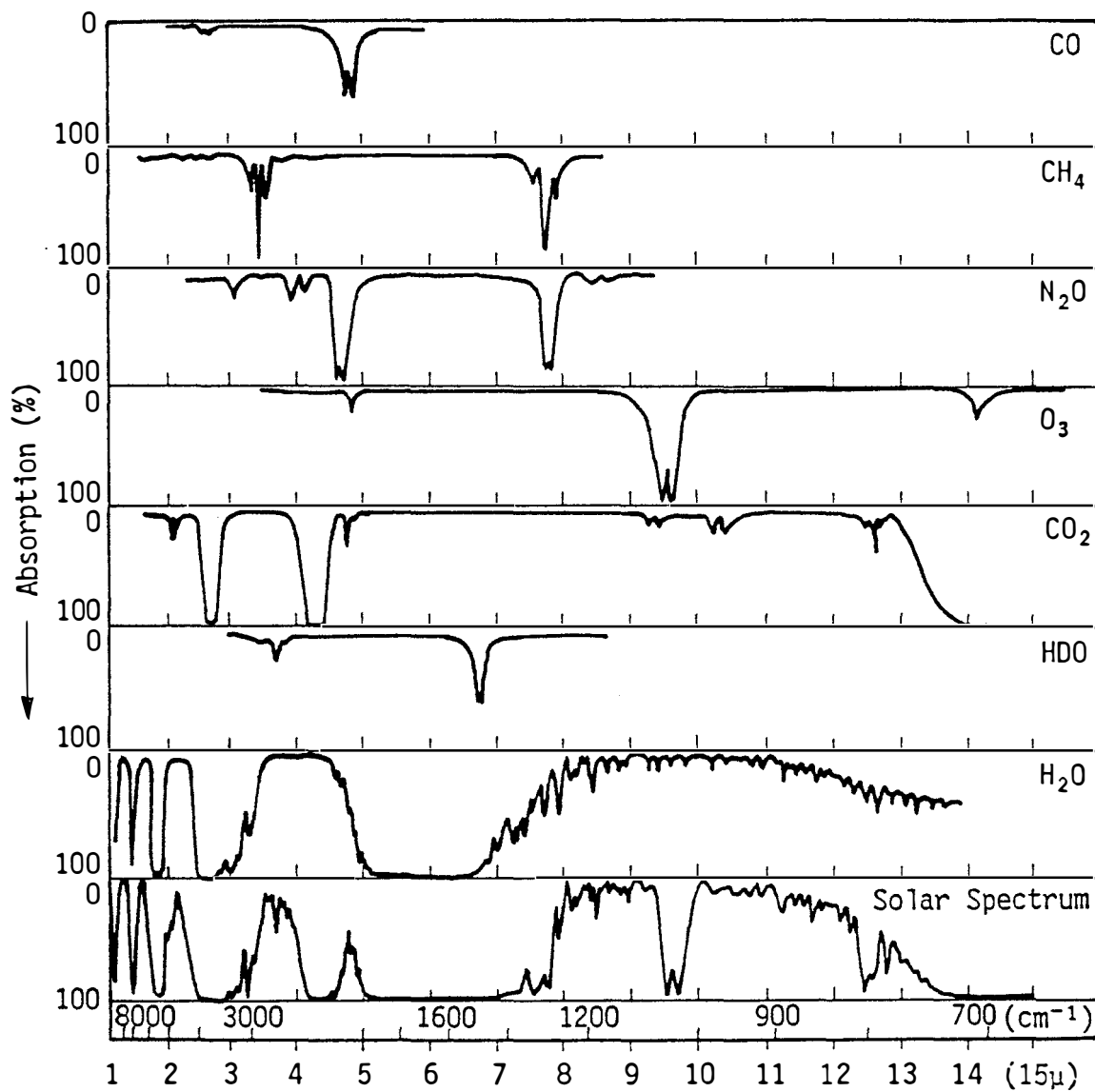


Figure 3.19 Comparison of the near infrared solar spectrum with laboratory spectra of various atmospheric gases (Valley, 1965).

wavenumbers over a wavenumber range from 350 to 40,000 corresponding to wavelengths $0.25 \leq \lambda \leq 28.5 \mu$. When used to calculate atmospheric radiance, LOWTRAN 6 provides calculations of radiant intensity at any altitude in units of watts per cm^2 per steradian along any line of sight direction (θ, ϕ) . LOWTRAN 6 is an extension and improvement of earlier versions of the LOWTRAN (Kneizys, et al. (1980), and Selby, et al. (1972, 1975, 1978)) series. It allows the calculation of atmospheric and ground emissions, direct solar radiance and single scattered solar radiance at any altitude and in any direction.

The LOWTRAN 6 model is a 33-layer spherical earth model with altitude layers defined from the surface to 100 Km. The model allows various options for defining atmospheric properties and gaseous constituents. Figure 3.20 illustrates the various choices of intrinsic LOWTRAN 6 models to define atmospheric temperature, pressure, (U.S. Standard Atmospheric Supplements (1966)), ozone, water vapor, tropospheric and stratospheric aerosol profiles. The model allows user defined boundary conditions for specification of ground temperature and a wavelength dependent ground albedo. Cloud properties can be used to define a lower or upper boundary cloud condition.

The radiance and/or transmission calculated in LOWTRAN 6 takes into account atmospheric molecular absorption, molecular scattering, aerosol extinction, and continuum absorption. Molecular absorption accounts for the absorbing influence of the vertical profiles of water vapor, ozone, nitric acid and other gases; CO_2 , N_2O , CH_4 , CO , O_2 and N_2 , that are assumed to be uniformly mixed throughout the atmosphere. A single parameter transmittance function is used to calculate absorption and scattering through each layer of the atmosphere for a given path

Atmospheric, Ozone, and Water Vapor Models:

Tropical Model Atmosphere

Mid-Latitude Summer

Mid-Latitude Winter

Sub-Artic Summer

Sub-Artic Winter

1962 U.S. Standard

Tropospheric Aerosol Models:

Rural Extinction, default VIS = 23 Km (visibility)

Rural Extinction, default VIS = 5 Km

Navy Maritime Extinction, sets own VIS

Maritime Extinction, default VIS = 23 Km (LOWTRAN 5 Model)

Urban Extinction, default VIS = 5 Km

Tropospheric Extinction, default VIS = 50 Km

User-Defined Extinction, default VIS = 23 Km

FOG1 (advection fog) Extinction, default VIS = 0.2 Km

FOG2 (radiation fog) Extinction, default VIS = 0.5 Km

Seasonal aerosol profile for each of the above:

Spring-Summer

Fall-Winter

Stratospheric Aerosol Models:

Background Stratospheric profile and extinction

Moderate Volcanic profile and Aged Volcanic extinction

High Volcanic profile and Fresh Volcanic extinction

High Volcanic profile and Aged Volcanic extinction

Moderate Volcanic profile and Fresh Volcanic extinction

Figure 3.20 Atmospheric profiles available in LOWTRAN 6.

length. The transmittance function can be written as $\tau = f(C_v \rho DS)$ where f is an empirically derived function, C_v is an empirically derived absorption coefficient for each absorber, ρ is the absorber density, and DS is the path length. The absorber density ρ is expressed as a function of pressure, temperature, the concentration of the absorber and an empirical constant. The total transmittance through a layer is then derived as the product of the transmission due to molecular absorption, molecular scattering, aerosol extinction and continuum absorption.

Atmospheric radiance is calculated from the numerical integration of the integral form of the equation of radiative transfer (Buglia (1986)). Extensive details about the development, capabilities and utilization of LOWTRAN 6 and other LOWTRAN codes are provided in Kneitzky, et al. (1980, 1983), and Selby, et al. (1972, 1975, 1976, 1978). LOWTRAN 6 has gained wide acceptance in the electro-optical and atmospheric propagation communities because of its computation speed, accuracy, flexibility, documentation and validation. The overall accuracy of the model is greater than 10%. It has been used extensively by government laboratories, private industries, and research organizations for calculating absorption and scattering of radiation transmitted through the atmosphere for both passive and active infrared and optical wavelength sensors. Other models have been reviewed before choosing LOWTRAN 6 (Suckling (1976, 1977), Babaro, et al. (1979), Hooper and Brunger (1980), Ideriah (1981), Hering and Johnson (1984)), but none possess all the advantages inherent in the LOWTRAN 6 model.

Several features available with LOWTRAN 6 makes it attractive for use in calculating the irradiance of the radiosonde thermistor by solar and infrared radiation under differing environmental conditions. Because LOWTRAN 6 allows the user to: a) chose from a menu of constituent, aerosol, and thermodynamic profiles; b) to specify the boundary conditions; and c) to define appropriate solar irradiance and scattering parameters, most environmental situations that commonly occur in nature can be approximated. Figure 3.21 summarizes the radiative properties utilized in LOWTRAN 6 and the input parameters used in specifying the radiation scenario. The following section describes the method used in calculating the heating of the radiosonde thermistor by utilizing results from LOWTRAN 6 computer runs.

3.6.3.1 Utilization of LOWTRAN 6 to Estimate Irradiance and Heating of the Radiosonde Thermistor

LOWTRAN 6 output provides a calculation of the radiance impinging upon an object at a specified altitude from a specified "look" direction (θ , ϕ). The radiant intensity is calculated in units of watts per cm^2 per steradian for a λ specified band of wavelengths. Calculation of the total irradiance of the thermistor requires the integration of a large number of intensity values arriving from all spherical directions for all wavelength bands of interest. The method used in calculating the heating rate of the thermistor from LOWTRAN 6 output differs slightly between daylight and nighttime conditions because of solar radiation. Figure 3.22 summarizes the technique for both conditions and is explained below. The technique assumes the thermistor is exposed only to atmospheric radiation and does not take into account the reflection and emission of radiation from the balloon

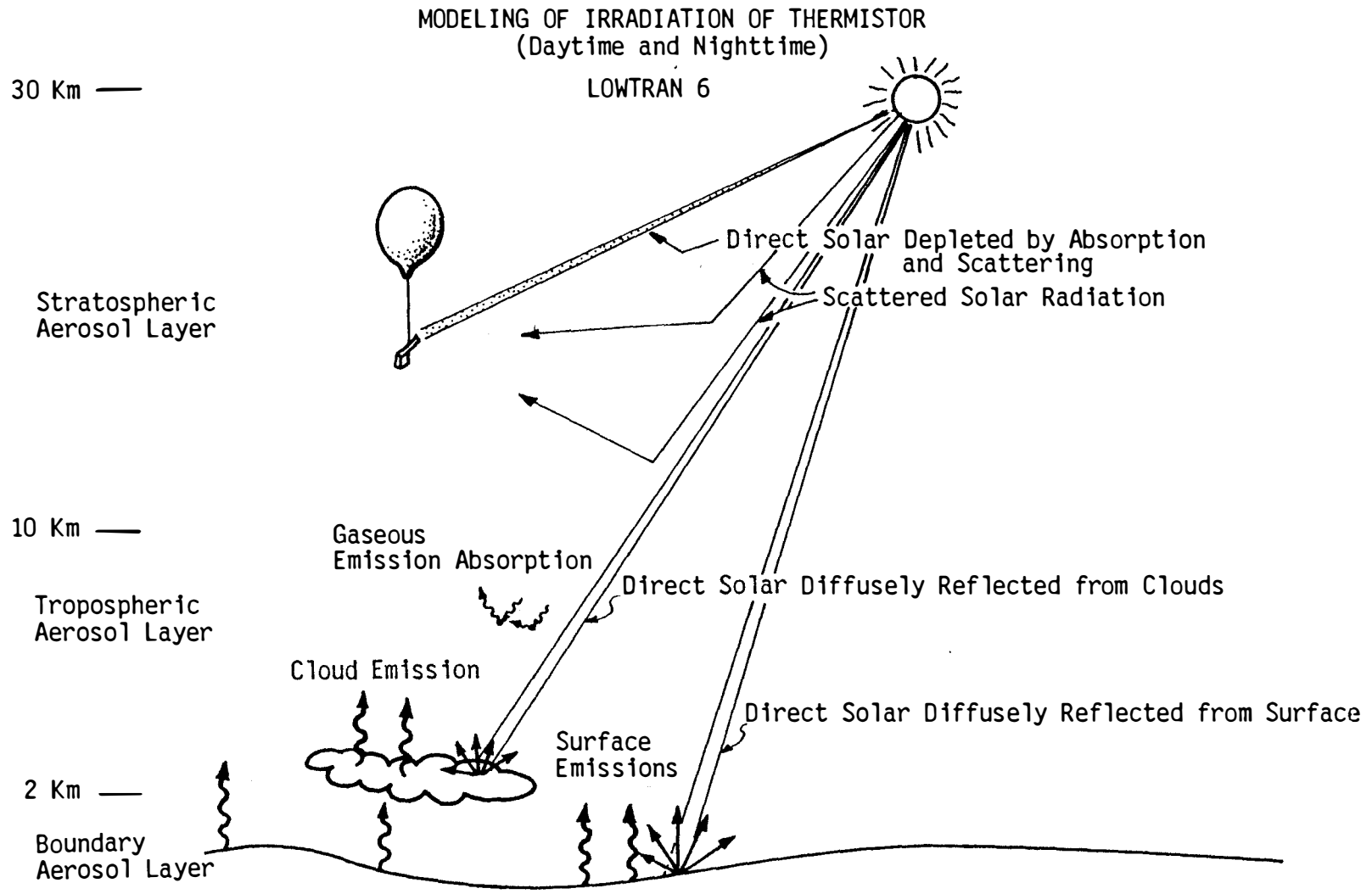


Figure 3.21 LOWTRAN Input: Aerosol profiles, solar elevation, lower boundary properties.

$$Q_{\text{abs}} = \int_{\lambda=0.25}^{40} \alpha(\lambda) \int_{\phi=0}^{2\pi} \int_{\theta=0}^{\pi} \bar{A}_p(\theta) I(\theta, \phi, \lambda) d\Omega d\lambda = \begin{cases} \sum_{j=1}^5 \alpha(\lambda_j) \sum_{i=1}^7 \bar{A}_p(\theta_i) I(\lambda_j, \theta_i) \Delta\Omega_i & \text{(NIGHT)} \\ \sum_{j=1}^5 \alpha(\lambda_j) \sum_{i=1}^7 \bar{A}_p(\theta_i) \sum_{k=1}^{12} I(\lambda_j, \theta_i, \phi_k) \frac{\Delta\Omega_i}{12} & \text{(DAY)} \end{cases}$$

Where:

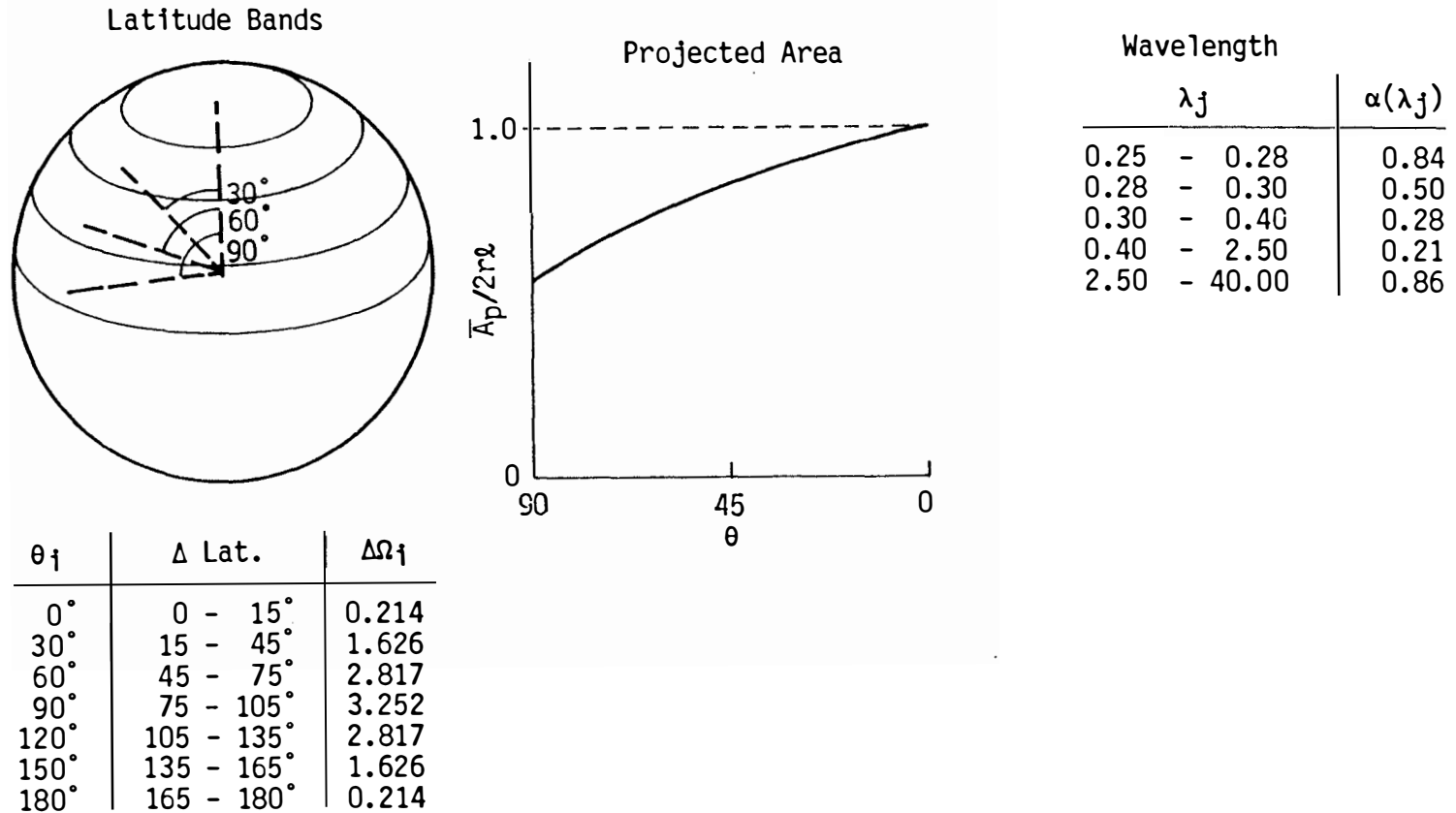


Figure 3.22 Method of calculating radiation absorbed by thermistor.

and radiosonde surfaces. Appendices 4 and 5 validate this assumption by calculating the magnitude of the balloon and radiosonde influences.

Consider first nighttime calculations. In the absence of solar radiation, the radiant intensity impinging upon an object can be considered independent of azimuthal direction. Thus, using Equation 3.5 to calculate q_{abs} (see Figure 3.22) the intensity is only a function of λ and θ . Consequently, the LOWTRAN 6 program need only generate radiances for variations in the elevation angle θ . The nighttime procedure is as follows.

- o A set of values of elevation angle, θ , is chosen based on previous studies with LOWTRAN 6 so as to quantify the variation in atmospheric radiance with elevation angle. The values used are: $\theta = 0, 30, 60, 90, 120, 150, 180^\circ$.
- o These elevation angles are used to decompose all spherical directions into bands of latitude (see Figure 3.22). The dividing lines are at latitudes of $\theta = 15, 45, 75, 105, 135,$ and 165° . The steradian content of each latitude band is calculated in Appendix 3 and designated as Ω_θ . The LOWTRAN 6 derived radiant intensity at the mid-latitude elevation angle is assigned as the value for the entire band.
- o Appropriate wavelength bands are defined (between 0.25 and 40.0 microns) such that the thermistor and lead wire absorptivity over each band can be approximated as a constant. Using absorptivity and emissivity properties given in Figure 3.4 and Table 3.1, the following five wavelength bands and absorptivity values were selected.

$\Delta\lambda(\mu)$	$\alpha(\Delta\lambda)$	$\alpha_w(\Delta\lambda)$
0.25 - 0.28	0.84	0.08
0.28 - 0.303	0.56	0.08
0.30 - 0.40	0.28	0.08
0.40 - 2.50	0.21	0.08
2.50 - 40.00	0.86	0.06

- o The LOWTRAN 6 code is executed at a given thermistor altitude, with specified environmental conditions for each elevation angle representing the mid-elevation of a latitude band. In running LOWTRAN 6, the five wavelength bands are specified so as to provide $I(\lambda_j, \theta_i)$ output over each wavelength band for each elevation angle.
- o The radiant intensity $I(\lambda_j, \theta_i)$ at the mid-elevation, θ_i , of latitude band (i), is then multiplied by the steradian content of that band ($\Delta\Omega_i$), and the average projected area of the thermistor $\bar{A}_p(\theta_i)$ as viewed from the elevation angle θ_i . This calculation provides the energy impinging upon the thermistor from the given latitude band over the wavelength interval λ_j . The azimuthally averaged thermistor projected area, $\bar{A}_p(\theta_i)$, and is derived in Appendix 1.
- o The rate of heat transfer to the thermistor is then calculated using the "night" equation of Figure 3.22 as the sum (integral) over the seven latitude bands (i), and five wavelength bands (j), of the energy impinging on the thermistor (per wavelength band, per latitude band) times the thermistor absorptivity for that wavelength band. A similar calculation is performed for the rate of heat transfer to the

lead wire per unit length.

For daytime calculations both direct and scattered solar radiation must be taken into consideration. Scattered solar radiation is azimuthally dependent. Consequently, LOWTRAN 6 radiance calculations must be made for appropriate values of azimuth angle, as well as elevation angle. Because of azimuthal symmetry about the solar reference azimuth, $\phi = 0$, only variations between $\phi = 0$ and $\phi = 180^\circ$ need be calculated. The influence of scattered solar radiance requires azimuthal integration for the calculation of q_{abs} . The integration is performed by dividing each latitude band into twelve azimuth (longitudinal) segments of $\Delta\phi = 30^\circ$. The heat transfer rate for each segment is the product of $I(\theta, \phi, \lambda)$ for that segment, times $1/12$ the solid angle $\Delta\Omega$ for that latitude band, times the appropriate projected area and absorptivity. The heat transfer rate is then summed over all segments, all latitude bands, and all wavelengths as delineated by the "day" equation in Figure 3.22.

The direct solar radiance is also provided from LOWTRAN 6 output as a function of solar elevation angle and wavelength band. The rate of thermistor heating due to direct solar radiation is calculated by performing a similar integration, taking into account $\bar{A}_p(\theta)$ and $\alpha(\lambda)$. The remaining procedure for calculating the daytime irradiation of the radiosonde thermistor is identical to that used for nighttime calculations.

3.6.3.2 Sensitivity of Atmospheric Parameters to Radiation Absorbed by Thermistor

The LOWTRAN 6 input parameters that define the atmospheric profiles and the boundary conditions affect the amount of radiation absorbed by

the thermistor. Several LOWTRAN 6 computer runs have been made by varying input parameters to establish the influence of each parameter on the radiation absorbed by the thermistor. A baseline set of input conditions from which variations in individual parameters were made is shown in Figure 3.23. The baseline was established for the 30 Km altitude region because it is the upper altitude range of the radiosonde system and, because in this altitude region, the temperature error was expected to be largest. The baseline parameters were chosen so as to be representative of conditions that occur during the summer at Wallops Island, VA, the launch site of two series of experimental radiosondes that provided direct measurement of the radiosonde temperature error. The parameters that were varied from the baseline values include altitude, the surface temperature and albedo, cloud cover, seasonal change from summer to winter temperature/constituent profiles, and a low visibility urban aerosol profile in place of the high visibility rural profile.

3.6.3.2.1 Nighttime Radiation

Results from the sensitivity analyses for nighttime radiation conditions are shown in Figure 3.24 for selective conditions as identified by the open circles. Several interesting conclusions can be drawn from inspection of this figure.

- o Above 20 Km there is essentially no change in the infrared radiation absorbed by the thermistor. The atmospheric constituents and aerosols present in this altitude region are transparent to infrared radiation. Below 20 Km, the irradiation of the thermistor increases gradually with decreased altitude until near 10 Km, a more rapid increase

Mid-Latitude Standard Atmosphere Summer Profiles:

Temperature

Pressure

Water Vapor

Ozone

Aerosol Profiles (Summer):

Rural, VIS = 5 Km (troposphere)

Background (stratospheric)

Surface Boundary Temp. = 300° K (no clouds)

Surface Albedo = 0.05 for all wavelengths (no clouds)

Altitude = 30 Km

Figure 3.23 Baseline input parameters for LOWTRAN 6.

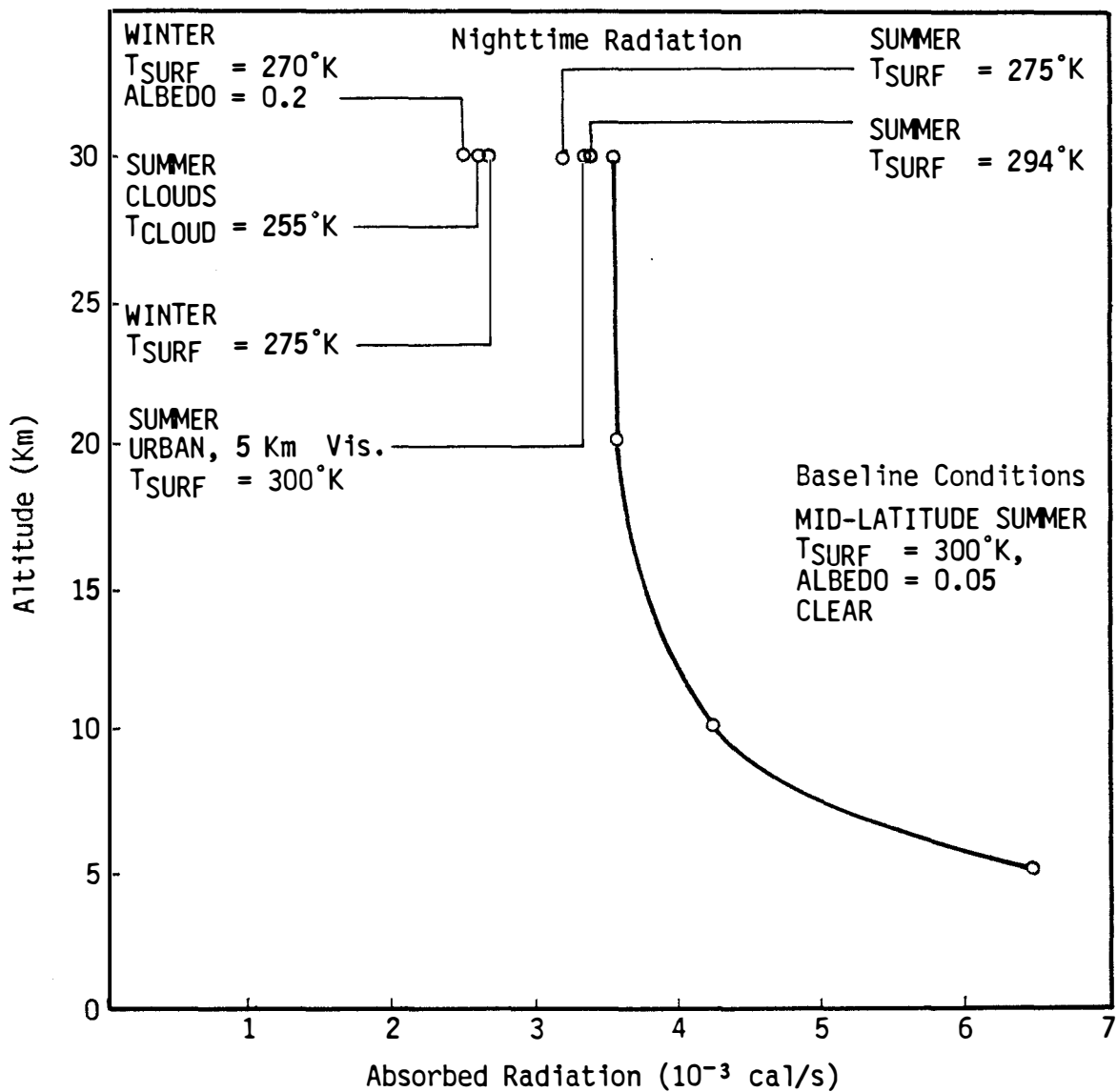


Figure 3.24 Nighttime radiation absorbed by thermistor under different environmental conditions.

begins. At 5 Km the thermistor absorbs nearly twice the infrared radiation absorbed at 30 Km.

- o A decrease in surface temperature of 25° K from the mid-latitude baseline surface temperature of 300 K results in a decrease in absorbed energy of approximately 0.4×10^{-3} cal/sec at 30 Km. Referring to the slope of the curve in Figure 3.6, this would produce a change in the radiosonde temperature error of 0.25° K.
- o A change from the mid-latitude summer profiles to the mid-latitude winter profiles decrease the absorbed radiation by 0.9×10^{-3} cal/sec. This includes a surface temperature reduction of 25° K. If the same summer and winter surface temperatures were assumed, a difference of only 0.5×10^{-3} cal/sec would occur. Thus, at 30 Km the change from an average summer to an average winter surface temperature changes ΔT by approximately -0.3° K whereas a change in the atmospheric constituent, aerosol and thermodynamic profiles, produces an additional change of approximately -0.2° K in ΔT for the winter profiles.
- o Winter snow cover, simulated by decreasing the surface emissivity from 0.95 to approximately 0.8 (see Table 3.7), produces only a small change in the radiation absorbed by the thermistor and is not a significant contributor to the radiosonde temperature error.
- o Summer cloud cover with cold cloud tops emitting at perhaps 255° K significantly decreases the radiation absorbed by the thermistor. A decrease of nearly 1×10^{-3} cal/sec occurs

between a cloudy and clear summer night which produces a change in the radiosonde temperature error of about -0.7° K (see Figure 3.6).

- o A change in the tropospheric aerosol profiles from a high visibility (25 Km) rural profile to a low visibility (5 Km) urban profile produces a small decrease in the radiation absorbed by the thermistor. However, the resulting contribution to the radiosonde temperature error is on the order of one tenth of a degree Kelvin.

From the above analysis we conclude that for a nighttime flight, the parameters having greatest influence on the amount of radiation absorbed by the thermistor and thus the radiosonde temperature error are: the surface temperature (in the absence of clouds), the cloud cover, the seasonal variation in the background atmospheric profiles; and below 20 Km a strong dependence on altitude.

3.6.3.2.2 Daytime Radiation

During the day the thermistor absorbs: a) infrared radiation from the ground and atmosphere; b) direct solar radiation from the sun; and c) scattered solar radiation off clouds, aerosols, molecules and the surface. The infrared irradiation of the thermistor during the daytime does not significantly differ from that occurring during the night, except for minor influences produced by changes in surface temperature and perhaps slight changes in the background atmospheric profiles. Therefore, the previous analysis performed for nighttime infrared radiation is also valid for the infrared component of daytime radiation.

The amount of direct solar radiation absorbed by the thermistor depends upon the solar elevation angle for two reasons. At low solar elevations the average cross-sectional area of the cylindrical thermistor exposed to radiation is less than at high solar elevation angles where a downward view exposes nearly half of the thermistor to direct solar radiation at all times. (Only at solar elevation angles exceeding 70° does the balloon shield the thermistor from direct sunlight. This case is not considered because U.S. radiosonde stations do not experience solar elevation angles exceeding 70° .) Appendix 1 derives the magnitude of this solar angle effect as a function of solar elevation angle. Based upon this analysis, a decrease of 35% in solar radiation incident on the thermistor occurs in going from a solar elevation of 90° to 0° .

A second influence of solar angle on the heating of the thermistor occurs because of the extended path length of radiation through the atmosphere as the solar elevation angle decreases. At altitudes above 20 Km this influence is minor because of the minimal absorbing and scattering constituents in the atmosphere (Jursa (1985)). However, when the radiosonde is at low altitudes, imbedded in aerosol and gaseous absorbing and scattering layers, a significant decrease in absorbed radiation occurs as the solar elevation angle decreases. The variation of absorbed radiation with solar elevation shown in Figure 3.25 includes both solar angle influences. Above 20 Km the variation shown results almost entirely from the change in the cross-sectional area. The change, which exceeds 1×10^{-3} cal/sec produces a change in the radiosonde temperature error at 30 Km of 0.7° K between 90° and 0° solar angles. At lower altitudes, the difference in absorbed radiation

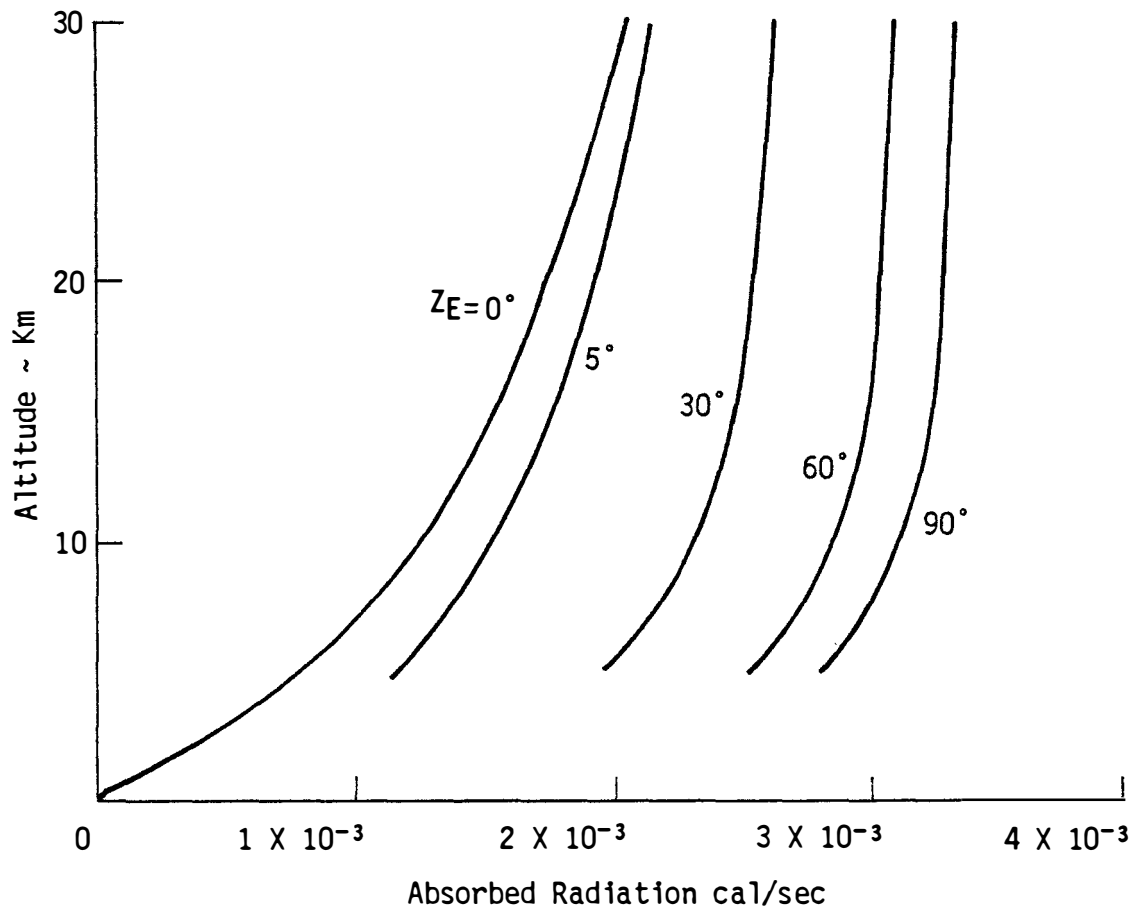


Figure 3.25 Direct solar radiation absorbed by thermistor versus altitude and solar elevation angle. The absorbed radiation is an average value over one revolution of the thermistor.

increases further due to the increased absorbing and scattering path length through the atmosphere. At 5 Km a difference of 2×10^{-1} cal/sec between 90° and 0° again produces a significant change in ΔT due to variation in solar angle.

The scattering of solar radiation changes appreciably with changes in atmospheric parameters (Ishimaru (1982)). An average earth albedo of 0.28 (Donn (1975)) indicates that, overall, 28% of incoming solar radiation is either scattered upwards to space or reflected off clouds and off the earth's surface to space. Clouds provide the largest number of scattering elements. Cloud cover routinely reduces to zero the amount of direct visible solar energy reaching the earth's surface thus scattering a high percentage of the energy content of the direct solar component. Aerosols and molecules also scatter significant amounts of solar radiation. The amount of solar radiation that is scattered and reflected back to space varies from a small percentage on a clear day in a clear atmosphere with an absorbing surface boundary such as water to in excess of 60% on a heavily overcast day (Ridgway and Davies (1983)). Figure 3.15 shows the large percentage of solar radiation that can be reflected from clouds when the thickness, h , is much larger than the mean free path length, L of a light ray.

An extensive number of computer runs would have been necessary to perform a complete sensitivity analysis on scattered solar radiation using the LOWTRAN 6 code. The run time on the IBM PC/AT used for this study exceeded 2 hours to generate the spherical irradiation of the thermistor at one altitude for each set of environmental input conditions. Thus, only selective runs were made to establish the magnitude of the scattering component between 10 to 30 Km under clear

sky conditions, as well as under overcast conditions with a 60% solar albedo. Under clear sky conditions the scattering component is small relative to the direct solar components and contributes less than 3% of the magnitude of the direct solar component for altitudes between 10 and 30 Km. In this case, the scattering component has no appreciable influence on the radiosonde temperature error. On overcast days, however, when perhaps 60% of incoming solar radiation is reflected upwards from clouds via Mie scattering, the influence is significant. From 10 to 30 Km, the scattering (reflected) component of radiation adds an approximate 30% to the direct solar component. The resulting increase in the radiosonde temperature error at 30 Km is in the range of 0.5 to 0.7° K.

3.7 Irradiation of the Thermistor From the Balloon and Radiosonde Instrument

Irradiation of the thermistor comes from the direct impingement of upwelling and downwelling atmospheric radiation and from radiation emitted by and reflected off the surface of the balloon and radiosonde instrument. The calculation of the irradiation of the thermistor can be simplified if it can be shown that the radiation exchange between the thermistor and both the balloon and radiosonde can be neglected. The influence of each (balloon and radiosonde) on the irradiation of the thermistor is two-fold. Not only does the thermistor receive radiation emitted and reflected from the balloon (radiosonde) surface, but the balloon (radiosonde) also acts as a shield to atmospheric radiation that would otherwise impinge upon the thermistor. Thus, the net influence of the balloon (radiosonde) on the irradiation of the thermistor is the difference between radiation arriving from the

balloon (radiosonde) surface and that atmospheric radiation shielded by the balloon (radiosonde) that would otherwise irradiate the thermistor if the balloon (radiosonde) were not present.

Appendices 4 and 5 calculate the influence of the balloon and radiosonde instrument, respectively, on the irradiation of the thermistor. The calculations in the Appendices include the influences of direct and diffuse solar radiation diffusely reflected off the balloon (radiosonde) surface, atmospheric infrared radiation diffusely reflected from the balloon (radiosonde) surface and radiation emitted by the balloon (radiosonde). Estimates of the magnitude of each term are made for environmental conditions likely to yield the maximum influence of radiation from the balloon (radiosonde).

In Appendix 4 the maximum nighttime influence of the balloon is calculated to make less than a 10% contribution to the total irradiation of the thermistor. During the daytime, the influence is even less with balloon reflected solar radiation contributing less than 4% to the total solar energy irradiating the thermistor.

In Appendix 5 the influence of the radiosonde instrument is derived in terms of radiation impinging on the thermistor from the sides S1 and S2 visible to the thermistor. The side S1 is the top side of the radiosonde oriented parallel to the earth and the side S2 is the vertical side of the radiosonde adjacent and visible to the thermistor (see Figure A5.1). For nighttime conditions the maximum combined influences of the sides S1 and S2 is calculated to be less than a few percent with the S2 contribution the larger. For daytime conditions with solar radiation present, the maximum combined influence of the sides S1 and S2 increases the solar irradiation of the thermistor by

less than 10%.

Consequently, in both daytime and nighttime situations, the heating rate of the thermistor due to radiation exchange with the balloon and radiosonde instrument is not appreciably different than if these influences were ignored and the thermistor heating rate were calculated assuming its exposure only to atmospheric radiation in all spherical directions. Thus, all further analysis excludes the influence of the balloon and radiosonde instrument.

4.0 RESULTS AND COMPARISONS WITH EXPERIMENTAL DATA

Direct measurements have been made of the radiosonde temperature error using special experimental radiosondes at Wallops Island, VA (Luers, et al. (1988, 1989), Schmidlin, et al. (1986, 1988)). Following the approach developed by Staffanson (1979) for rocketsonde measurements, each experimental radiosonde was equipped with 4 thermistors; the standard radiosonde thermistor, a black coated thermistor, and 2 thermistors coated with an aluminum paint. The error in the standard radiosonde thermistor is derived from the differences in the temperature measurements between three thermistors having different coatings. The fourth thermistor provides redundancy for verification of the accuracy of the measurement (Cox, et al. (1968)). Luers and Schmidlin (1989), Schmidlin, et al. (1986) describe in detail the theoretical basis of this technique.

Briefly, the technique is based upon deriving the steady state heat balance equation for each of the three thermistors in terms of the solar and infrared radiation absorbed by the thermistor, the radiation emitted by the thermistor and the convective heat transfer to the thermistor. The conduction through the lead wires and other second-order influences are not included in the analysis, leading to a small error in the results. Since the temperature of each thermistor is a measured quantity from its resistance, and the solar absorption and infrared emission properties of each thermistor have been experimentally measured in the laboratory, only three unknowns remain in the heat balance equations: the air temperature, the solar power, and the infrared power irradiating the sensor. The three equations are

solved simultaneously for the unknowns and the radiosonde temperature error derived from the difference between the temperature of the standard coated thermistor and the air temperature.

This technique allows the determination of the radiosonde temperature error for both daytime and nighttime flights. The accuracy of the derived temperature error has been verified to be within $\pm 0.5^\circ$ K at each data point. Smoothing of the many measurements obtained from each profile generates a smoothed profile with estimated accuracy of $\pm 0.2^\circ$ K. During the initial development of this special radiosonde instrument a series of 15 flights were conducted in 1983 (Schmidlin and Luers 1987)). Four of these flights provided measurements of the profile of the nighttime temperature error of the standard radiosonde thermistor. This test series also provided several measurements of the daytime temperature error. A more extensive series of experimental radiosonde flight tests (Schmidlin and Luers (1988)) was conducted at Wallops Flight Center during 1987. Most of these flights consisted of daytime launches. However, several nighttime and twilight flights also provided valid data.

Four nighttime, three daytime and one twilight flights were chosen from the two test series for comparison with simulation results based upon LOWTRAN 6 generated atmospheric radiation profiles. The method used in producing the simulation results is summarized as follows. The LOWTRAN 6 program was run to determine the irradiation of the thermistor, using as input representative atmospheric profiles and boundary conditions appropriate for each of the eight flight conditions. Mid-latitude summer and winter profiles were used for the June and February flights, respectively. The March and September

flights used interpolated values between the winter and summer results using, however, the proper boundary temperature and emissivity for each particular flight. The output data from each LOWTRAN 6 run was processed as described in Section 3.6.3.1 to determine the amount of radiation absorbed by the thermistor and lead wires. These values were then included with other necessary input data into the heat balance equation which was solved as described in Section 3.4. The temperature value obtained from each individual radiosonde flight at a given altitude was used in the heat balance equation to solve for the temperature error at that altitude.

4.1 Comparison of Measurement With Simulation Results: Night Flights

The four nighttime flights chosen for comparison consisted of one from each season of the year. A different structure in the temperature error profiles was observed in the measured data from each flight. The simulated and experimental results are compared in Figures 4.1 - 4.4. The profiles represent the experimental data and the dots the simulated results. Simulations were made at 5 Km increments in altitude. The atmospheric profiles used as the input to LOWTRAN 6 are identified in each figure. The winter flight of 17 February (Figure 4.1) shows excellent agreement between the measurements and simulated results. This particular flight only reached an altitude of 24 Km at which time the balloon burst. The temperature error remained small throughout the flight. The comparisons are exceptionally good above 10 Km.

The March 8 flight (Figure 4.2) shows a bias of 0.4 - 0.5° K between the simulated results and the experimental measurements of ΔT . Assuming the experimental measurements to be correct, the "too warm" values from the simulations indicate that the atmospheric radiation

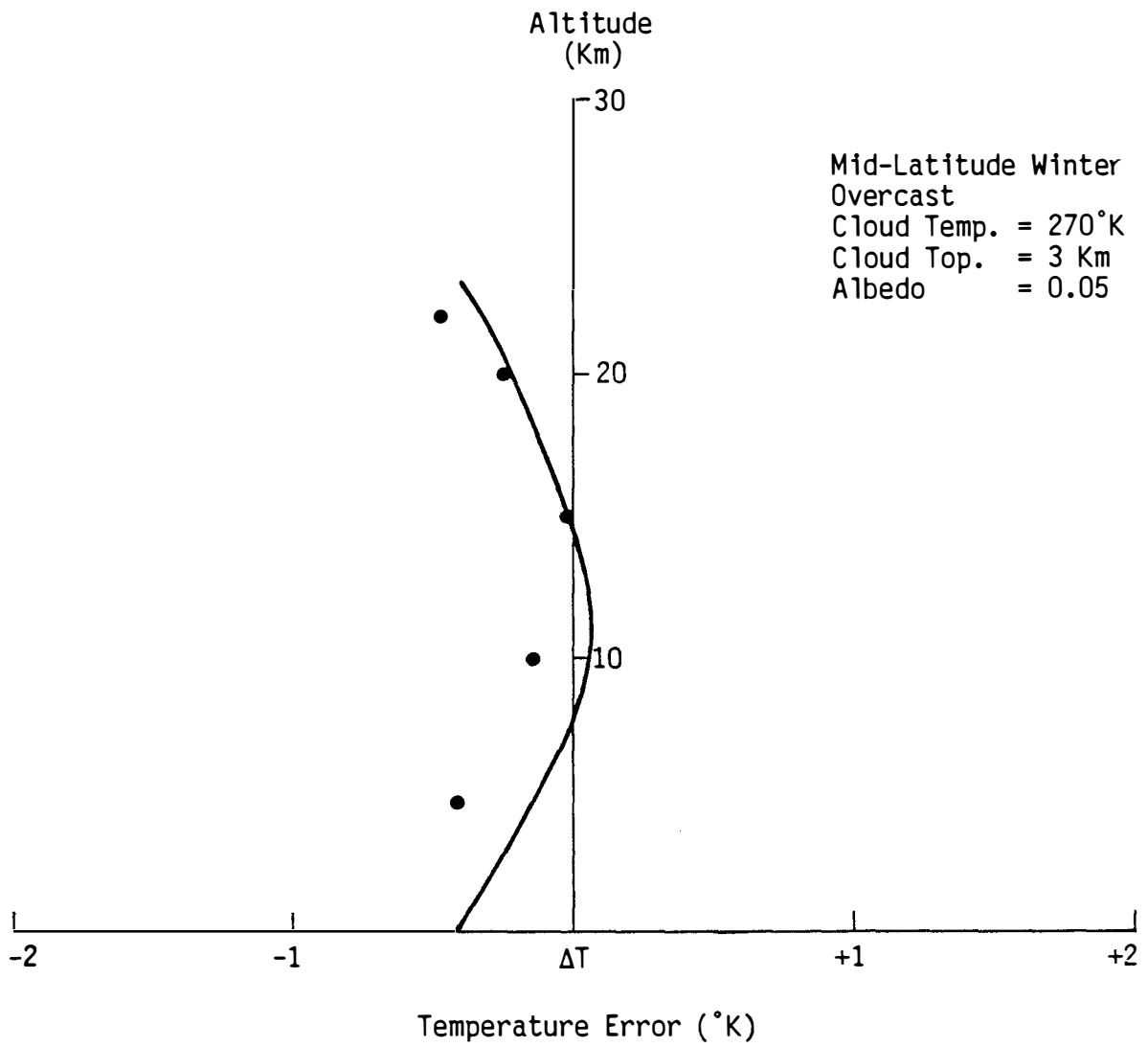


Figure 4.1 Temperature error profile: Nighttime Flight, 17 Feb 83, 01:51 Z.

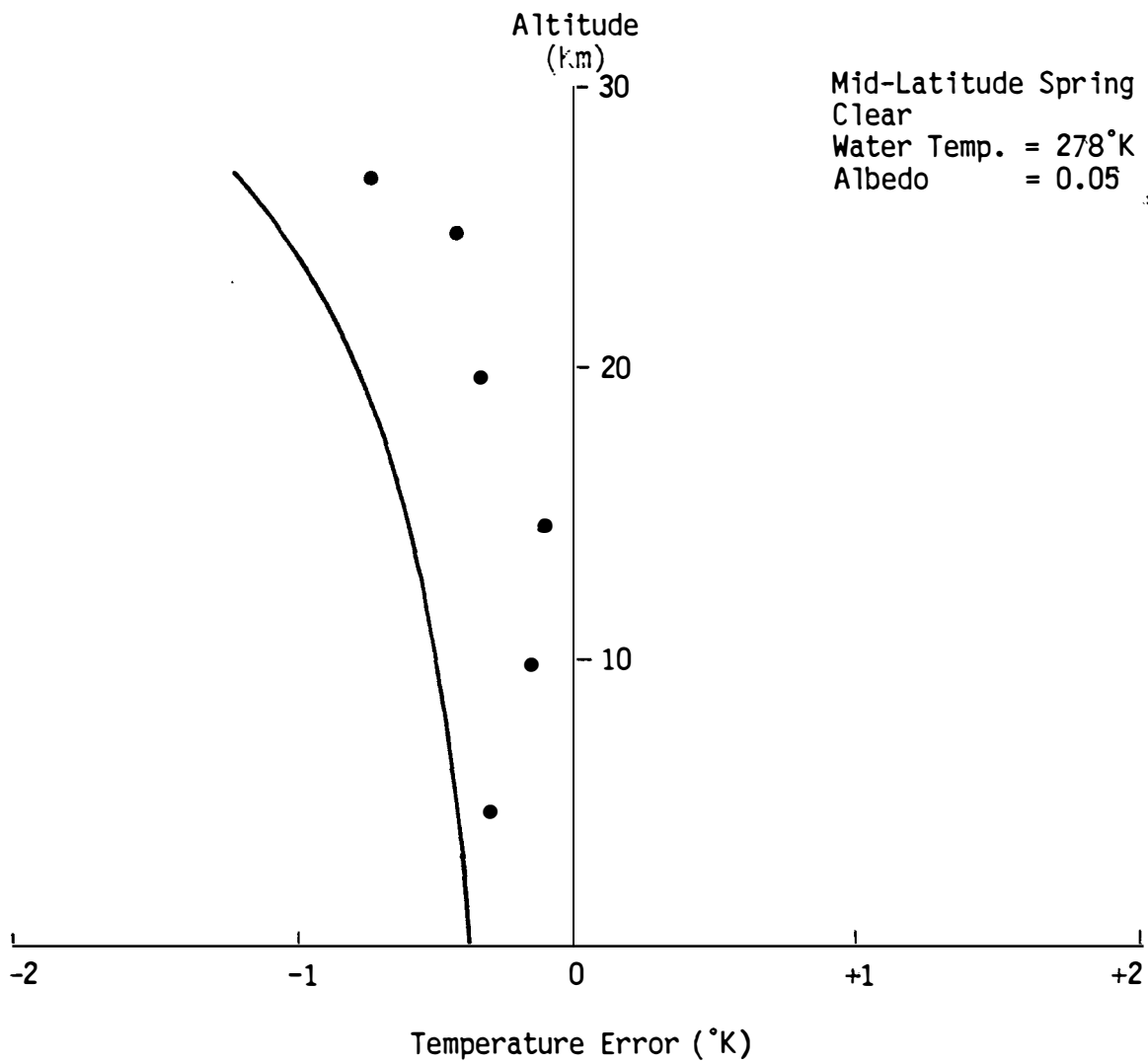


Figure 4.2 Temperature error profile: Nighttime Flight, 8 Mar 83, 23:07 Z.

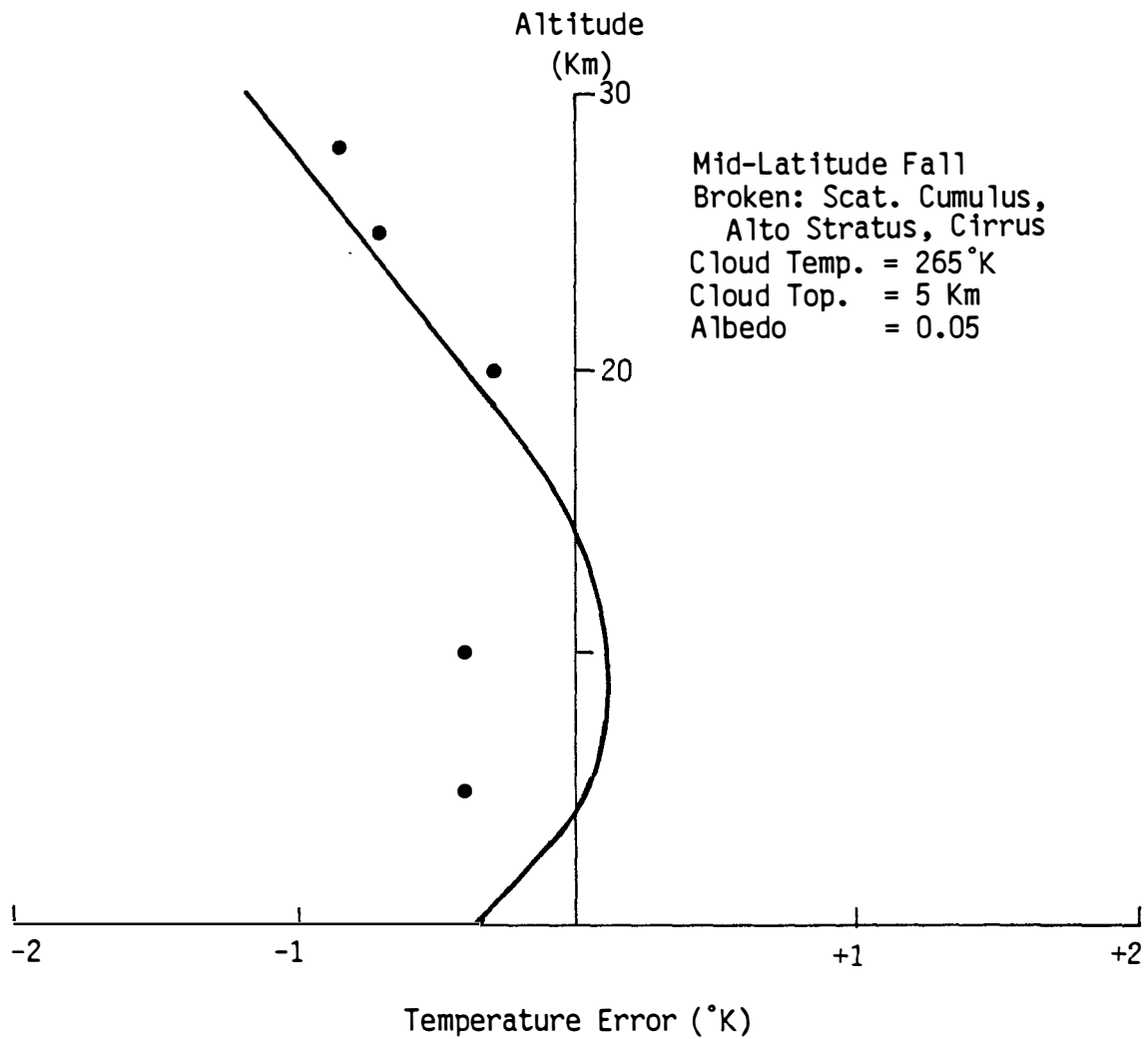


Figure 4.3 Temperature error profile: Nighttime Flight, 13 Sept 83, 23:17 Z.

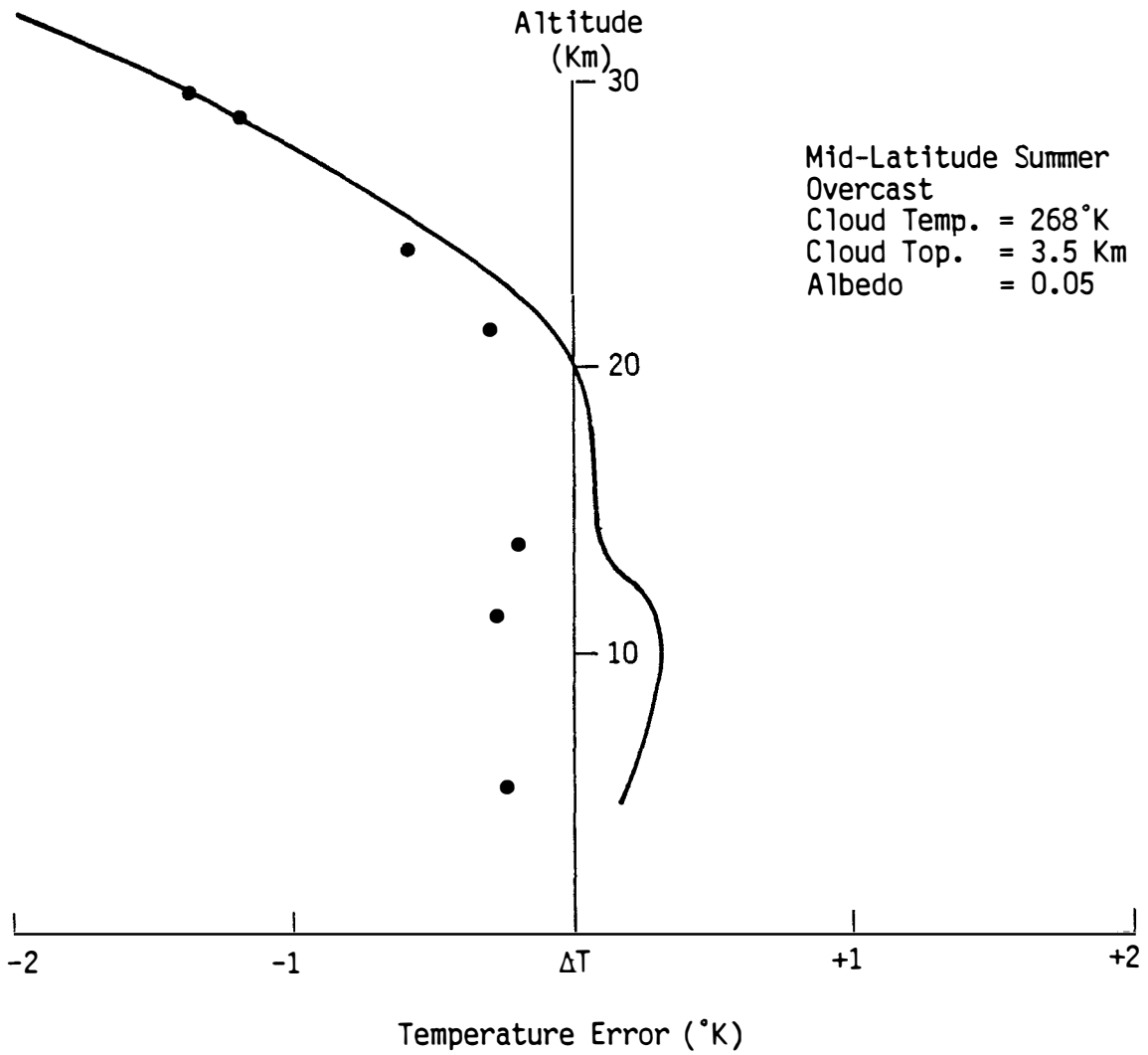


Figure 4.4 Temperature error profile: Nighttime Flight, 23 June 87, 23:33 Z.

estimated by LOWTRAN 6 was too large. The cause of this bias is unknown, perhaps a cloud deck of high cirrus partially shielded the radiosonde from upwelling radiation from the water surface.

Results from the nighttime flight on September 13 is shown in Figure 4.3. Again the agreement is excellent above 10 Km. A cloud top temperature of 265° K with emissivity of 0.95 at 5 Km, was used as the lower boundary for LOWTRAN 6. At 10 Km and below the simulated results appear too cold perhaps because of downwelling radiation from higher clouds not taken into account. Scattered clouds cannot be adequately addressed with the LOWTRAN 6 code.

Results from the summer flight on June 23, 1987 are shown in Figure 4.4. In this flight the temperature error takes on large negative values in excess of -2° K above 30 Km. The cause of the large temperature error at high altitudes can be traced to a warmer than usual atmospheric temperature profile in that altitude region. A warmer thermistor temperature produces a greater heat loss due to emissions from the thermistor and an increase in negative ΔT . The simulated results agree favorably with the actual empirical data. Only below 15 Km is there any appreciable discrepancy. Slight errors at the lower levels are probably the result of inadequate modeling of the atmospheric profiles in this region.

In summary the analysis of four nighttime flights shows the simulation results to provide excellent agreement with experimental measurements. The agreement is most impressive at altitudes above 10 Km where the radiosonde temperature error is the largest. Flights conducted during all four seasons of the year and under clear sky, overcast, and scattered cloud conditions were used in the analysis. In

only one case, the March 8, 1987 case, was there a significant bias ($\approx 0.5^\circ \text{ K}$) between the experimental data and simulation results. The experimental data indicated less radiation than that predicted. Nevertheless, the overall results must be considered to be in good agreement when one takes into account the inaccuracy of the experimental measurements, as well as the assumptions required in defining the atmospheric parameters used in the LOWTRAN 6 model.

4.2 Comparison of Measurements With Simulation Results: Day Flights

Four experimental daytime radiosonde flights, launched during the 1987 test series were chosen for comparison with simulation results. Two summer flights during June, a winter February flight, and a March twilight flight were chosen. The flight conditions included: broken, scattered, and overcast cloud conditions and a solar elevation angle variation from 45° , near noon, during the winter flights to in excess of 65° for the summer flights and from 12° (through 0° into darkness) for the twilight flight. Figures 4.5 - 4.8 show a comparison of the experimentally measured radiosonde temperature error versus the results simulated using the LOWTRAN input parameters specified in each figure. Since broken and scattered cloud conditions could not be directly incorporated into LOWTRAN 6, a compensation was made to the input data by slightly increasing the surface albedo for solar wavelengths to account for reflection off of cloud surfaces.

Figure 4.5 shows the results for the February 26 flight at 15:33 zulu. An approximate 5 hour time difference between sun time and Greenwich mean time at Wallops Island, VA results in a sun launch time about 10:30 AM. The radiosonde rises from the surface to 30 Km in approximately 90 minutes resulting in a sun time of near noon at 30 Km.

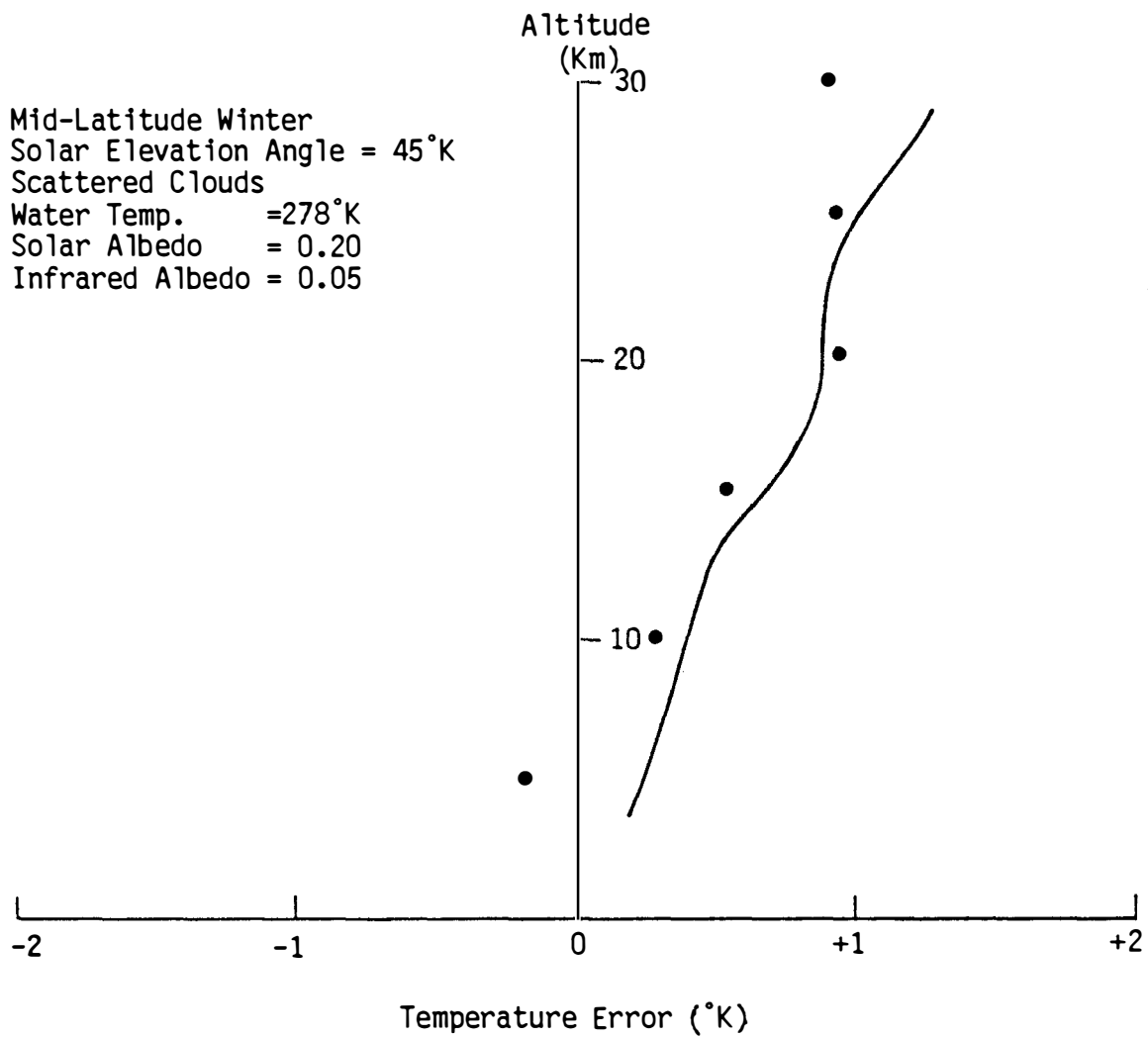


Figure 4.5 Temperature error profile: Daytime Flight, 26 Feb 87, 15:33 Z.

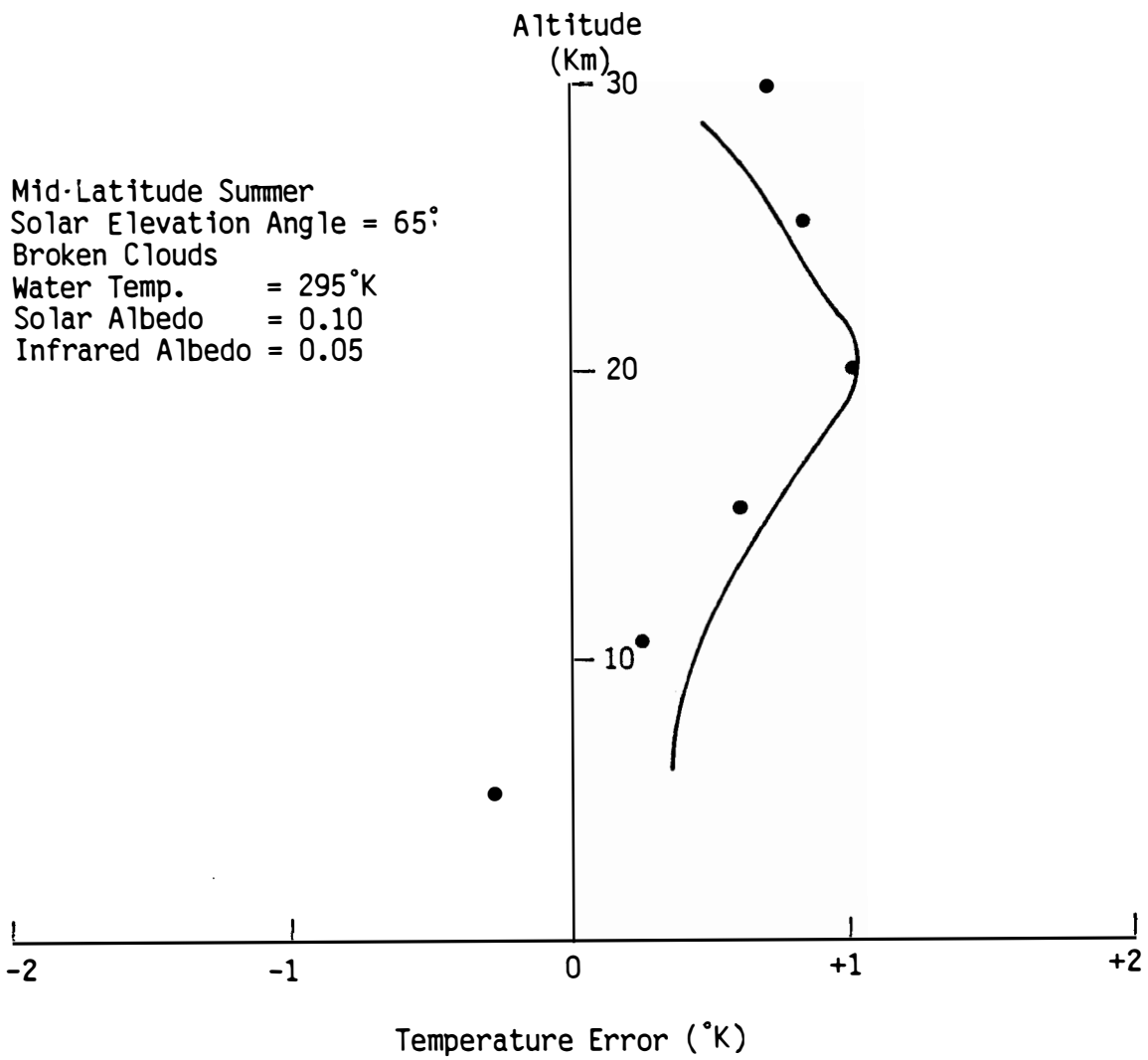


Figure 4.6 Temperature error profile: Daytime Flight, 19 June 87, 15:01 Z.

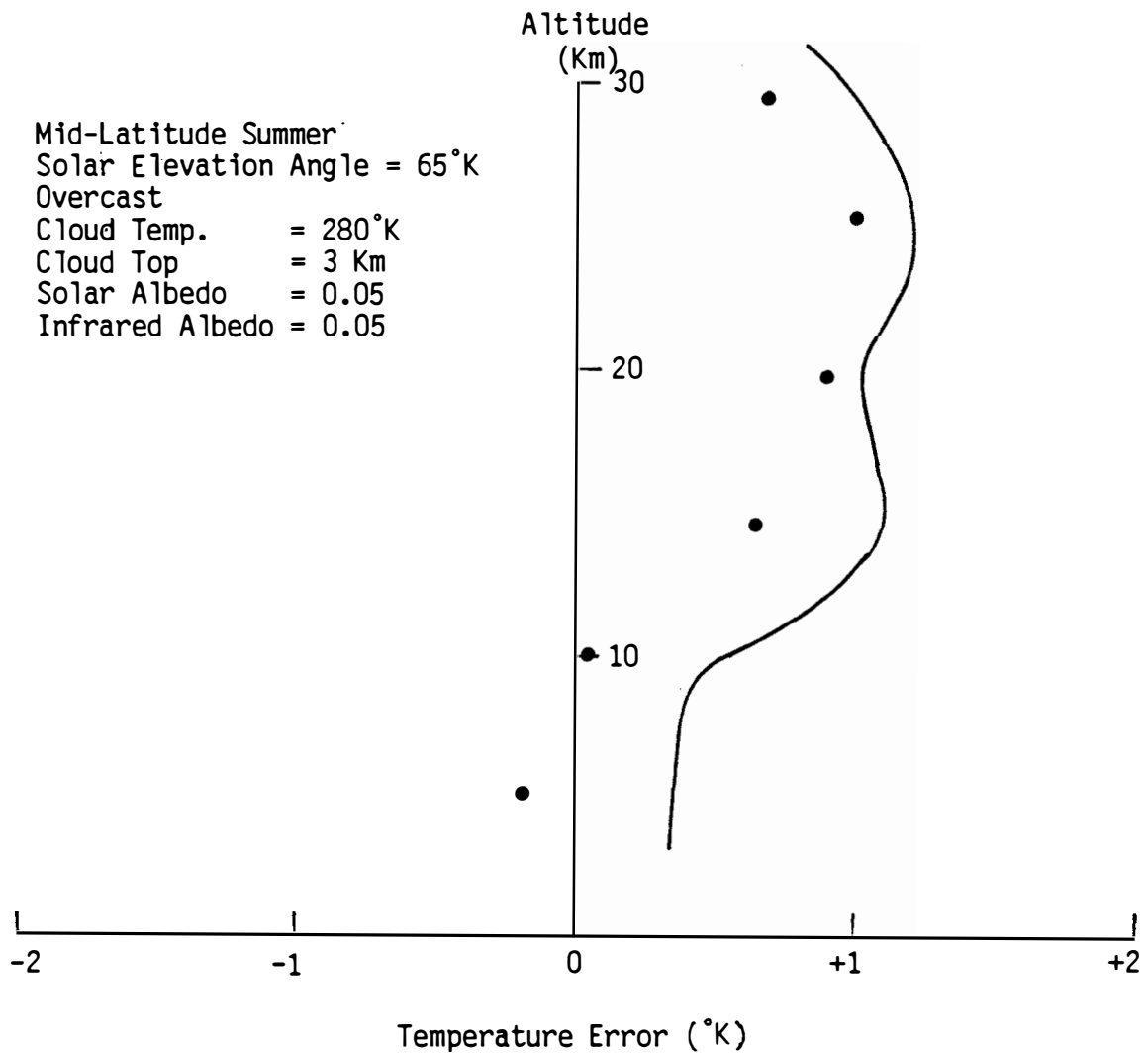


Figure 4.7 Temperature error profile: Daytime Flight, 23 June 87, 15:47 Z.

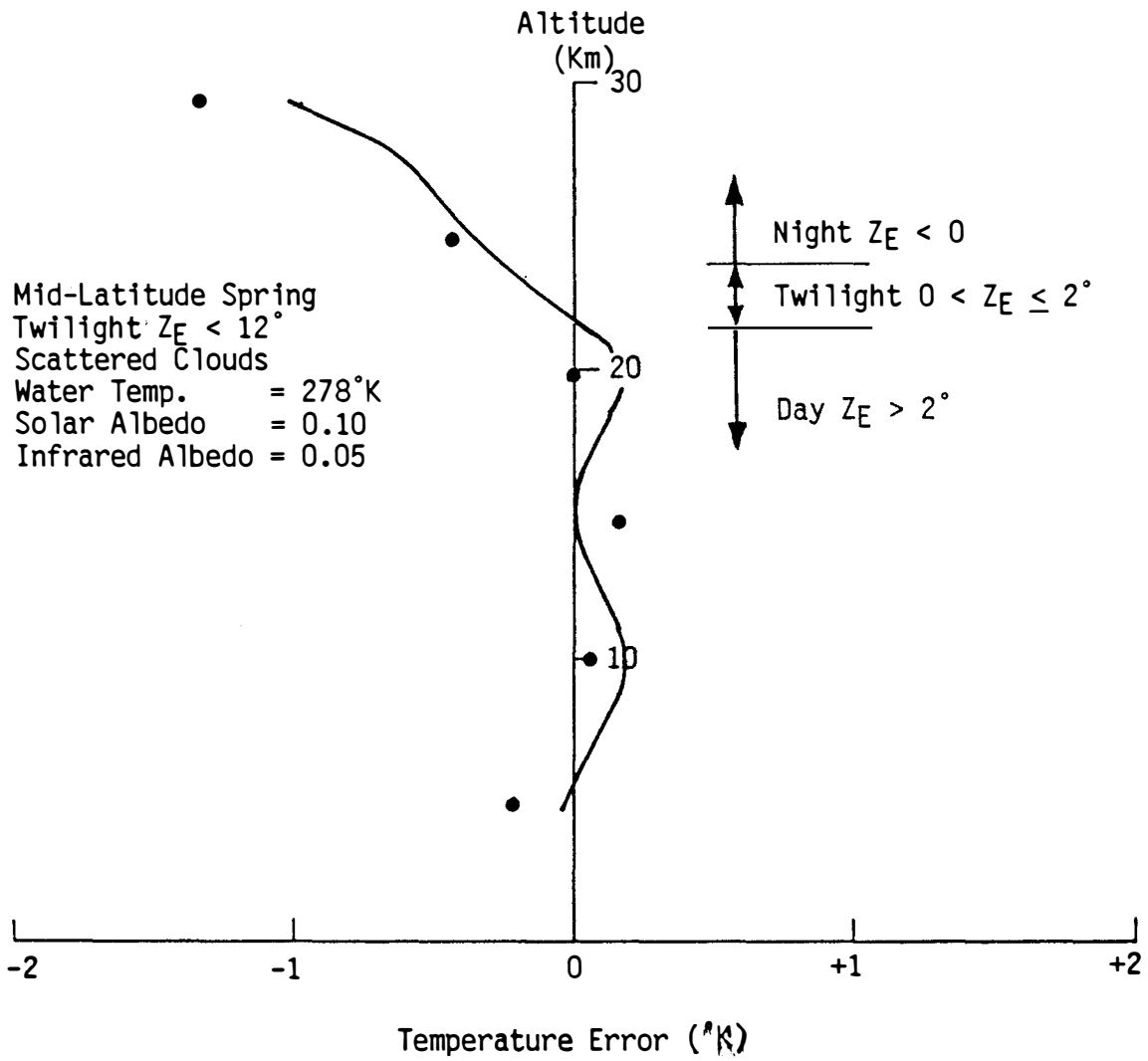


Figure 4.8 Temperature error profile: Twilight Flight, 5 Mar 87, 21:54 Z.

A solar elevation angle of 45° was chosen as representative of this flight at Wallops latitude for the February 26 date. Excellent agreement is seen between the simulation and experimental results. A detailed review of the LOWTRAN output shows that the irradiation of the thermistor was near equally partitioned between infrared radiation and the direct components of solar radiation. The contribution due to the scattering of the solar component was small, less than 10% of the direct solar component. An increase in the surface albedo to 0.2 for solar radiation, to account for reflections off the scattered clouds (Schmetz (1984)), generated only a small increase in the thermistor heating from the reflected solar radiation. The slight under estimation in Figure 4.5 of the temperature error at the 5 Km level may be due to enhanced low level reflections and scatterings off of isolated clouds.

Results from the summer flight of June 19, 1987 are shown in Figure 4.6. A sun time at launch of approximately 10 AM at a date near the summer solstice produces a representative solar elevation angle of 65° for the flight. A review of the LOWTRAN output data shows that the infrared and direct solar radiation contributions to the thermistor heating are of approximately equal magnitude above 15 Km. The magnitude of each, however, is somewhat larger than for the February flights. The increase in infrared radiation is due to a warmer surface temperature while the increased direct solar radiation results from a higher solar elevation angle. At altitudes below 10 Km the infrared heating of the thermistor predominates over the solar component. The scattered and reflected solar components of radiation, amount to less than 10% of the direct solar component. Although more radiation is

absorbed by the thermistor during the summer flight than the February 26 flight, the radiosonde temperature error is of the same magnitude for both flights. The reason is that the summer temperature profile is approximately 10° warmer (at the higher altitudes) than the winter temperature profile. This produces a higher emission rate for the thermistor and largely compensates for the increased irradiation of the thermistor.

The radiosonde launch of June 23 with overcast conditions is shown in Figure 4.7. An albedo for solar radiation of 0.6 was used to simulate the solar wavelength reflections off the cloud lower boundary. A cloud top temperature of 280° K at 3 Km was used to define the lower boundary for the infrared component of radiation. The cloud emissivity was taken to be 0.95. With this scenario the direct solar radiation heating the balloon above 20 Km somewhat exceeded the infrared component. The scattering component, however, is significant and contributes approximately 30% of the direct solar component. Agreement between simulated results and experimental measurements is very good especially at the higher altitudes. The simulation results appear to underestimate the thermistor heating at altitudes below 10 Km where the infrared component predominates.

The balloon launch of March 5 (Figure 4.8) occurred about 30 minutes before sunset with the balloon entering into darkness near 25 Km altitude. The solar elevation at launch approached 12° . As the balloon ascended it remained exposed to direct sunlight aloft even though sunset already occurred at the surface. Between 22 and 25 Km the balloon went through twilight into darkness. Figure 4.8 compares the temperature error measurements from those predicted using the

simulation technique. In performing the simulation a calculation was made at increments of 5 Km using the solar elevation angle appropriate for that altitude. The agreement between measurement and prediction is excellent. The lack of a significant positive error in the 10 to 20 Km region, even with sunlight present, is due to the greatly reduced solar intensity at low elevation angles as shown in Figure 3.24.

4.3 Conclusions

Agreement is generally good between simulation results and experimental measurements of the radiosonde temperature error for all flights considered. Agreement is especially good when one takes into account the error in the experimental measurements, as well as the uncertainty in the estimate of environmental conditions used in the generation of the simulated irradiance values. Important insights have been gained concerning the magnitude of the temperature error in the radiosonde under different daytime environmental conditions, as well as those factors having greatest influence on the temperature error. For both winter and summer daytime flights, a positive temperature error of up to $+1^{\circ}$ K at altitudes of 20 Km and above has been observed. The magnitude of the error stabilizes, in the 20 to 30 Km region, as a result of a decrease in atmospheric temperature with increasing altitude. For nighttime flights the temperature error was generally negative and increased in magnitude with increased altitudes. The twilight flight showed less heating in the sunlit segment of the flight, because of a low solar angle, with the appropriate magnitude for the nighttime error in the darkness segment of the flight. It should be cautioned, however, that the above results will considerably change under different vertical profiles of atmospheric temperature.

At altitude below 10 Km the infrared component of heating predominates while at altitudes above 20 Km the infrared and direct solar components contribute approximately equally to the heating of the thermistor. The scattered solar component is generally small, however, with a heavy layer of clouds the reflected solar energy off the cloud tops can contribute significantly to the thermistor heatings.

Summer time temperature errors for the daytime flights considered were of about the same magnitude as that of the winter profile. The increased solar and infrared radiation present during the summer was compensated for by increased thermistor emissions due to a warmer summer temperature profile.

5.0 CONCLUSIONS AND RECOMMENDATIONS

A technique has been developed to calculate the temperature error of the radiosonde as a function of the environmental parameters that influence the solar and infrared irradiation of the thermistor. The technique has been tested and validated using eight experimental flights in which good comparisons were achieved. The flights used in testing the technique included both day and night flights under clear and cloudy conditions, during all seasons of the year, and with differing solar elevation angles. The comparisons between experimental measurements and the simulated results were within the agreement expected when one takes into account inaccuracies in experimental data and the approximating profiles used in identifying and modeling the atmospheric conditions present at the time of the balloon launch. Noteworthy results achieved in this study can be summarized as follows:

- o Variations in the absorption and emission properties of the standard radiosonde thermistor is not a source of significant error in the radiosonde temperature measurement.
- o Variations in the dimensions of radiosonde thermistors is not a significant source of error in the radiosonde temperature measurement.
- o Variations in the solar and infrared intensity irradiating the thermistor has a major influence on the radiosonde temperature error. The radiant intensities, in turn, are influenced by; the surface (lower boundary) temperature and emissivity, by the seasonally dependent constituent, aerosol and thermodynamic atmospheric profiles, by the solar elevation

angle, and by the cloud cover. The influence of each is as follows.

- o A change in surface temperature (boundary temperature) of 25° K produces a change in thermistor absorbed radiation of 0.5×10^{-3} cal/sec which, in turn, produces a change in the temperature error at (30 Km) of approximately 0.3° K. A change in emissivity of 0.15 (indicative of snow), makes a negligibly small change in the temperature error.
- o Seasonal changes in constituent and background profiles produce on the average, a change in the temperature error of 0.2° K between summer and winter profiles. Combining the surface temperature and background profile changes, between the winter and summer seasons, produces on the average a change in the temperature error of 0.5° K above 20 Km.
- o The solar elevation angle influences the radiosonde temperature correction for two reasons. As the solar elevation angle decreases, the rotating cylindrical thermistor is exposed to less solar radiation because of a smaller average projected area per revolution. Secondly, as the solar elevation decreases, additional scattering and absorption of radiation occurs because of the longer path length through the atmosphere. At altitudes above 20 Km only the projected area affect is significant and produces a change in the temperature error of 0.7° K between 0° and 90° solar elevation

angles. At low altitudes, especially below 10 Km, the increased path length significantly decrease the solar irradiation of the thermistor and an additional change in ΔT of 0.2 to 0.4° K results.

- o Cloud cover changes the irradiation of the thermistor because of: a) infrared emissions at the cloud top temperature, and b) increased reflected solar energy off the cloud tops. In summer cold cloud tops can greatly decrease the infrared irradiation of the thermistor over what would occur on a clear day when the thermistor is irradiated by a warm surface. Under extreme conditions with a very high cloud layer, a decrease in the temperature error of 0.6° K at 30 Km can result from the decrease in the infrared component of radiation. The decreased infrared radiation, however, is partially compensated for by increased reflected solar radiation off the cloud layer. The magnitude of this contribution depends upon the density of the cloud layer but can be in excess of 0.3° K. The amount of solar radiation scattered by molecules and aerosols that irradiates the thermistor is small compared to the direct component and contributes less than a 0.1° K to the radiosonde temperature error.
- o The structure of the atmospheric temperature profile has a major influence on the radiosonde temperature error. At a given altitude a decrease in the atmospheric temperature will make the radiosonde temperature error increase in a positive

sense. The magnitude of the influence of atmospheric temperature depends to some extent on the magnitude of the temperature error itself. However, changes in temperature error of 0.5° K for a 15° K change in atmospheric temperature are not uncommon at the higher altitudes.

- o An increase in altitude increases the temperature error because the more rarified air diminishes the convective heat transfer from the thermistor. The larger the magnitude of the temperature error at a given altitude, the greater will be its increase at higher altitudes. Increases in the magnitude of the temperature error of 0.5° K due to altitude are possible from 20 and 30 Km. Generally, however, the altitude effect is less.

The results from this study lend itself to further research and applications in several different areas. This initial study was restricted to developing a technique for estimating the radiosonde temperature error and verifying the method by making comparisons with experimental measurements from Wallops Island, VA. This technique should also be applied to data sets from other geographic locations where the radiation input and/or background temperature profiles differ significantly from the mid-latitude Wallops Island, VA site. Specifically, the technique might be applied to polar locations and tropical locations. Additionally, the technique should be applied to unique meteorological events, such as stratospheric warmings and volcanic eruptions that drastically change the background temperature profile or the aerosol content of the atmosphere. Historic radiosonde profiles from these type events could be obtained and the radiosonde

temperature error that occurred with these measurements determined.

A simplification of the technique developed in this study has potential for the operational reduction of National Weather Service radiosonde data. A method would have to be developed and verified for estimating the radiation absorbed by the thermistor as a function of environmental conditions without relying on LOWTRAN 6 computer runs for providing the necessary data. However, many of the main contributors to the temperature error can be easily identified and their contributions calculated directly. These include solar elevation angle, the atmospheric temperature profile, and the influence of altitude. The infrared and solar irradiance of the thermistor could be estimated empirically based upon the cloud cover established from the radiosonde humidity profile and the surface temperature. It is recommended that a further study be conducted to test a simplified approach for calculating the radiosonde temperature error, that can be utilized for operational reduction of radiosonde flights.

The technique that has been developed and applied to the U.S. radiosonde is also applicable to radiosonde instruments used by other countries, as well as new radiosonde instruments being developed in the U.S. and abroad. Although the heat transfer equations may need minor revision for each radiosonde instrument, the basic approach could be easily implemented and comparisons made between the radiosonde temperature errors from different sensors under varying environmental conditions. New sensors in the design stage could be evaluated in terms of the accuracy of their measurements using the technique developed in this report.

REFERENCES

- Arpaci, V., Conduction Heat Transfer, Addison-Wesley, 1966.
- Badgley, F.I., "Response of Radiosonde Thermistor," Rev. Sci. Instr., 28, pp. 1079-1984, 1957.
- Ballard, H.N. and R. Rubio, "Corrections to Observed Rocketsonde and Balloonsonde Temperatures," Journal of Applied Meteorology, 7(5), pp. 919-928, October 1968.
- Barbaro, S., S. Coppolino, C. Leone, and E. Sinagra, "An Atmospheric Model for Computing Direct and Diffuse Solar Radiation," Solar Energy, 22, 1979, pp. 225-228.
- Belt, C., and H. Fuelberg, "The Effects of Random Errors in Rawinsonde Data and Derived Kinetic Quantities," Monthly Weather Review, Vol. 110, February 1982, pp. 91-101.
- Bingxun, H., "The Radiation and Lag Errors of GZZ-7 Radiosonde," NASA Translation TT-20099, Sept. 1987.
- Buglia, J., "Introduction to the Theory of Atmospheric Radiative Transfer," NASA Ref. Pub. 1186, July 1986.
- Choudhury, B.J., and A.T.C. Chang, "The Albedo of Snow for Partially Cloudy Skies," Boundary-Layer Meteorology, 20, 1981, pp. 371-389.
- Coombes, C., and A. Harrison, "Angular Distribution of Downward Longwave Radiance and Their Meteorological Applications," J. Applied Meteorology, Vol. 25, pp. 1134-1143, 1986.
- Cox, S., J. Maynard, and V. Suomi, "Radiosonde Temperature-Baseline Inaccuracy," J. of Appl. Met., Vol. 7, No. 4, August 1968, pp. 691-696.
- Daniels, G.E., "Errors of Radiosonde and Rocketsonde Temperature Sensors," Bulletin of the American Meteorological Society, 49(1), pp. 16-18, January 1968.
- Down, W., Meteorology, 4th Edition, McGraw-Hill, Inc. 1975.
- Fan, D.R., and K. Keswani, "A Continuous Correlation Equation for Heat Transfer from Cylinders to Air in Crossflow for Reynolds Numbers From 10^{-2} to 2×10^5 ," International Journal of Heat and Mass Transfer, 15, pp. 559-562, 1972.
- Friedman, M., "Radiosonde Set VIZ 1292 and 1293," Tech Publication 730919, VIZ Manufacturing Co., Philadelphia, PA.
- Gergen, J., "Atmosphere Infrared Radiation Over Minneapolis to 30 Millibars," J. Applied Meteorology, Vol. 14, December 1957, pp. 495-504.

- Harney, P., "Tests on Ventilation Rates and Other Factors in Radiosonde Performance," J. of Applied Meteorology, Vol. 10, April 1971, pp. 295-301.
- Henninger, J., "Solar Absorptance and Thermal Emittance of Some Common Spacecraft Thermal-Control Coatings," NASA Ref. # 1121, 1984, pp. 43.
- Hering, W., and R. Johnson, "The FASCAT Model Performance Under Fractional Cloud Conditions and Related Studies," AFGL-TR-84-0168, S10 Ref. 85-7, 1984.
- Hodge, M., and C. Harmantas, "Compatibility of United States Radiosondes," Monthly Weather Review, Vol. 93, No. 4, April 1965, pp. 253-266.
- Hooper, F.C., and A.P. Brunger, "A Model for the Angular Distribution of Sky Radiance," Journal of Solar Energy Engineering, 102, August 1980, pp. 196-202.
- Ideriah, F.J.K., "A Model for Calculating Direct and Diffuse Solar Radiation," Solar Energy, 26, 1981, pp. 447-452.
- Ishimaru, A., "Multiple Scattering Effects on Transmission Through the Atmosphere," ONR-TR-4, August 1982.
- Johnson, K.W. and R.M. McInturff, "Day-Night Differences in Radiosonde Observations in the Stratosphere and Troposphere," proceedings of the Conference of Atmospheric Environmental Aerospace Systems and Applied Meteorology, New York, NY, pp. 186-189, November 1978.
- Johnson, R., W. Hering, J. Gordon, B. Fitch, and J. Shields, "Preliminary Analysis and Modeling Based Upon Project OPAQUE Profile and Surface Data," AFGL-TR-79-0285, 1979.
- Jursa, A.S. (editor), "Handbook of Geophysics and Space Environments," U.S. Air Force Geophysics Laboratory, 1985.
- Kays, W., and M. Crawford, Convective Heat and Mass Transfer, McGraw-Hill, Inc., 1980.
- Kneizys, E., E. Shettle, and W. Gallery, "Atmospheric Transmission and Radiance: LOWTRAN 5 Code," SPIE Vol. 277, Atmospheric Transmission, 1981, pp. 116-124.
- Kneizys, F., E. Shettle, W. Gallery, J. Chetwynd, L. Abreu, J. Shelby, S. Clough, and R. Fenn, "Atmospheric Transmittance/Radiance Computer Code LOWTRAN 6, AFGL-TR-83-0-0187, pp. 20, 1983.
- Kreith, F., Radiation Heat Transfer, International Textbook Co., 1962.
- Krummins, M.V., "A Study of Corrections for the Loop Mounted Sensor," PhD. Thesis, University of Maryland, 1978.

- Lenhard, R., "Accuracy of Radiosonde Temperature and Pressure Height Determination," Bulletin of American Meteorological Society, Vol. 51, No. 9, Sept. 1970,
- Lenhard, R., "A Revised Assessment of Radiosonde Accuracy," Bulletin of American Meteorological Society, Vol. 54, No. 7, July 1973, pp. 691-693.
- Luers, J.K., "Effect of Rawinsonde Errors on Rocketsonde Density and Pressure Profiles - An Error Analysis of the Rawinsonde System," University of Dayton Research Institute, TR-80-87, January 1980.
- Luers, J., and F. Schmidlin, "Corrections for the Standard U.S. Radiosonde Temperature Sensor - Part 1: Theory and Techniques," Sub. to Bulletin of American Meteorological Society, 1989.
- McInturff, R.W. and F.G. Finger, "The Compatibility of Radiosonde Data at Stratospheric Levels Over the Northern Hemisphere," ESSA TM WBTM-DATAC2, December 1968.
- McInturff, R.W., F.G. Finger, K.W. Johnson, and J.D. Laver, "Day-night Differences in Radiosonde Observations of the Stratosphere and Troposphere," NOAA Technical Memo, NWS NMC 63, pp. 47, 1979.
- McMillin, L., M. Gelman, and A. Sylva, "A Method for the Use of Satellite Retrievals as a Transfer Standard to Determine Systematic Radiosonde Errors," Monthly Weather Review, Vol. 116, May 1988, pp. 1091-1102.
- Miyake, Y., R. Shimokawa, and Y. Hamakawa, "Global Radiation Model and Angular Distribution of the Diffuse Irradiance," Solar Cells, 20, 1987, pp. 127-143.
- Morcrette, J.J., and J.F. Geleyn, "On the Influence of Different Radiation Parameterization on Model-Generated Radiation Fields," Quart. J.R. Met., Vol. 111, p. 565, 1985.
- Nash, J., and F.J. Schmidlin, "Final Report of the WMO International Radiosonde Intercomparison," WMO Report No. 30, 1987.
- Nestler, M., "A Comparative Study of Measurements from Radiosonde Rocketsondes and Satellites," NASA CR-168343, April 1983.
- Ney, E.P., R.W. Maas, and W.F. Huch, "The Measurement of Atmospheric Temperature," Journal of Meteorology, Vol. 18, pp. 60-80, February 1961.
- Pearson, P., "An Investigation Into the Response and Corrections to a Thermistor and a Platinum Wire Resistance Thermometer for Temperature Measurement in the Upper Atmosphere," Australian Weapons Res. Est. Tech. Note PAD 83, Adelaide, Australia, 1967.

- Powell, A., Jr., "A Simple Solar, Spectral Model for Studying the Effects of Cloud Cover and Surface Albedo on the Incoming Solar Radiation," AFIT/CI/NR 86-123D, 1986.
- Ridgway, W.L., and R. Davies, "Interpretation of Spectral Reflection from Cloud Tops," Fifth Conference on Atmospheric Radiation, Oct. 31-Nov. 4, 1983, Baltimore, MD, American Meteorological Society, pp. 524-527.
- Schmetz, J., "On the Parameterization of the Radiative Properties of Broken Clouds," Tellus, 36A, 1984, pp. 417-432.
- Schmidlin, F., "A Statistical Comparison of Winter-Summer Rocketsonde-Radiosonde Temperatures in the 20 to 34 Kilometer Region of the Stratosphere," Monthly Weather Review, Vol. 97, No. 8, August 1969, pp. 607-611.
- Schmidlin, F.J., J.K. Luers and P.D. Huffman, "Preliminary Estimates of Radiosonde Thermistor Errors," NASA Technical Paper # 2637, September 1986.
- Schmidlin, F.J., "WMO International Radiosonde Intercomparison Phase II," WMO Report No. 29, 1987.
- Schmidlin, F., and J. Luers, "U.S. Radiosonde Temperature Errors, Methods of Correction, and Evidence of Data Improvements," Sixth Symposium on Meteorological Observations and Instrumentation, January 1987, New Orleans, LA.
- Schmidlin, F.J., "Comparisons of Radiosonde and Radar Geopotential Heights," Proceedings of the Sixth Symposium on Meteorological Observations and Instrumentation, Jan. 12-16, 1987, New Orleans, LA.
- Schmidlin, F.J., and F.G. Finger, "Conclusions and Recommendations Resulting from the WMO International Radiosonde Intercomparison," Proceedings of the Sixth Symposium on Meteorological Observations and Instrumentation, Jan. 12-16, 1987, New Orleans, LA.
- Schmidlin, F., and J. Luers, "Development and Application of Corrections to the U.S. Radiosonde Rod Thermistor Temperature Measurements," WMO Conference on Measurements and Instrumentation, Leipzig, F.R.G., May 1987.
- Selby, J.E.A., and R.A. McClatchey, Atmospheric Transmittance from 0.25 to 28.5 μm : Computer Code LOWTRAN 2, AFCRL-TR-72-0745, AD A763721, 1972.
- Selby, J.E.A., and R.A. McClatchey, Atmospheric Transmittance from 0.25 to 28.5 μm : Computer Code LOWTRAN 3, AFCRL-TR-75-0255, AD A017734, 1975.

- Selby, J.E.A., E.P. Shettle, and R.A. McClatchey, Atmospheric Transmittance from 0.25 to 28.5 μ m: Supplement LOWTRAN 3B, AFGL-TR-76-0258, AD A040701, 1976.
- Selby, J.E.A., F.X. Kneizys, J.H. Chetwynd, Jr., and R.A. McClatchey, Atmospheric Transmittance/Radiance: Computer Code LOWTRAN 4, AFGL-TR-78-0053, AD A058643, 1978.
- Sparrow, E., and R. Cess, Radiation Heat Transfer, McGraw-Hill, Inc. 1978.
- Staffanson, F.L., "Rocketsonde Data Processing and Participation in the NASA Wallops Flight Center Meteorological Rocket/Nimbus Satellite Comparison Project," Final Report Contract NAS6-2627, University of Utah, 1979.
- Suckling, P.W., and J.E. Hay, "Modelling Direct, Diffuse and Total Solar Radiation for Cloudless Days," Atmosphere, 14(4), 1976, pp. 298-308.
- Suckling, P.W., and J.E. Hay, "A Cloud Layer-Sunshine Model for Estimating Direct Diffuse and Total Solar Radiation," Atmosphere, 15(4), 1977, pp. 194-207.
- Sutherland, R., and J. Bartholic, "Significance of Vegetation in Interpreting Thermal Radiation from a Terrestrial Surface," Journal of Applied Meteorology, Vol. 16, No. 8, August 1977, pp. 759-763.
- Talbot, J.E., "Radiation Influences on a White-Coated Thermistor Temperature Sensor in a Radiosonde," Australian Meteorology Magazine, Vol. 20, pp. 22-33, March 1972.
- Tam, W., and R. Corriveau, "Infrared Spectral Radiance of the Sky," Infrared Phys., (16) pp. 129-134, 1976.
- U.S. Standard Atmosphere Supplements, U.S. Government Printing Office, Washington, DC, 1966.
- Unsworth, M.H., and J.L. Monteith, "Longwave Radiation at the Ground. I. Angular Distribution of Incoming Radiation," Quart. J. Roy. Met. Soc., (101), pp. 13-24, 1975.
- Valley, S.L. (editor), Handbook of Geophysics and Space Environments, Air Force Cambridge Research Laboratories, 1965.
- Wenkert, D., "Empirical Relations Between the Earths Radiation Budget, Cloudiness and Various Meteorological Parameters," Ph.D. Thesis, Cal. Inst. of Tech., October 1985.
- Whitney, C., and H. Malchow, "Study of Radiative Transfer in Scattering Atmospheres," AFGL-TR-78-0101, June 1977.
- Williams, S.L. and D.G. Acheson, "Thermal Time Constant of U.S. Radiosonde Sensors Used in GATE," NOAA TM-EDS-CEDDA-7, May 1976.

APPENDICES

APPENDIX 1: AVERAGE PRESENTED AREA, AND FRACTIONAL PERCENTAGE OF MAXIMUM IRRADIATION OF THERMISTOR

The amount of energy coming from a fixed direction (θ, ϕ) that irradiates a cylindrical thermistor oriented parallel to the earth's surface depends upon the elevation angle θ and the azimuth angle, ϕ' of the thermistor relative to the azimuth, ϕ , of the incoming radiation. For convenience the azimuth ϕ of incoming radiation can be taken as 0. The geometry is shown in Figure A1.1. The line \overline{OL} represents the length of the thermistor ℓ . The line \overline{LP} is the projected length of the thermistor in the direction of the incoming irradiation $(\theta, 0)$. For a cylindrical thermistor of radius r the projected width of the thermistor in the direction $(\theta, 0)$ is $2r$. Thus, the thermistor receives radiation over $A_p = 2r \times \overline{LP}$ from the direction $(\theta, 0)$.

The length of LP is:

$$\overline{LP} = \ell \sin \gamma = \ell \left[\cos^2 \phi' + \sin^2 \phi' \cos^2 \theta \right]^{1/2}$$

The average (projected) area A_p of sunlight intercepted by the thermistor over one rotation of the thermistor is:

$$\overline{A}_p(\theta) = \frac{2r\ell}{\pi} \int_0^\pi \left[\cos^2 \phi' + \sin^2 \phi' \cos^2 \theta \right]^{1/2} d\phi'$$

The fraction of the maximum thermistor cross-section that the parameter A_p takes on as a function of θ is:

$$F_r(\theta) = \frac{1}{\pi} \int_0^\pi \left[\cos^2 \phi' + \sin^2 \phi' \cos^2 \theta \right]^{1/2} d\phi'$$

Thus, $1 - F_r(\theta)$ is the percent reduction in the irradiance of the thermistor, from its maximum value, versus elevation angle. Note that the maximum occurs $F_r(0^\circ) = 1$ when irradiation impinges from the vertical direction. Figure A1.2 shows the graph of $F_r(\theta)$. The average projected area of the thermistor is derived from Figure A1.2 as:

$$\overline{A}_p(\theta) = 2r\ell F_r(\theta).$$

(Note that when these results are applied to incoming solar radiation the relationship $Z_E = \frac{\pi}{2} - \theta$ holds.)

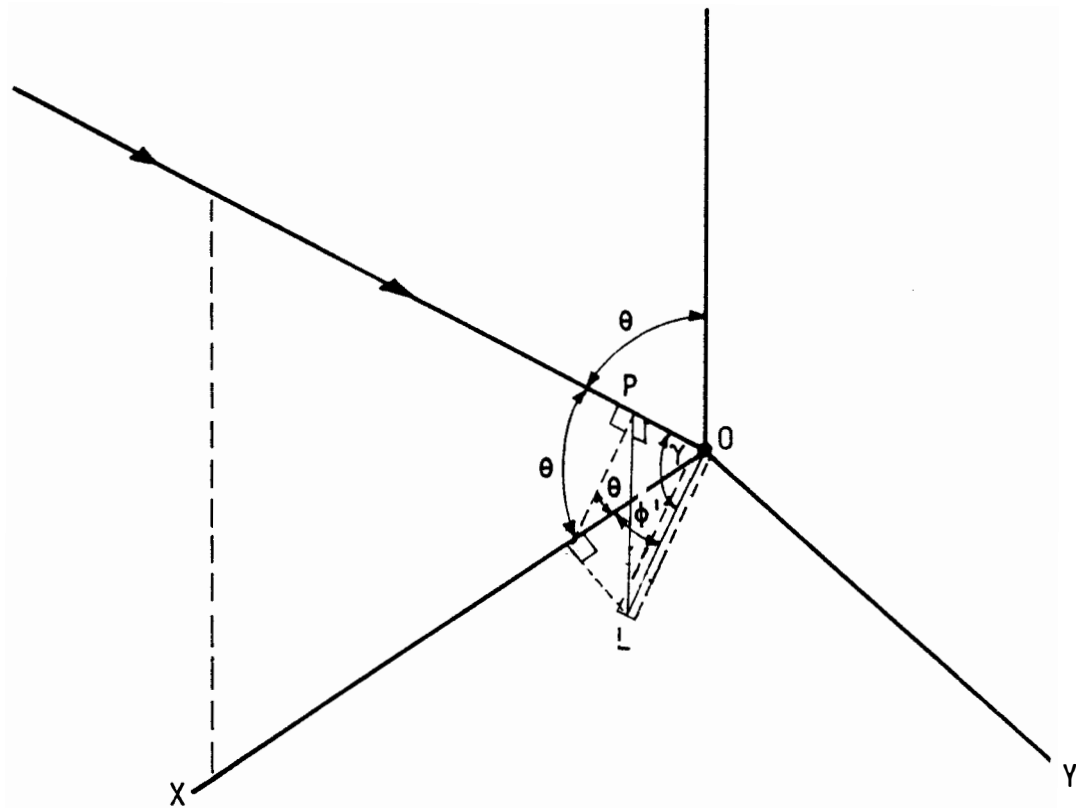


Figure A1.1 Geometry describing irradiation of the thermistor.

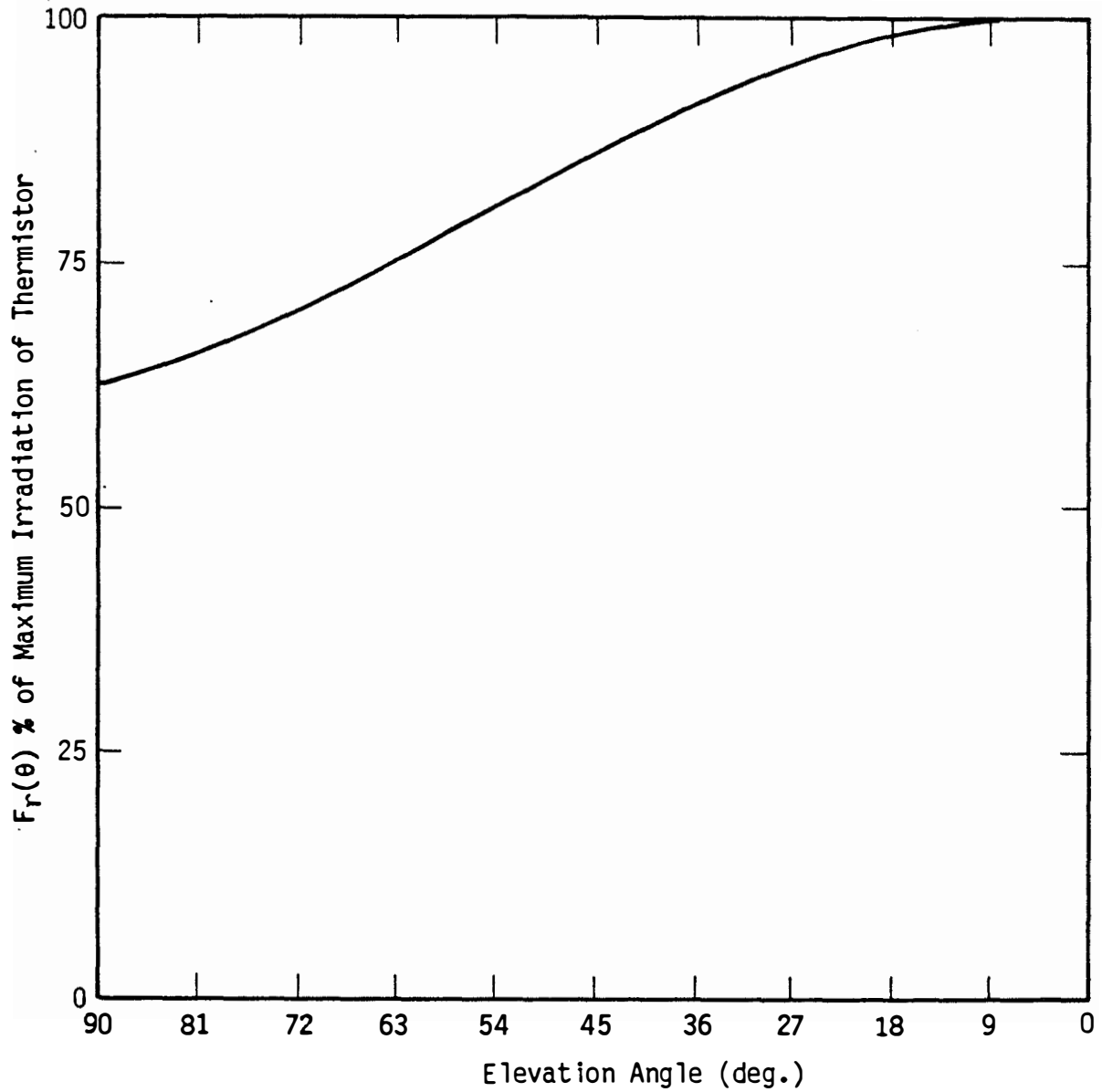


Figure A1.2 Average percent of maximum irradiation of thermistor versus elevation angle.

APPENDIX 2: ORDER OF MAGNITUDE OF TERMS IN HEAT BALANCE EQUATION

Representative values of variables (Henninger (1984)) used in the heat transfer equations are shown in Table A2.1. These values are used in the following calculations to estimate the magnitude of the various terms.

Thermistor Heat Balance Equation

a) Time rate of change

$$mC \frac{dT}{dt}$$

Assume net flux of 1×10^{-2} cal/sec then,

$$1.68 \times 10^{-2} \frac{dT}{dt} = 10^{-2}$$

$$\frac{dT}{dt} = 0.6^\circ \text{ K/sec}$$

b) Absorption

Solar (0.25 - 2.5 μ) and infrared (2.5-40 μ)

$$\text{max solar} = (I_0 + \frac{1}{2} I_0) 2\pi r l F_r \alpha,$$

F_r , Solar angle dependent rotation factor, = 0.8 at $Z_E = 30^\circ$

$$q_{\text{abs}} = 2.88 \times 10^{-3} \text{ cal/sec (maximum)}$$

Infrared (2.5-40 μ) absorption

$$q_{\text{abs}} = \sigma T_E^4 2\pi r(r+l) \epsilon, \quad T_E = \text{Equivalent blackbody background temperature}$$

$$q_{\text{abs}} = 6.96 \times 10^{-3} \text{ cal/sec } (T_E = 250^\circ \text{ K) maximum}$$

$$q_{\text{abs}} = 2.32 \times 10^{-3} \text{ cal/sec } (T_E = 190^\circ \text{ K) minimum}$$

c) Emission

$$q_{\text{emis}} = -2\pi (r l + r^2) \sigma T^4 \epsilon n$$

$$q_{\text{emis}} = 1.44 \times 10^{-2} \text{ cal/sec } (T = 300^\circ \text{ K) maximum}$$

$$q_{\text{emis}} = 2.85 \times 10^{-3} \text{ cal/sec } (T = 200^\circ \text{ K) minimum}$$

d) Convection: Sides of Cylindrical Thermistor

$$q_{\text{conv}} = -2\pi r l h_c (T - T_\infty)$$

Table A2.1: Typical and Extreme Value of Variables Used in Order of Magnitude Analysis

Variable	Value
m	0.12 g
C	0.14 cal/g °C
r	0.06 cm
ℓ	4 cm
σ	1.354×10^{-12} cal/sec cm ² °K ⁴
ε	0.86
η	1.0
h _C	4 X 10 ⁻³ cal/s cm ² at surface (Nu = 10) 6.8 X 10 ⁻⁴ cal/s cm ² at 30 Km (Nu = 1.7)
T - T _∞	3° K (maximum)
\dot{z}	5 m/sec
E	18 volts
R	12,000 ohms (+40° C) → 3,500,000 ohms (-70° C)
R _f	1,000,000 ohms
r _w	0.0125 cm
k _w	0.92 cal/sec cm °K
$\frac{dl_w}{d\ell}$	5°/cm (max)
ρ _w	8.9 g/cm ³ (copper)
C _w	0.093 cal/g °K (copper)
ε _w	0.06 (tin coating)
R _w	0.0035 ohm/cm
h _{CW}	1.92 X 10 ⁻² cal/s cm ² at surface (Nu = 10) 3.26 X 10 ⁻³ cal/s cm ² at 30 Km (Nu = 1.7)
T	300° K (maximum) 200° K (minimum)
h _d	2 X 10 ⁻³ cal/s cm (Nu = 5)
I ₀	3335 X 10 ⁻² cal/cm ² sec
α _{S1}	0.15
α _w	0.08 (tin coating)

$q_{\text{conv}} = 3.08 \times 10^{-3}$ cal/sec at 30 Km (maximum occurs at 30 Km, near the surface h_c is larger)

Ends of Cylinder $-2\pi r^2 h_d (T - T_\infty)$

$q_{\text{conv}} = 4.62 \times 10^{-5}$ cal/sec

Note that $\frac{q_{\text{conv}} (\text{sides})}{q_{\text{conv}} (\text{walls})} = 0.015$.

Thus only 1.5% of the convective transfer occurs through the end plates.

c) Electrical Heating

$q_{\text{elect}} = \frac{E^2 R}{(R_f + R)^2}$ assume fixed resistor is 1,000,000 ohms

At 310° K

$q_{\text{elect}} = 9.1 \times 10^{-7}$ cal/sec (negligible)

At -200° K

$q_{\text{elect}} = 1.34 \times 10^{-5}$ cal/sec (negligible)

f) Conduction Lead Wires

$2\pi r_w^2 k_w \frac{dT_w}{d\ell} \Big|_{\ell=0}$

Assume $\frac{dT_w}{d\ell} = 5^\circ/\text{cm}$ (max)

$q_{\text{cond}} = 1.05 \times 10^{-1}$ cal/sec (maximum)

Lead Wire Heat Balance

a) Time rate of change

$\pi r_w^2 \rho_w C_w \frac{dT}{dt} = 4.11 \times 10^{-4} \frac{dT}{dt}$

b) Absorption

q_{abs}^i

max Solar $(I_0 + \frac{1}{2} I_0) 2r_w F_r \alpha_w$

$q_{\text{abs}}^i = 8 \times 10^{-5}$ cal/cm sec (max solar abs $Z_E = 30^\circ$,

albedo = 0.5 $\alpha_w = 0.08$)

Longwave Absorption

$q_{\text{abs}} = \sigma T_E^4 2\pi r_w \epsilon_w$

$$q_{\text{abs}} = 1.67 \times 10^{-5} \text{ cal/sec cm } (T_E = 250^\circ \text{ K}) \text{ maximum}$$

$$q_{\text{abs}} = 5.54 \times 10^{-6} \text{ cal/sec cm } (T_E = 190^\circ \text{ K}) \text{ maximum}$$

c) Emission

$$q_{\text{emis}} = -2\pi r_w \epsilon_w \sigma T_w^4$$

$$q_{\text{emis}} = 3.34 \times 10^{-5} \text{ cal/sec cm } (T = 300^\circ \text{ K}) \text{ maximum}$$

$$q_{\text{emis}} = 6.7 \times 10^{-6} \text{ cal/sec cm } (T = 200^\circ \text{ K}) \text{ minimum}$$

d) Convection

$$q_{\text{conv}} = -2\pi r_w h_{cw} (T_w - T_\infty)$$

$$q_{\text{conv}} = 7.68 \times 10^{-4} \text{ cal/sec cm at 30 Km, maximum}$$

e) Conduction

$$q_{\text{cond}} = -\pi r_w^2 k_w \frac{dT_w}{d\ell}$$

$$\text{assume } \frac{dT_w}{d\ell} = 1^\circ \text{ K/cm, (maximum)}$$

$$q_{\text{cond}} = 4.5 \times 10^{-4}, \text{ maximum}$$

f) Electrical

$$q_{\text{elect}} = I^2 R_w = \frac{E^2}{(R_f + R)^2} R_w$$

At 310° K

$$q_{\text{elect}} = 2.16 \times 10^{-11} \text{ cal/cm sec (negligible)}$$

At -200° K

$$q_{\text{elect}} = 2.09 \times 10^{-14} \text{ cal/cm sec (negligible)}$$

APPENDIX 3: SOLID ANGLE INCREMENTS OF SPHERE

A solid angle Ω , in steradians, is defined in terms of the surface area contained within the angle at a distance r from its vertex as:

$$\Omega = \frac{\text{AREA}}{r^2}$$

The solid angle from the center of a sphere encompassing the entire sphere (i.e., all directions) is:

$$\Omega_{\text{sp}} = \frac{4\pi r^2}{r^2} = 4\pi \text{ steradians}$$

Thus, there are 4π steradians in a sphere. If a sphere is divided into bands of latitude, and incoming radiation assumed constant for each latitude band, then the total radiation, irradiating the center of the sphere is determined by summing the radiation from each latitude band relative to the contribution of that band to the total 4π steradians of the sphere.

The area of a spherical segment is given by:

$$A = 2\pi r h$$

where

r = the sphere radius

h = distance between chord line and sphere surface along the bisector.

Thus,

$$h = r - r \cos \gamma$$

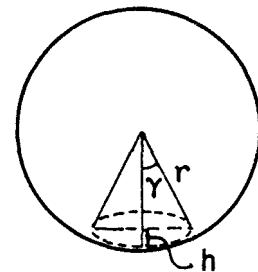
or

$$A = 2\pi r^2 (1 - \cos \gamma)$$

Evaluating the solid angle for latitude bands defined as:

$$\begin{aligned} \gamma_0 &= 0 \leq \gamma < 15^\circ \\ \gamma_{30} &= 15 \leq \gamma < 45^\circ \\ \gamma_{60} &= 45 \leq \gamma < 75^\circ \\ \gamma_{90} &= 75 \leq \gamma < 105^\circ \\ \gamma_{120} &= 105 \leq \gamma < 135^\circ \\ \gamma_{150} &= 135 \leq \gamma < 165^\circ \\ \gamma_{180} &= 165 \leq \gamma < 180^\circ \end{aligned}$$

gives



$$\Omega_0 = 2\pi (1 - \cos 15^\circ) = 0.214 = \Omega_{180^\circ}$$

$$\Omega_{30} = 2\pi \left[(1 - \cos 45^\circ) - (1 - \cos 15^\circ) \right] = 1.626 = \Omega_{150^\circ}$$

Similarly,

$$\Omega_{60} = \Omega_{120} = 2.817$$

$$\Omega_{90} = 3.252$$

Summing

$$2(\Omega_0 + \Omega_{30} + \Omega_{60}) + \Omega_{90} = 4\pi$$

APPENDIX 4: INFLUENCE OF THE BALLOON ON RADIOSONDE TEMPERATURE ERROR

A4.1 Irradiation of the Thermistor From the Balloon

The purpose of this section of the report is to derive the equations necessary to calculate the heating rate of the thermistor due to radiation emitted and reflected from the surface of the balloon. These equations are then evaluated and compared with the total thermistor heating from all sources to see if the balloon influence can be ignored in the heat transfer analysis.

The heating rate of the thermistor due to radiation emitted from and reflected off the balloon can be written in terms of the notation of Equation 3.5 and 3.6 as:

$$q_{b \rightarrow th} = \int_{\lambda} \alpha(\lambda) \int_{\Omega_b} \bar{A}_p(\theta) I_b(\theta, \phi, \lambda) \sin \theta d\theta d\phi d\lambda \quad (A4.1)$$

$$\text{where } \bar{I}_b(\theta, \lambda) = \frac{1}{\pi} \int_0^{\pi} I_b(\theta, \phi, \lambda) d\phi$$

The integration is performed over the solid angle encompassing the thermistors view of the balloon. The difficulty in directly evaluating Equation A4.1 arises in deriving the intensity $I_b(\theta, \phi, \lambda)$ of the radiation from the balloon to the thermistor in terms of reflected atmospheric radiation $I^*(\theta, \phi, \lambda)$ and the radiation emitted by the balloon. In this section we derive a method for evaluating the heating rate of the thermistor due to radiation from the balloon (Equation A4.1), using exchange factors.

The radiosonde thermistor exchanges radiation with the balloon as shown in Figure A4.1. If the balloon is of radius r_b and the tether length to the radiosonde S , then the angle ξ is given by:

$$\cos \xi = \frac{[(S + r_b)^2 - r_b^2]^{\frac{1}{2}}}{S + r_b} \quad (A4.2)$$

The chord length $2c$ is given by:

$$2c = 2r_b \cos \xi \quad (A4.3)$$

The thermistor exchanges radiation with less than half of the balloon. The thermistor's view of the balloon is that of a disc of radius C . In calculating the radiation exchange between the thermistor and balloon the following assumptions are made.

- o The balloon emits as a gray body at uniform temperature T_b .
- o The emissivity of the balloon, ϵ_b , is constant for any value of T_b .

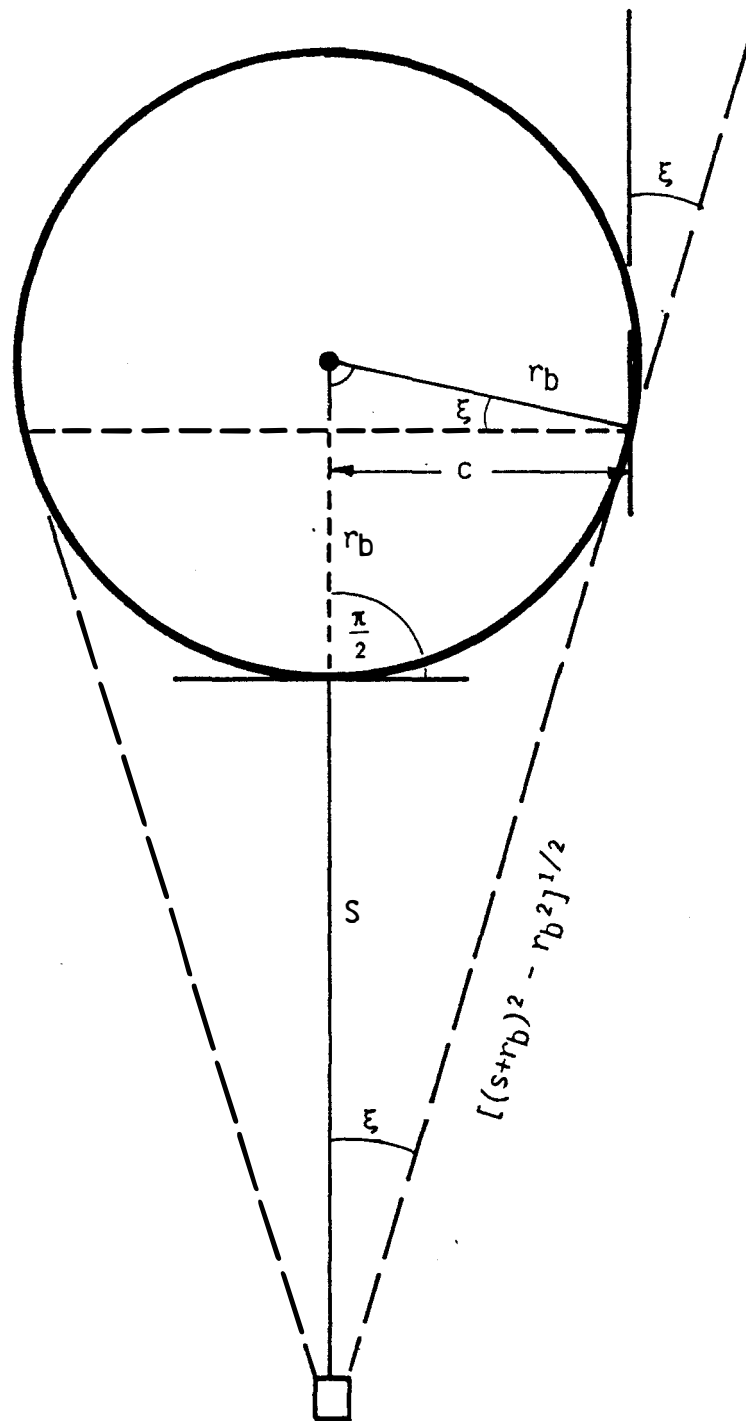


Figure A4.1 Geometry of balloon and thermistor.

o $\rho_b(\lambda)$ the reflectivity of the balloon is such that:

$$\rho_b = \rho_b(\lambda) \text{ for } 0.25 \leq \lambda \leq 2.5\mu$$

$$\rho_b = \text{constant for } 2.5 \leq \lambda \leq 40\mu$$

o The balloon is a diffuse reflector for all λ ($0.25 \leq \lambda \leq 40\mu$)

o The emissivity of the thermistor ϵ is constant for $2.5 \leq \lambda \leq 40\mu$

o The absorptivity of the thermistor, $\alpha(\lambda)$ is a function of λ for $0.25 \leq \lambda \leq 2.5\mu$.

The radiation emitted by the balloon that is absorbed by the thermistor is:

$$q_{em} = 4\pi r_b^2 \epsilon_b \sigma T_b^4 \epsilon F_{b \rightarrow th} \quad (A4.4)$$

where,

$4\pi r_b^2$ = the surface area of the balloon

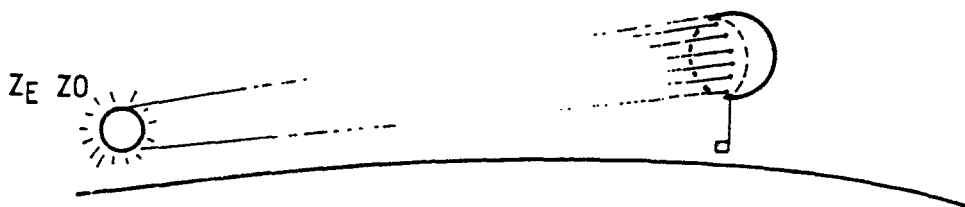
$F_{b \rightarrow th}$ = exchange factor between the balloon and thermistor.

In this formulation the entire surface area of the balloon is assumed to be emitting and the exchange factor is the percentage of the total emissions that irradiate the thermistor.

An approximating approach is used to assess the reflected radiation from the balloon surface that strikes the thermistor.

The radiation reflected off the balloon that irradiates the thermistor is divided into two components - the direct solar reflected component and the diffuse reflected component (solar and infrared). A maximum in direct reflected solar energy irradiates the thermistor when the solar elevation angle is zero as shown in the sketch below. In this case, depending on balloon altitude, slightly over one-half of the balloon area visible to the thermistor is receiving direct solar radiation. For simplicity, consider this case. The heating rate of the thermistor due to balloon reflector direct solar radiation then is:

$$q_{sb} = \pi r_b^2 F_{b \rightarrow th} \int_{\lambda} \alpha(\lambda) \rho_b(\lambda) I_0(\lambda) d\lambda \quad (Z_E = 0) \quad (A4.5)$$



The factor $I_0(\lambda)\pi r_b^2$ is the solar energy intercepted by the balloons' cross-sectional area. For the case of a low (near zero) solar elevation angle, the sun's rays are parallel to the axis of the thermistor. In this case the sun's irradiation of the balloon bisects the thermistor view of the balloon and the exchange factor for the entire balloon to the thermistor is identical to that for half the view. At a high solar elevation $Z_E \geq \pi/2 - \xi$ (see Figure A4.1), the thermistor is not in view of any part of the balloon exposed to direct solar radiation as shown in Figure A4.2. At some intermediate solar elevation angle, Z_E , we approximate the balloon reflected direct solar radiation that is absorbed by the thermistor by cosine interpolation as:

$$q_{sb} = \pi r_b^2 \cos Z_E F_{b \rightarrow th} \int_{\lambda} \alpha(\lambda) \rho_b(\lambda) I_0(\lambda) d\lambda \quad (A4.6)$$

The diffuse irradiation of the balloon that is reflected from its surface and absorbed by the thermistor is divided into two wavelength region. A shortwave solar region $0.25 \leq \lambda \leq 2.5\mu$ in which the reflection and absorption coefficients are a function of wavelength and the infrared region $2.5 \leq \lambda \leq 40\mu$ in which the absorption (emission) and reflection coefficients are constant. Consider first the diffuse solar radiation that is reflected off the balloon surface and absorbed by the thermistor. Most of the scattering and reflection of solar radiation that makes up the diffuse component occurs in the first few kilometers of the atmosphere - below the altitudes of interest for the radiosonde temperature error problem. Thus, at altitudes of interest it is assumed that the diffuse solar energy is upwelling radiation that irradiates only the lower half of the balloon. The intensity of this radiation is approximated by specifying the earth's albedo $AL(\lambda)$. That is, assume upwelling radiation of power $AL(\lambda)I_0(\lambda)$ irradiates the underside of the balloon. The heating rate of the thermistor due to diffuse solar radiation reflecting off the balloon and absorbed by the thermistor is approximately:

$$q_{sdb} \approx \pi c^2 F_{b \rightarrow th}^* \int_{0.25}^{2.5} \alpha(\lambda) \rho_b(\lambda) AL(\lambda) I_0(\lambda) d\lambda \quad (A4.7)$$

where πc^2 is the cross-sectional area of the balloon visible to the thermistor and $F_{b \rightarrow th}^*$ is the exchange factor between the balloon area visible to the thermistor, and the thermistor.

The diffuse component of infrared radiation ($2.5 \leq \lambda \leq 40\mu$) reflected from the balloon that irradiates the thermistor is also analyzed using an approximation technique. We assume the infrared radiation impinging upon the balloon surface consists of upwelling blackbody radiation at temperature T_u , and downwelling blackbody radiation at temperature T_d (Tam and Corriveau (1976), and Unsworth and Monteith (1975)). The bottom most point, P_b , (see Figure A4.2) on the sphere is exposed only to radiation from below. The energy irradiating an incremental area dA_p surrounding the point P is:

$$dq_p = dA_p \sigma T_u^4 \epsilon \quad (A4.8)$$

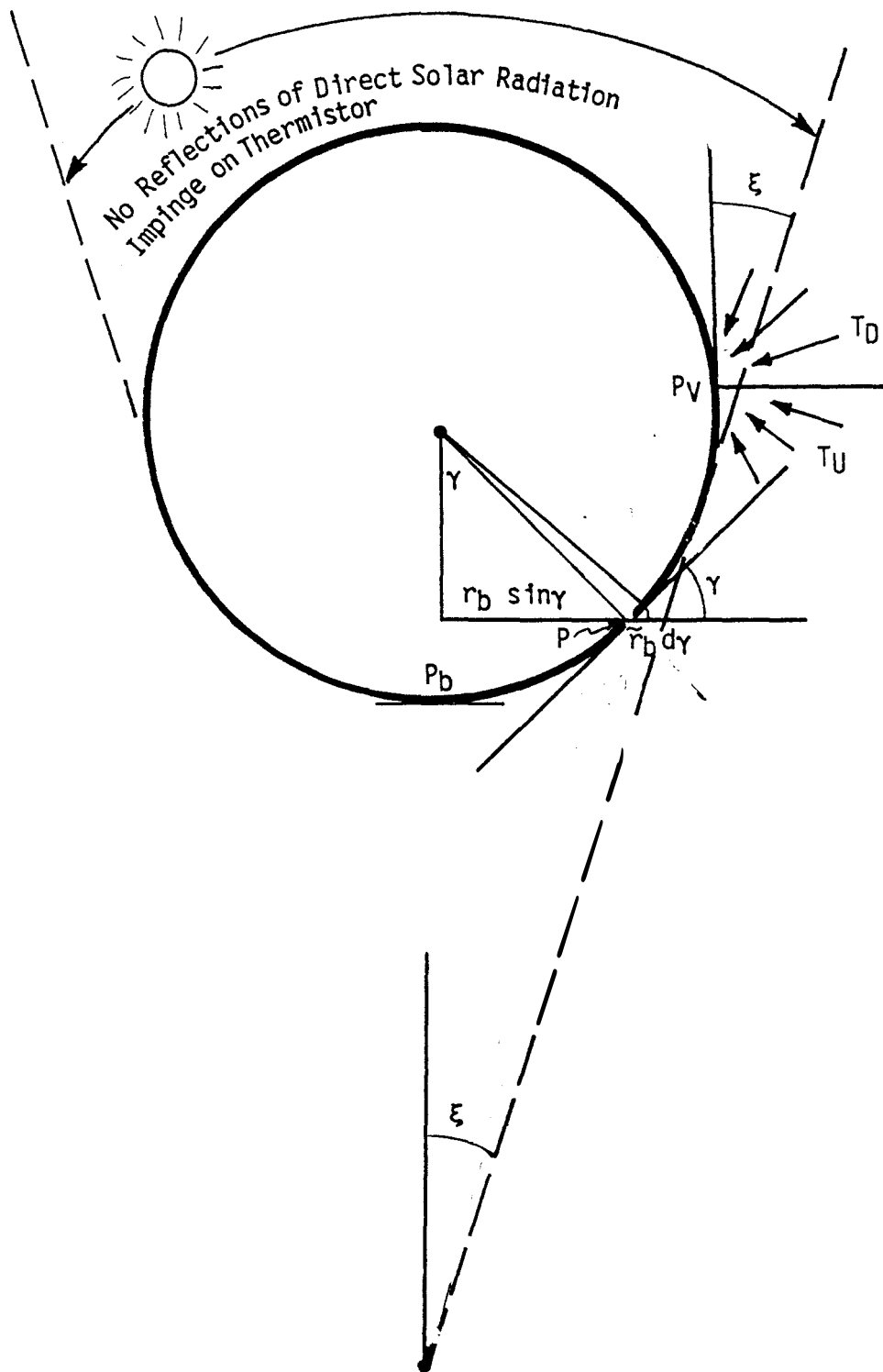


Figure A4.2 Geometry for reflections off balloon.

A point on the sphere whose tangent plane is vertical is irradiated equally by upwelling and downwelling radiation. The energy irradiating on incremental area surrounding the point P_V is:

$$dq_V = dA_V \sigma (T_U^4 + T_D^4)/2 \quad (\text{A4.9})$$

Summing incrementally a width $r_b d\gamma$ about the circumference of the balloon gives a circumferential irradiation of:

$$dq_{A_V} = 2\pi r_b^2 \sigma d\gamma (T_U^4 + T_D^4)/2 \quad (\text{A4.10})$$

If a point is located arbitrarily on the lower segment of the balloon visible to the thermistor, such that its tangent plane makes the angle γ with the vertical (see Figure A4.2), then the irradiation of a circumferential slice of surface area about the point P can be approximated by a sinusoidal variation between the points P_b and P_V as:

$$dq_A \approx 2\sigma\pi r_b^2 \sin\gamma d\gamma \left[\frac{1}{2} T_D^4 \sin \gamma + T_U^4 \left(1 - \frac{1}{2} \sin \gamma\right) \right] \quad (\text{A4.11})$$

Integrating over the appropriate limits of γ that define the segment of the balloon visible to the thermistor gives the total irradiance of the balloon (visible to the thermistor) from upwelling and downwelling radiation as:

$$q = 2\pi r_b^2 \sigma \int_0^{\frac{\pi}{2} - \xi} \left(\frac{1}{2} T_D^4 \sin^2 \gamma + T_U^4 \sin \gamma - \frac{1}{2} T_U^4 \sin^2 \gamma \right) d\gamma \quad (\text{A4.12})$$

Integration gives:

$$q = 2\pi r_b^2 \sigma \left\{ \frac{1}{2} T_D^4 \left[\frac{1}{2} \left(\xi - \frac{\pi}{2} \right) + \frac{1}{4} \sin(\pi - 2\xi) \right] - T_U^4 \left(1 - \cos \left(\frac{\pi}{2} - \xi \right) \right) - \frac{1}{2} T_U^4 \left[\frac{1}{2} \left(\xi - \frac{\pi}{2} \right) + \frac{1}{4} \sin(\pi - 2\xi) \right] \right\} \quad (\text{A4.13})$$

The infrared energy reflected off the balloon that is absorbed by the thermistor is:

$$q_{db} = 2\pi r_b^2 \sigma F_{b \rightarrow th}^* (1 - \epsilon_b) \epsilon \left\{ (T_U^4 - T_D^4) \left(\frac{1}{4} \xi - \frac{\pi}{8} + \frac{1}{8} \sin(\pi - 2\xi) \right) + T_U^4 \left(1 - \cos \left(\frac{\pi}{2} - \xi \right) \right) \right\} \quad (\text{A4.14})$$

where $F_{b \rightarrow th}^*$ is the exchange factor between the balloon area visible to the thermistor and the thermistor and $(1 - \epsilon_b) = \rho_b$ is the infrared reflectivity of the balloon. The exchange factors $F_{b \rightarrow th}$ and $F_{b \rightarrow th}^*$, defined in terms of total surface area and that visible to the thermistor are related through the equation:

$$F_{b \rightarrow th}^* = \frac{4\pi r_b^2}{A_{vis}} F_{b \rightarrow th} \quad (A4.15)$$

where A_{vis} is the balloon area visible to the thermistor. A_{vis} is evaluated utilizing the geometry of Figure A4.2 as:

$$A_{vis} = 2\pi r_b^2 \int_0^{\frac{\pi}{2} - \xi} \sin \gamma d\gamma = 2\pi r_b^2 (1 - \cos(\frac{\pi}{2} - \xi)) \quad (A4.16)$$

Thus,

$$F_{b \rightarrow th}^* = \frac{2}{1 - \cos(\frac{\pi}{2} - \xi)} F_{b \rightarrow th} \quad (A4.17)$$

Combining the solar direct, solar diffuse, diffuse infrared, and emission heating terms, the total heating of the thermistor from radiation emitted from the balloon surface, as well as radiation reflected from the balloon surface and absorbed by the thermistor is given as:

$$\begin{aligned} q_b = & 4\pi r_b^2 \epsilon_b \sigma T_b^4 \epsilon F_{b \rightarrow th} + \pi r_b^2 \cos Z_E F_{b \rightarrow th} \int_{\lambda} \alpha(\lambda) \rho_b(\lambda) I_0(\lambda) d\lambda \\ & + \pi c^2 F_{b \rightarrow th}^* \int_{0.25}^{2.5} \alpha(\lambda) \rho_b A L(\lambda) I_0(\lambda) d\lambda \\ & + 2\pi r_b^2 \sigma (1 - \epsilon_b) \epsilon F_{b \rightarrow th}^* \left[(T_u^4 - T_d^4) \left(\frac{1}{4} \xi - \frac{\pi}{8} + \frac{1}{8} \sin(\pi - 2\xi) \right) \right. \\ & \left. + T_u^4 (1 - \cos(\frac{\pi}{2} - \xi)) \right] \quad (A4.18) \end{aligned}$$

where

$F_{b \rightarrow th}$ = Exchange factor from balloon to thermistor

$F_{b \rightarrow th}^*$ = Exchange factor from balloon in view of thermistor to thermistor

We now derive an expression for the exchange factors $F_{b \rightarrow th}$ and $F_{b \rightarrow th}^*$.

A4.2 Exchange Factor Balloon to Thermistor

Consider the thermistor to be suspended from the balloon at a string length, S , from the balloon of radius r_b as shown in Figure A4.1. The thermistor can be considered as an infinitesimal area in that the geometry of any point on the thermistor visible to the balloon is identical with respect to the balloon. The radiant power from the balloon to the thermistor is that intercepted by a flat plate, parallel to the earth, at the location of the thermistor having area essentially equal to the cross-sectional area of the thermistor. This radiant power is given by:

$$q_{th} = B A_b F_{b \rightarrow th} \quad (A4.19)$$

where

B = Radiosity of balloon

A_b = Area of balloon

$F_{b \rightarrow th}$ = Exchange factor of balloon with thermistor, i.e., percent of radiant power from entire balloon surface that strikes a thermistor.

The exchange factor $F_{b \rightarrow th}$ can most easily be derived using reciprocity.

From reciprocity

$$A_b F_{b \rightarrow th} = A_b F_{b \rightarrow FP} = A_{FP} F_{FP \rightarrow b} \quad (A4.20)$$

where

A_{FP} = Area of flat plate at location of thermistor having area equal to cross-sectional area of thermistor

$F_{b \rightarrow FP}$ = Exchange factor between balloon and flat plate at thermistor location

The first equality states that the irradiation of the thermistor is the same as that for a flat plate of area equal to that of the thermistor cross-section at the location of the thermistor. The second equality defines reciprocity between the flat plate and the balloon.

The exchange factor from an infinitesimal flat plate of area dA , to a sphere a radius r_b , a distance S away titled at an angle Λ is given in Kreith (1962), Appendix V, p. 214, Configuration 33 as:

$$F_{dA \rightarrow b} = \cos \Lambda \left(\frac{r_b}{S + r_b} \right)^2 \quad (A4.21)$$

Since every infinitesimal area dA on the thermistor is assumed to have the same orientation with respect to the balloon, the exchange factor from the flat plate of finite area onto the balloon is the same as that for an infinitesimal segment. That is, the percent radiation from an infinitesimal flat plate projection of a thermistor element onto the balloon is equal to the percent radiation from a flat plate (finite) area equal to the cross-sectional area of the thermistor onto the balloon.

Thus for $\Lambda = 0$

$$F_{FP \rightarrow b} = \left(\frac{r_b}{S + r_b} \right)^2 \quad (A4.22)$$

Using reciprocity

$$F_{b \rightarrow th} = \frac{A_{FP}}{A_b} F_{FP \rightarrow b}$$

Thus

$$F_{b \rightarrow th} = \frac{2r\ell}{4\pi r_b^2} \left[\frac{r_b}{S + r_b} \right]^2 \quad (A4.23)$$

The exchange factor $F_{b \rightarrow th}^*$ that provides the percent radiation from the lower segment of the balloon visible to the thermistor, to the thermistor is derived from Equation A4.17 as:

$$F_{b \rightarrow th}^* = \frac{r\ell}{(1 - \cos(\frac{\pi}{2} - \xi)) \pi(S + r_b)^2} \quad (A4.24)$$

The exchange factors $F_{B \rightarrow th}^*$ and $F_{B \rightarrow th}$ are evaluated for representative balloon diameters in the following section.

A4.3 Evaluation of Exchange Factor From Balloon to Thermistor

The balloon expands as it rises through the atmosphere until near 30 Km (or above) the balloon bursts. Assuming the original inflation diameter of the balloon to be 2 meters and assuming the internal pressure of the balloon is essentially equal to the exterior pressure, the balloon diameter can be calculated as a function of altitude assuming a standard atmosphere pressure profile.

At the surface: $P = 1013 \text{ mb}$

$$V = \frac{4}{3} \pi (r_b)^3 = 4.17 \text{ m}^3$$

$$T = 290^\circ \text{ K}$$

From the equation of state, where the subscripts denote altitude in Km:

$$\frac{PV}{T} = \frac{P_{20}V_{20}}{T_{20}} = \frac{P_{25}V_{25}}{T_{25}} = \frac{P_{30}V_{30}}{T_{30}} \quad (A4.25)$$

Assuming the 1966 Standard Atmosphere Mid-Latitude values of temperature and pressure and solving the above equation for the balloon radius at 20, 25, and 30 Km gives:

$$r_{20} = 2.3 \text{ m}$$

$$r_{25} = 3.1 \text{ m}$$

$$r_{30} = 4.0 \text{ m}$$

From Equation A4.23 the exchange factor from the balloon to the thermistor is:

$$F_{b \rightarrow th} = \frac{2r\ell}{4\pi r_b^2} = \left[\frac{r_b}{S + r_b} \right]^2 \quad (A4.26)$$

The exchange factor is evaluated at different altitudes with appropriate balloon radius and a representative string length of 10 m. The resulting values of the exchange factor are:

$$F_{b \rightarrow th} = 3.47 \times 10^{-7} \text{ (surface)}$$

$$F_{b \rightarrow th} = 3.10 \times 10^{-7} \text{ (20 Km)}$$

$$F_{b \rightarrow th} = 2.92 \times 10^{-7} \text{ (25 Km)}$$

$$F_{b \rightarrow th} = 2.73 \times 10^{-7} \text{ (30 Km)}$$

A4.4 Atmospheric Radiation Shielded by Balloon

The balloon acts as a shield for atmospheric radiation coming from the direction above the balloon as seen in Figure A4.3. This shielded radiating term, if significant, can be subtracted from Equation 4.18 to determine the net thermistor heating due to the thermistor exchange with the balloon. This term is negative and employing the same assumptions as previously with $A_{fp} \approx 2r_l$ gives:

$$q_{sh/b} = -2r_l \int_{\lambda} \alpha(\lambda) \int_{\Omega_b} \cos \theta I^*(\theta, \phi, \lambda) \sin \theta \, d\theta d\phi d\lambda \quad (A4.27)$$

This term is evaluated by establishing the integration limits for the solid angle Ω_b between the balloon and thermistor as shown in Figure A4.3.

Equation A4.27 is used to calculate the radiant power contained in the solid angle defined in Figure A4.3.

where

$$r^* = \left[(s + r_b)^2 - r_b^2 \right]^{1/2}$$

$$d\Omega = \frac{dA}{r^2} = \sin \theta \, d\theta d\phi$$

assigning the appropriate limits

$$\theta_{max} = \tan^{-1} \left(\frac{r_b}{r^*} \right)$$

$$\theta_{min} = 0$$

$$0 \leq \phi \leq 2\pi$$

Applying these limits to the above equation gives:

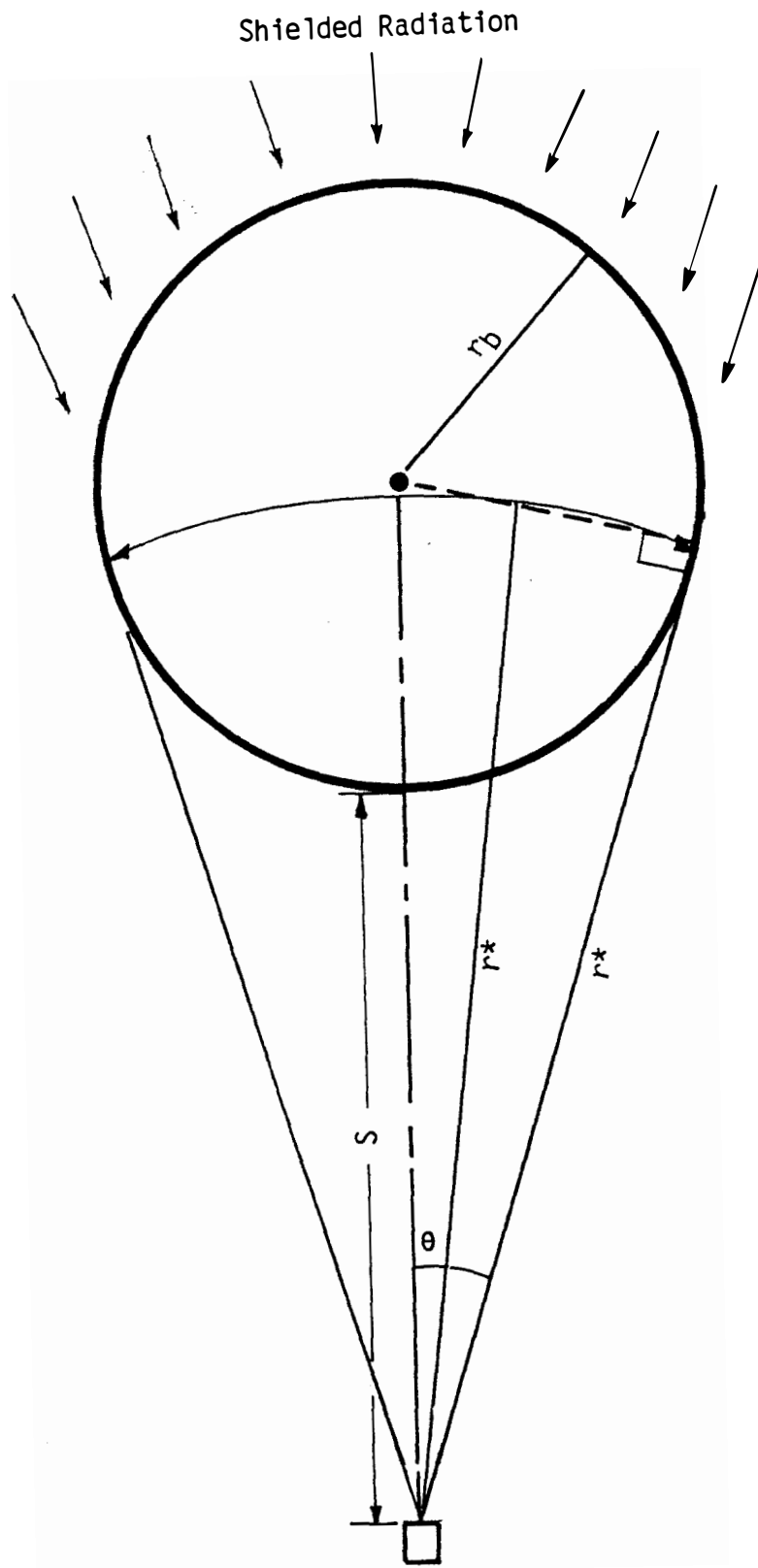


Figure A4.3 Solid angle defining thermistor view of balloon.

$$q_{sh/b} = -2r\ell \int_{\lambda} \alpha(\lambda) \int_{\phi=0}^{2\pi} \int_{\theta=0}^{\theta=\tan^{-1}(r_b/r^*)} \cos \theta I^*(\theta, \phi, \lambda) \sin \theta d\theta d\phi d\lambda$$

and assuming azimuthal symmetry in intensity within Ω_b gives:

$$q_{sh/b} = 4\pi r\ell \int_{\lambda} \alpha(\lambda) \int_{\theta=0}^{\tan^{-1}(r_b/r^*)} \cos \theta I^*(\theta, \lambda) \sin \theta d\theta d\lambda \quad (A4.28)$$

Typical values of balloon radius required for evaluating Equation A4.28 as a function of altitude and tether length were derived in the previous section.

A4.5 Influence of Balloon on Temperature of Thermistor

We now apply the results of the previous sections to calculate the balloon influence on the thermistor temperature error. The balloon influences the temperature of the thermistor because, a) the thermistor receives emitted and reflected radiation from that part of the balloon visible to the thermistor; and b) the balloon shields the thermistor from atmospheric radiation along the solid angle subtended by the balloon. The percent change in the radiation absorbed by the thermistor due to the presence of the balloon can be written as:

$$\frac{\Delta q_b}{q_{abs}} = \frac{|q_b - q_{sh/b}|}{q_{abs}} \quad (A4.29)$$

where

q_b is given by Equation A4.18, $q_{sh/b}$ by Equation A4.28 and q_{abs} given by Equation 3.5.

To establish the significance of including the balloon terms in the heat balance equations, the terms in the above equation have been evaluated for extreme cases in both day and night situations to establish the maximum influence of each term.

Nighttime Radiation

In the absence of solar radiation the radiation spectrum of interest can be restricted to $2.5 \leq \lambda \leq 40$ microns. In this wavelength region the absorptivity, emissivity and reflectivity of the thermistor, balloon and radiosonde surface are assumed independent of wavelength. The radiation emitted by the balloon that is absorbed by the thermistor is given by Equation A4.4 as:

$$q_{eb} = 4\pi r_b^2 \epsilon_b \sigma T_b^4 \epsilon F_{b \rightarrow th} \quad (A4.30)$$

The exchange factor from a balloon of radius r_b to the thermistor is given by Equation A4.23 as:

$$F_{b \rightarrow th} = \frac{2r_b}{4\pi r_b^2} \left(\frac{r_b}{S + r_b} \right)^2 \quad (A4.31)$$

Substituting into Equation A4.30 gives:

$$q_{eb} = 2r_b \epsilon_b \sigma T_b^4 \epsilon \left(\frac{r_b}{S + r_b} \right)^2 \quad (A4.32)$$

Evaluating q_{eb} at 30 Km with $r_b = 4.0$ m, $S = 10.0$ m, $220^\circ \text{ K} \leq T_b \leq 240^\circ \text{ K}$ and $\epsilon = 0.86$ gives:

$$9.6 \times 10^{-5} \leq q_{eb} \leq 1.36 \times 10^{-4} \text{ cal/sec}$$

as the magnitude of the balloon emission term.

The magnitude of the reflected radiation term is calculated by assuming that the underside of the balloon is uniformly exposed to upwelling black body radiation at the surface temperature of the earth and downwelling black body radiation at $T_d = 200^\circ \text{ K}$. The infrared energy reflected from the underside of the balloon and absorbed by the thermistor is deduced from Equation A4.14 to be:

$$q_{db} = 2\pi r_b^2 \sigma \epsilon (1 - \epsilon_b) \left[(T_u^4 - T_d^4) \left(\frac{\xi}{4} - \frac{\pi}{8} + \frac{1}{8} \sin(\pi - 2\xi) \right) + T_u^4 (1 - \cos(\frac{\pi}{2} - \xi)) \right] F_{b \rightarrow th}^* \quad (A4.33)$$

where

$$\cos \xi = \frac{\left[(S + r_b)^2 - r_b^2 \right]^{\frac{1}{2}}}{S + r_b}$$

and the balloon is assumed to be opaque in the infrared and a diffuse reflector with reflectivity $\rho_b = (1 - \epsilon_b)$. The above equation is evaluated at 30 Km for its maximum influence with $T_u = 300^\circ \text{ K}$ and

$\xi = 0.29$ radians (16.5°) as:

$$q_{db} = 5.4 \times 10^{-5} \text{ cal/sec}$$

The magnitude of the balloon emission and reflected infrared radiation terms can be compared with representative values of the total nighttime thermistor irradiation q_{abs} under different environmental conditions as derived from the LOWTRAN 6 program. The calculations from the LOWTRAN 6 program assumed that the thermistor was irradiated only by atmospheric radiation from all spherical directions. For a

mid-latitude location, the range of infrared flux absorbed by the radiosonde thermistor under minimal radiation winder conditions to maximal summer conditions has been calculated using LOWTRAN 6 runs as:

$$2.0 \times 10^{-3} \leq q_{\text{abs}} \leq 4.0 \times 10^{-3} \text{ cal/sec}$$

The combined maximum influences of nighttime radiation both emitted and reflected from the balloon, that is absorbed by the thermistor, obtained by summing the previous results is:

$$q_b = 1.90 \times 10^{-4} \text{ cal/sec}$$

Thus, the maximum increase in thermistor absorbed radiation due to the presence of the balloon, in nighttime conditions, is less than 10% of the total radiation. In non-extreme environmental conditions, the increase would be expected to be considerably smaller. Not only were the assumed conditions extreme, but additionally, the amount of downwelling atmospheric radiation shielded by the balloon subtracts from the value above. Consequently, we conclude that it is permissible to neglect the radiation exchange from the balloon when calculating the temperature error in the radiosonde for a nighttime flight. This is indeed fortunate. Modeling of the radiation exchange from the balloon would severely complicate the calculations by requiring that the balloon's view of radiation of varying intensity versus elevation angle be taken into account. Also, the balloon temperature, an unknown, is a necessary parameter in calculating the balloon emissions.

Daytime Radiation

During a daytime flight the balloon is additionally exposed to direct and diffuse solar radiation. The balloon emission is again given by Equation A4.4. During the day direct solar radiation is reflected from the balloon which irradiates the thermistor. At sunrise the sun irradiates approximately half of the balloon area visible to the thermistor. At higher solar elevations less of the balloon surface area that is exposed to the sun, is visible to the thermistor. The balloon is assumed to be a diffuse reflector of solar radiation. The direct solar energy reflected from the balloon that is absorbed by the thermistor has been approximated as a function of solar elevation angle by Equation A4.6 as:

$$q_{\text{sb}} = \pi r_b^2 \cos Z_E F_{\text{b} \rightarrow \text{th}} \int_{\lambda} \alpha(\lambda) \rho_b(\lambda) I_0(\lambda) d\lambda \quad (\text{A4.34})$$

The integral in the above equation is evaluated by utilizing an integrated value of I_0 over all wavelengths, and a spectrally weighted absorptivity, α , for the thermistor relative to the solar spectrum. With these assumptions Equation A4.34 is written as:

$$q_{\text{sb}} \pi r_b^2 \cos Z_E F_{\text{b} \rightarrow \text{th}} \alpha \rho_b I_0 \quad (\text{A4.35})$$

Evaluating Equation A4.35 with representative values of $\alpha = 0.15$ (Luers (1988)), $\rho_b = 0.8$, $I_0 = 0.03335 \text{ cal/sec cm}^2$, at $Z_E = 0$ gives:

$$q_{sb} = 3.3 \times 10^{-5} \text{ cal/sec}$$

Consider next the diffuse solar radiation which reflects off the balloon and irradiates the thermistor. To maximize the influence, assume 50% of the solar radiation irradiating the earth's surface is lost to space by scattering. Also, since nearly all of this scattering occurs at altitudes lower than 10 Km, then when the balloon is above 20 Km only the underside of the balloon is essentially irradiated by the earth's albedo (scattered radiation to space). The diffuse solar radiation reflected from the lower half of the balloon visible to the thermistor and absorbed by the thermistor is calculated from Equation A4.7 for 50% albedo as:

$$q_{sdb} = \pi c^2 \frac{I_0}{2} \rho_b \alpha F_{b \rightarrow th}^* \quad (A4.36)$$

Evaluating Equation A4.36 at 30 Km gives:

$$q_{sdb} \approx 3.9 \times 10^{-5} \text{ cal/sec}$$

Thus, the heating rates of the thermistor due to reflected direct solar radiation and reflected diffuse solar radiation are approximately equal. The magnitude of these terms is now compared to the heating rate of the thermistor due to the direct and diffuse solar components of radiation directly impinging (not reflected off another surface) on the thermistor. Calculation of solar absorption by the thermistor from direct and diffuse solar radiation under differing environmental conditions at a mid-latitude site is obtained from running the LOWTRAN 6 program. The results give a range of total absorbed atmospheric solar radiation from:

$$2 \times 10^{-3} < q_{abs} < 4.0 \times 10^{-3} \text{ cal/sec}$$

By comparison, the combined influence of both direct and diffuse solar radiation reflected off the balloon contribute less than 4% to the total absorbed solar radiation. Again a great simplification results in being able to ignore the influence of the balloon in calculating the radiosonde temperature error for daytime conditions.

APPENDIX 5: INFLUENCE OF THE RADIOSONDE INSTRUMENT ON THE
RADIOSONDE TEMPERATURE ERROR

A5.1 Irradiation of the Thermistor from the Radiosonde

The heating rate of the thermistor due to radiation emitted from and reflected off the radiosonde can be written in terms of the notation of Equation 3.5 and Equation 3.6 as:

$$q_{rs \rightarrow th} = \int_{\lambda} \alpha(\lambda) \int_{\Omega_{rs}} \bar{A}_p(\theta) I_{rs}(\theta, \phi, \lambda) \sin \theta d\theta d\phi d\lambda \quad (A5.1)$$

The integration limits for the solid angle, Ω_{rs} , define the boundaries of the thermistor's view (considered as a point) of the radiosonde instrument. The intensity $I_{rs}(\theta, \phi, \lambda)$ of radiation coming from the radiosonde is the sum of that emitted by the radiosonde and that reflected from the sonde. The development of an expression equivalent to Equation A5.1 follows the exchange factor approach taken in Appendix 4 for irradiation from the balloon.

The radiosonde thermistor exchanges radiation with sides S1 and S2 of the radiosonde instrument as shown in Figure A5.1. Assuming the thermistor temperature does not effect the temperature of sides S1 and S2 the only exchange that must be considered is the radiation from S1 and S2 that strikes the thermistor. Consider first the top side S1. Radiation coming from S1 consists of that emitted by the surface S1 and that atmospheric radiation propagating downward that reflects off of S1. In deriving the radiation from side S1 that is absorbed by the thermistor several assumptions are made:

- o S1 emits as a gray body at temperature T_{S1}
- o ϵ_{S1} , the emissivity of S1, is constant for any value of the temperature of S1.
- o ρ_{S1} , the reflectivity of the surface S1 is, a function of λ for $0.25 \leq \lambda \leq 2.5\mu$; $\rho_{S1} = \text{constant}$ for $2.5 \leq \lambda \leq 40\mu$
- o The surface S1 is a diffuse reflector of all radiation $0.25 \leq \lambda \leq 40\mu$
- o The emissivity of the thermistor, ϵ , is constant for $2.5 \leq \lambda \leq 40\mu$
- o The absorptivity of the thermistor is a function of λ for $0.25 \leq \lambda \leq 2.5\mu$

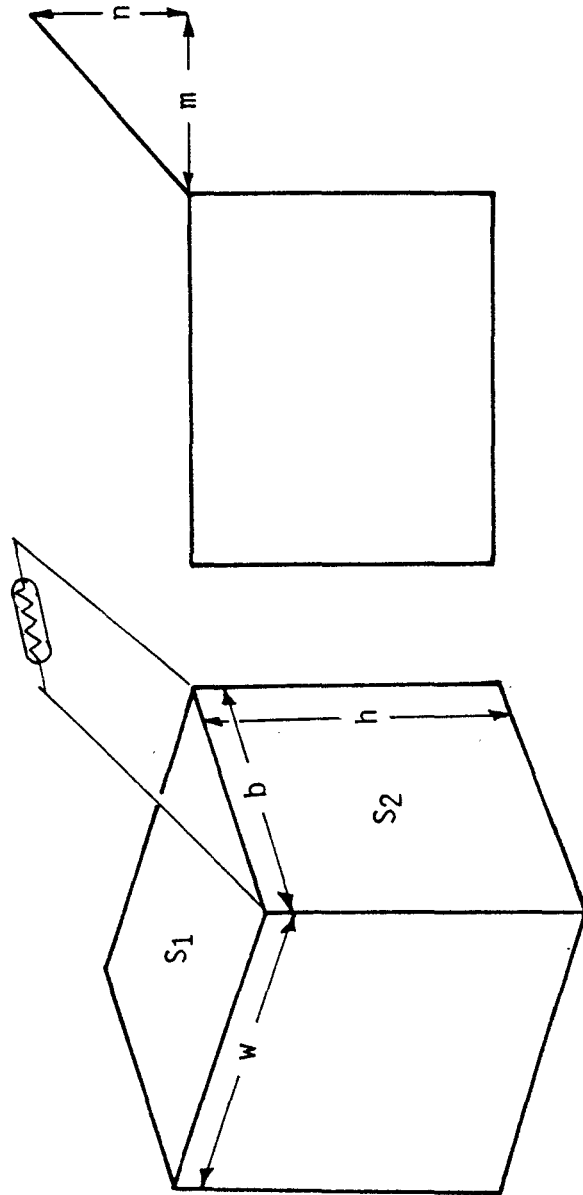


Figure A5.1 Idealized geometry of the radiosonde.

With these assumptions, the radiant power emitted by S1 that is absorbed by the thermistor is:

$$q_{eS1} = wb\sigma T_{S1}^4 \epsilon_{S1} \epsilon_{FS1 \rightarrow th} \quad (A5.2)$$

where the dimensions w , b and h are defined in Figure A5.1 and $F_{S1 \rightarrow th}$ is the exchange factor for side S1 to the thermistor.

The radiant power reflected from S1 that is absorbed by the thermistor is written as the sum of three components, a wavelength dependent direct and a diffuse solar component for $0.25 \leq \lambda \leq 2.5\mu$ and a diffuse infrared component for $2.5 \leq \lambda \leq 40 \mu$. The diffuse solar power reflected from S1 and absorbed by the thermistor is:

$$q_{sdS1} = wb F_{S1 \rightarrow th} \int_{\lambda=0.25}^{\lambda=2.5} F_{\downarrow}(\lambda) \rho_{S1}(\lambda) \alpha(\lambda) d\lambda \quad (A5.3)$$

where $F_{\downarrow}(\lambda)$ is the total downwelling radiant power at wavelength λ and is given by:

$$F_{\downarrow}(\lambda) = \int_{\phi=0}^{2\pi} \int_{\theta=\frac{\pi}{2}}^{\pi} I^*(\theta, \phi, \lambda) \cos \theta \sin \theta d\theta d\phi \quad (A5.4)$$

The diffuse infrared component reflected from S1 and absorbed by the thermistor is:

$$q_{dS1} = wb F_{S1 \rightarrow th} (1 - \epsilon_{S1}) \epsilon \int_{\lambda=2.5}^{40} F_{\downarrow}(\lambda) d\lambda \quad (A5.5)$$

The solar power directly irradiating the side S1 and reflecting diffusely onto the thermistor is dependent on the solar elevation angle. At a solar elevation, near zero when the sun's rays are parallel to the top side, S1, of the radiosonde no solar energy irradiates S1. At an arbitrary solar elevation angle of Z_E the heating rate of the thermistor due to direct solar energy reflected off side S1 and irradiating the thermistor is given by:

$$q_{sS1} = wb \sin Z_E F_{S1 \rightarrow th} \int_{\lambda=0.25}^{2.5} \rho_{S1}(\lambda) \alpha(\lambda) I_0(\lambda) d\lambda \quad (A5.6)$$

Summing Equations A5.2, A5.3, A5.5 and A5.6 gives the heating rate of the thermistor from the surface S1:

$$q_{S1} = wb F_{S1 \rightarrow th} \left\{ \sigma T_{S1}^4 \epsilon_{S1} \epsilon + \int_{\lambda=0.25}^{\lambda=2.5} F_{\downarrow}(\lambda) \rho_{S1}(\lambda) \alpha(\lambda) d\lambda + (1 - \epsilon_{S1}) \epsilon \int_{\lambda=2.5}^{40} F_{\downarrow}(\lambda) d\lambda + \sin Z_E \int_{\lambda=0.25}^{\lambda=2.5} \rho_{S1}(\lambda) \alpha(\lambda) I_0(\lambda) d\lambda \right\} \quad (A5.7)$$

The parameter $F_{\downarrow}(\lambda)$ can be derived from the modeling of the atmospheric intensity using LOWTRAN 6 and Equation A5.4. All other parameters in Equation A5.7 have known or measured values. The expression for the exchange factor is derived in a latter part of Appendix 5. The magnitude of each of the terms in Equation A5.7 and the significance of their contribution to the heating of the thermistor is also calculated in a latter part of this Appendix.

A similar but more complex analysis is required for determining the radiant power absorbed by the thermistor from the surface S2. The same assumptions used for side S1 are also valid for the vertical side S2. The radiant power emitted by S2, at temperature T_{S2} and absorbed by the thermistor is:

$$q_{eS2} = bh F_{S2 \rightarrow th} \sigma T_{S2}^4 \epsilon_{S2} \epsilon \quad (A5.8)$$

where $F_{S2 \rightarrow th}$ is the exchange factor from side S2 to the thermistor. Because the radiosonde rotates as it ascends through the atmosphere, the side S2 is exposed to direct solar radiation during only one-half of a rotation and only during daytime flights. It is exposed to diffuse radiation at all times. Thus, the radiation reflected from the side S2 is again considered as a sum of three terms, a direct and diffuse solar component, and a diffuse infrared component.

The direct solar power striking S2 when it is facing perpendicular to the sun is:

$$q_{S2} = bh \cos Z_E \int_{\lambda=0.25}^{\lambda=2.5} I_0(\lambda) d\lambda \quad (A5.9)$$

where I_0 is the solar intensity, depleted by absorption and scattering, at a given point in the atmosphere. Z_E is the solar elevation angle.

Averaging q_{S2} over one-half revolution in which some exposure occurs gives:

$$\bar{q}_{S2/2} = bh \cos Z_E \frac{1}{\pi} \int_{\lambda=0.25}^{\lambda=2.5} I_0(\lambda) d\lambda \int_{\phi'=-\frac{\pi}{2}}^{\frac{\pi}{2}} \cos \phi' d\phi'$$

and evaluating

$$\bar{q}_{S2/2} = \frac{2bh \cos Z_E}{\pi} \int_{\lambda=0.25}^{\lambda=2.5} I_0(\lambda) d\lambda \quad (A5.10)$$

During the other one-half of rotation, side S2 receives no direct solar radiation. Thus, the average direct solar power striking S2, during one complete revolution is:

$$\bar{q}_{S2} = \frac{bh \cos Z_E}{\pi} \int_{\lambda=0.25}^{\lambda=2.5} I_0(\lambda) d\lambda \quad (A5.11)$$

The average direct solar power striking S2 that is diffusely reflected from S2 and absorbed by the thermistor is:

$$\bar{q}_{sS2} = \frac{bh \cos Z_E F_{S2 \rightarrow th}}{\pi} \int_{\lambda=0.25}^{\lambda=2.5} \rho_{S2}(\lambda) \alpha(\lambda) I_0(\lambda) d\lambda \quad (A5.12)$$

In considering the diffuse solar and infrared components, it will be assumed that the radiosonde's shielding of the sun does not influence the local distribution of the diffuse component that irradiates side S2. The diffuse radiant power at wavelength λ irradiating S2 when S2 is oriented azimuthally at the angle ϕ_0 with respect to the X-axis is:

$$q_d(\lambda, \phi_0) = bh \int_{\phi=\phi_0-\frac{\pi}{2}}^{\phi_0+\frac{\pi}{2}} \int_{\theta=0}^{\theta=\pi} I^*(\lambda, \theta, \phi) \cos\left(\frac{\pi}{2} - \theta\right) \sin \theta d\theta d\phi$$

where the factor $\cos\left(\frac{\pi}{2} - \theta\right)$ reduces the flux relative to its angle of incidence (see Figure A5.2)

or equivalently:

$$q_d(\lambda, \phi_0) = bh \int_{\phi=\phi_0-\frac{\pi}{2}}^{\phi_0+\frac{\pi}{2}} \int_{\theta=0}^{\pi} I^*(\lambda, \theta, \phi) \sin^2 \theta d\theta d\phi \quad (A5.13)$$

The average diffuse radiant power at wavelength λ irradiating S2 during one revolution is:

$$\bar{q}_d(\lambda) = \frac{1}{\pi} \int_{\phi_0=0}^{\phi_0=\pi} q_d(\lambda, \phi_0) d\phi_0$$

(Recall: $I^*(\lambda, \theta, \phi)$ is axially symmetric about $\phi_0=0$) (A5.14)

Dividing the diffuse radiation into its solar and infrared components, the average diffuse radiation striking S2 that is diffusely reflected from S2 and absorbed by the thermistor is:

$$\bar{q}_{dS2} = F_{S2 \rightarrow th} \left\{ \int_{\lambda=0.2}^{2.5} \bar{q}_d(\lambda) \rho_{S2}(\lambda) \alpha(\lambda) d\lambda + (1 - \epsilon_{S2}) \epsilon \int_{\lambda=2.5}^{40} \bar{q}_d(\lambda) d\lambda \right\} \quad (A5.15)$$

Summing Equations A5.8, A5.12, and A5.15 gives the heating rate of the thermistor from energy exchange with side S2 as:

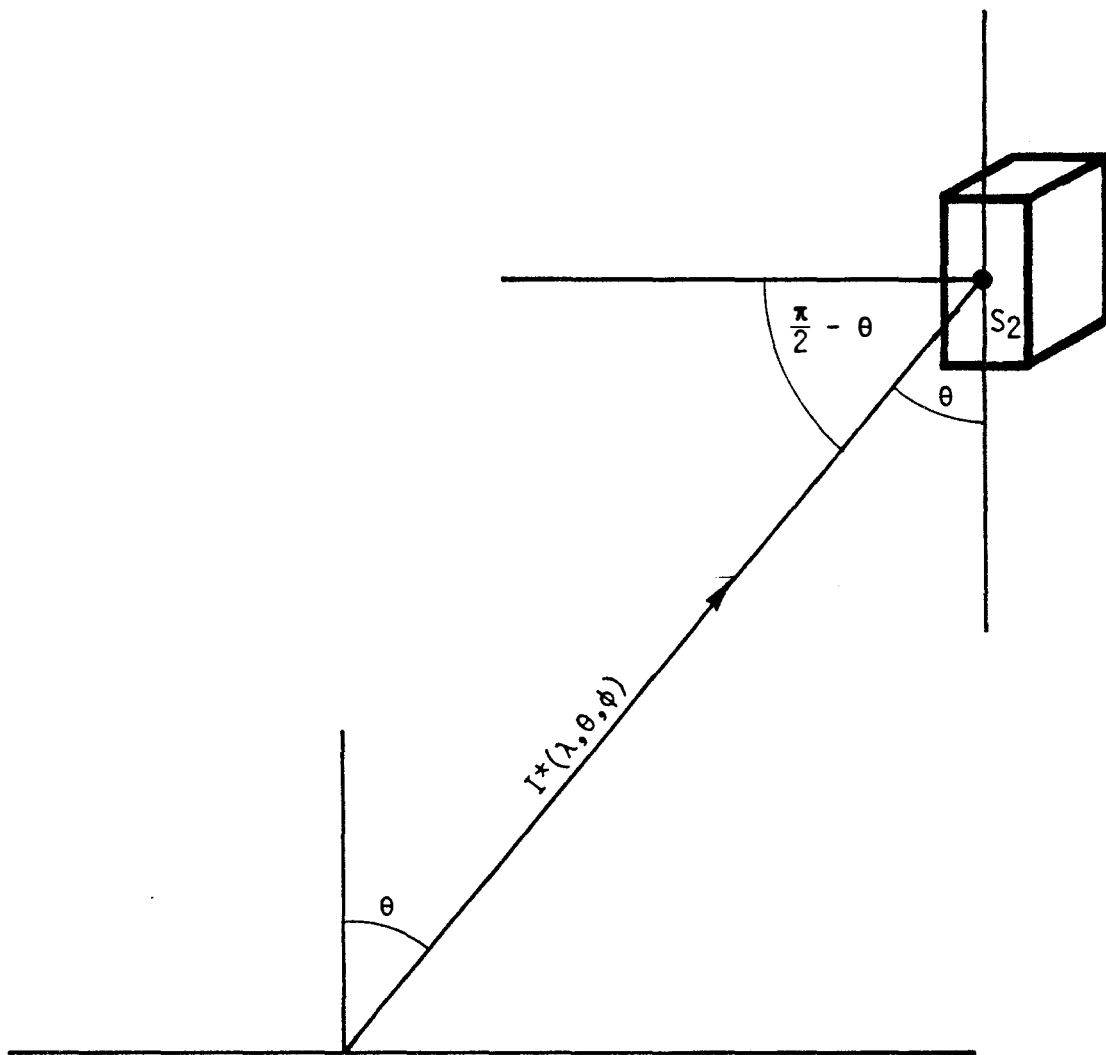


Figure A5.2 Geometry for calculating radiant power irradiating S_2 .

$$\begin{aligned}
q_{S2} = F_{S2 \rightarrow th} \left\{ bh \sigma T_{S2}^4 \epsilon_{S2} \epsilon + \frac{bh \cos Z}{\pi} \int_{\lambda=0.25}^{2.5} \rho_{S2}(\lambda) \alpha(\lambda) I_0(\lambda) d\lambda \right. \\
\left. + \int_{\lambda=0.25}^{2.5} \bar{q}_d(\lambda) \rho_{S2}(\lambda) \alpha(\lambda) d\lambda + (1 - \epsilon_{S2}) \epsilon \int_{\lambda=2.5}^{40} \bar{q}_d(\lambda) d\lambda \right\}
\end{aligned} \tag{A5.16}$$

where

$F_{S2 \rightarrow th}$ = The exchange factor between S2 and the thermistor

$I_0(\lambda)$ = Direct solar intensity at a specified altitude

$$\bar{q}_d(\lambda) = \frac{1}{\pi} \int_{\phi_0=0}^{\phi_0=\pi} Q_d(\lambda, \phi_0) d\phi_0$$

$$q_d(\lambda, \phi_0) = bh \int_{\phi=\phi_0-\frac{\pi}{2}}^{\phi_0+\frac{\pi}{2}} \int_{\theta=0}^{\pi} I^*(\theta, \phi, \lambda) \sin^2 \theta d\theta d\phi$$

Equation A5.16 gives the heating rate of the thermistor from radiation coming from the vertical side S2. All parameters except the temperature T_{S2} in Equation A5.16 are known, can be estimated, or are output parameters from the atmospheric modeling of $I^*(\theta, \phi, \lambda)$ using LOWTRAN 6 (the exchange factors are derived in the next section). Equations A5.6 and A5.16 combine to give the heating rate of the thermistor due to radiant exchange with the radiosonde instrument. Later in this Appendix the magnitude of each term in Equation A5.16 is evaluated in terms of its significance in contributing to the heating rate of the thermistor.

A5.2 Exchange Factor for Side S1 with Thermistor

The irradiation of the thermistor from the surface S1 can be considered as that irradiating a flat plate at the location of the thermistor having cross-sectional area defined by the impingement limits of S1 on the thermistor.

The length of this flat plate (projection of the thermistor) is l and its width (from Figure A5.3) is $2c = 2a \sin(\frac{\delta-\beta}{2})$. The angle of tilt between the flat plate and side S1 is $\psi = \frac{\pi}{2} - \frac{\delta+\beta}{2}$, where

$$\delta = \tan^{-1} \frac{n}{m}, \quad \beta = \tan^{-1} \frac{n}{m+w}, \quad \text{and } a = r \cot \left(\frac{\delta-\beta}{2} \right).$$

To derive the exchange factor from S1 to the thermistor, first the exchange factor from a flat plate thermistor to S1 is derived and then the reciprocity theorem is used for exchange factors between flat surfaces. The flat plate is considered as an infinitesimal source in

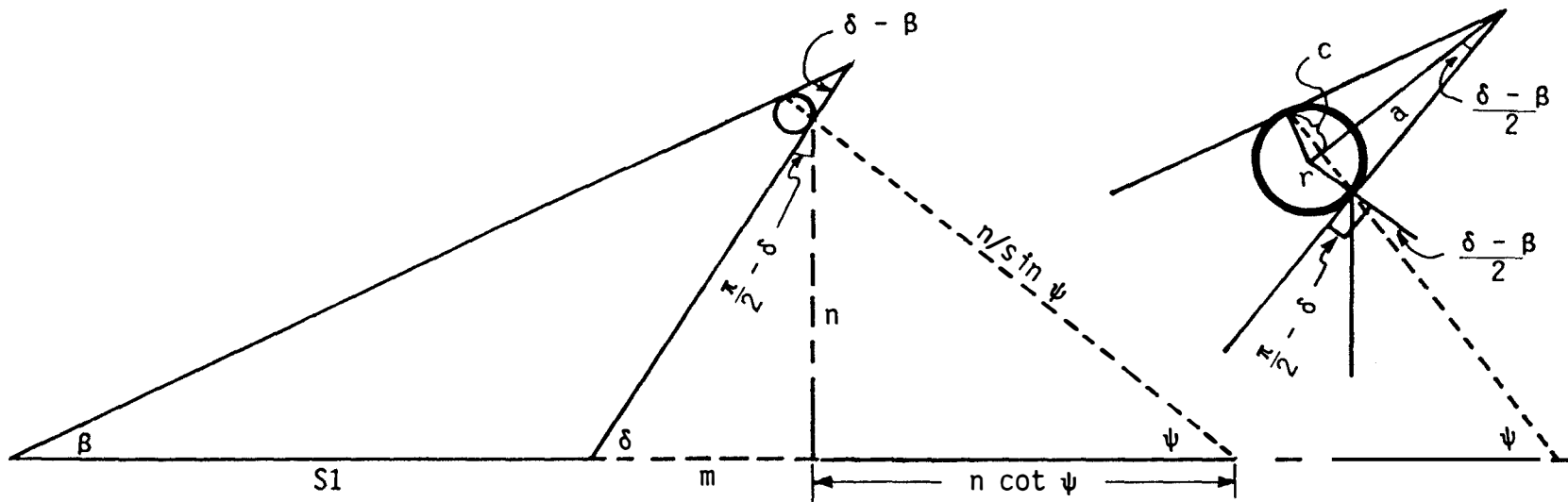


Figure A5.3 Geometry for thermistor view of side S1.

that all points are assumed to have the same geometric relationship with the side S1. The exchange factor between an infinitesimal flat plate source and another plane representing half of the side S1 is given in Kreith (1962), Appendix V, Configuration # 2. A description of the variables used in Configuration # 2 are shown in Figure A5.4. The exchange factor from an infinitesimal flat plate source dA, to the side S1 is derived from the summation relationship for exchange factors (see Figure A5.5, A5.6, A5.7 and A5.8) as:

$$F_{dA_1 \rightarrow S1} = 2F_{dA_1 \rightarrow \frac{S1}{2}} = 2(F_{dA_1 \rightarrow A_2} - F_{dA_1 \rightarrow A_3}) \quad (A5.17)$$

where for $F_{dA_1 \rightarrow A_2}$

$$\begin{aligned} \bar{\Phi} = \psi &= \frac{\pi}{2} - \frac{\delta + \beta}{2} \\ a^* &= m + n \cot \psi + w \\ b^* &= \frac{b}{2} \\ c^* &= n / \sin \psi \end{aligned}$$

and for $F_{dA_1 \rightarrow A_3}$

$$\begin{aligned} \bar{\Phi} = \psi &= \frac{\pi}{2} - \frac{\delta + \beta}{2} \\ a^* &= m + n \cot \psi \\ b^* &= \frac{b}{2} \\ c^* &= n / \sin \psi \end{aligned}$$

The exchange factors are plotted in Figure V-2 (Kreith (1962)) and are given by:

$$\begin{aligned} F_{dA_1 \rightarrow A_2} = \frac{1}{2\pi} & \left\{ \tan^{-1} \left(\frac{1}{L} \right) + V(N \cos \bar{\Phi} - L) \tan^{-1} V \right. \\ & \left. + \frac{\cos \bar{\Phi}}{W} \left[\tan^{-1} \left(\frac{N - L \cos \bar{\Phi}}{W} \right) + \tan^{-1} \left(\frac{L \cos \bar{\Phi}}{W} \right) \right] \right\} \quad (A5.18) \end{aligned}$$

where

$$V = \frac{1}{[N^2 + L^2 - 2NL \cos \bar{\Phi}]^{1/2}}$$

$$W = [1 + L^2 \sin^2 \bar{\Phi}]^{1/2}$$

$$N = \frac{a^*}{b^*}$$

$$L = \frac{c^*}{b^*}$$

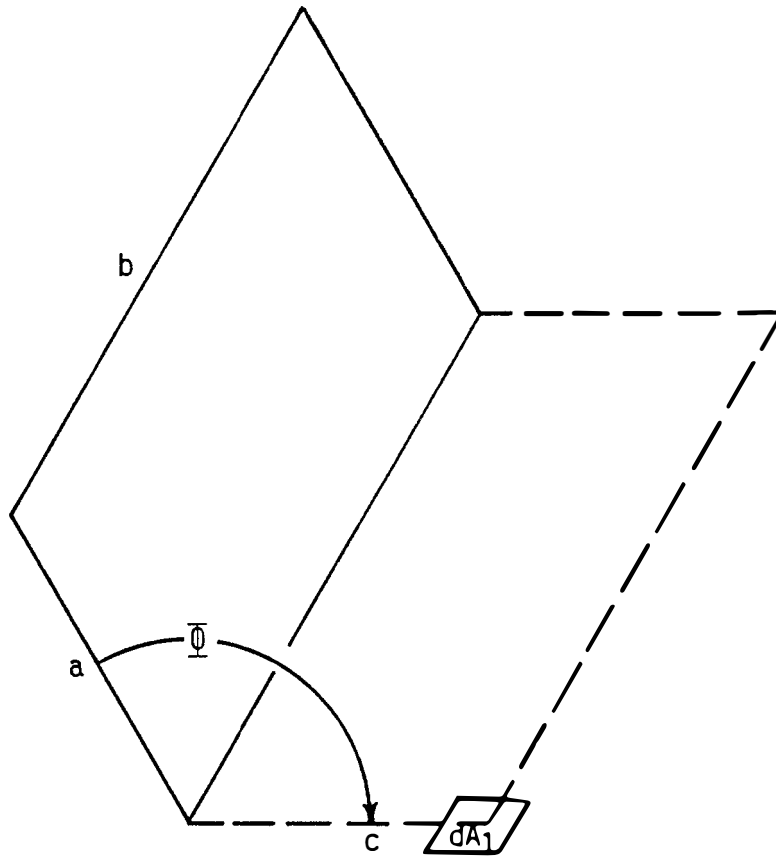


Figure A5.4 Geometry applicable to configuration # 2 (Kreith, 1962).

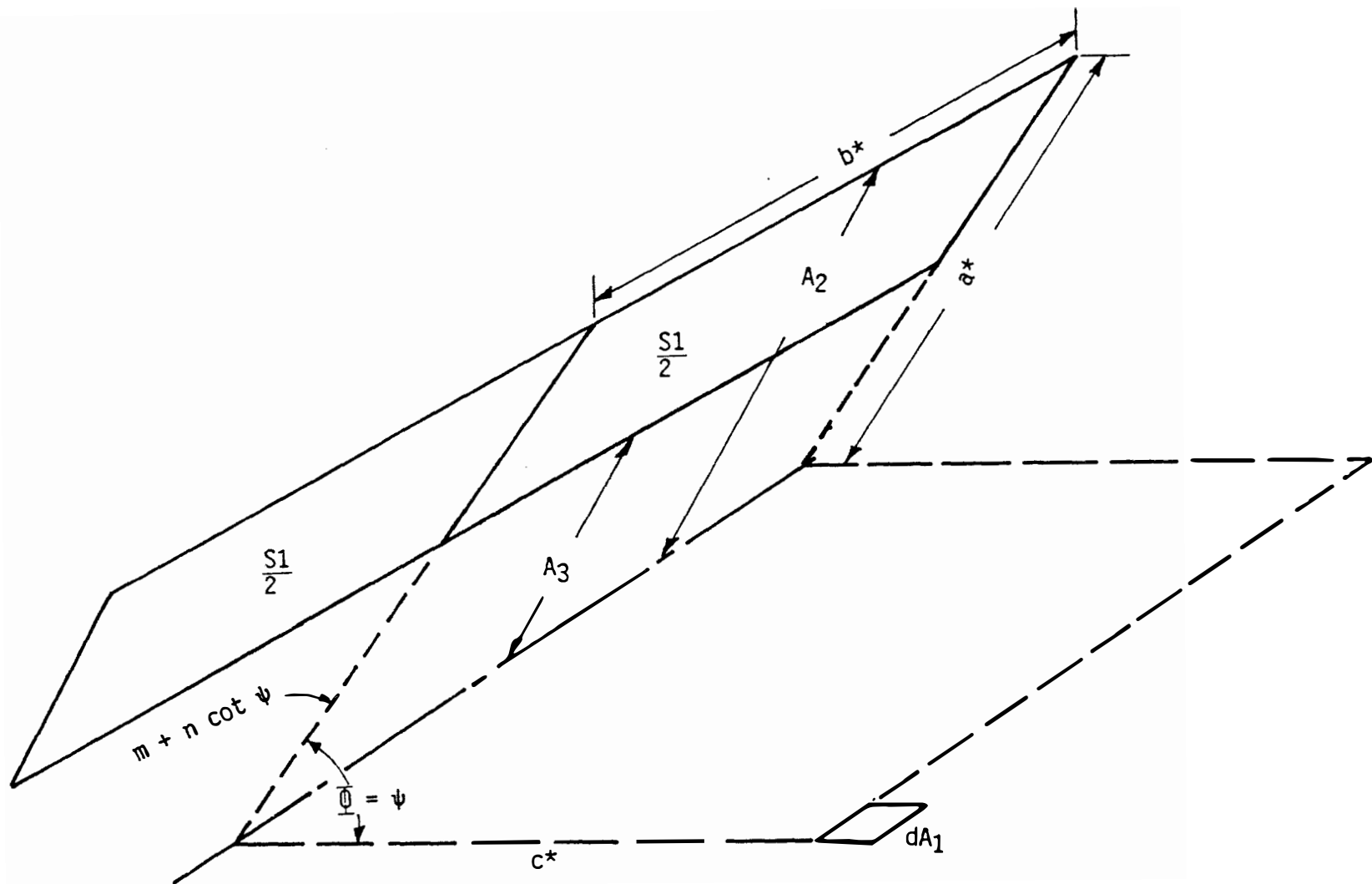


Figure A5.5 Application of configuration # 2 geometry to thermistor → S_1 exchange factor.

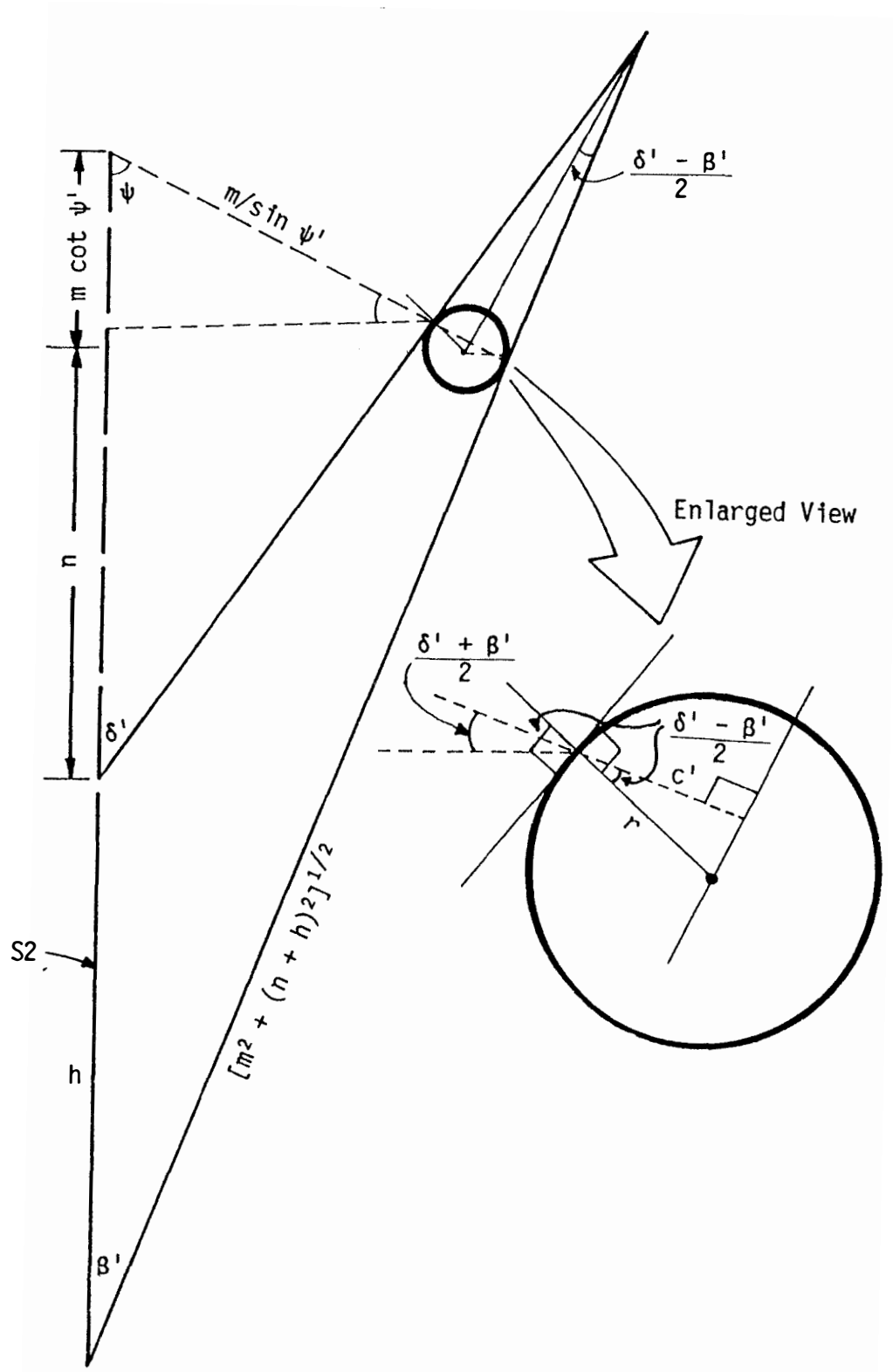


Figure A5.6 Geometry of thermistor view of side S2.

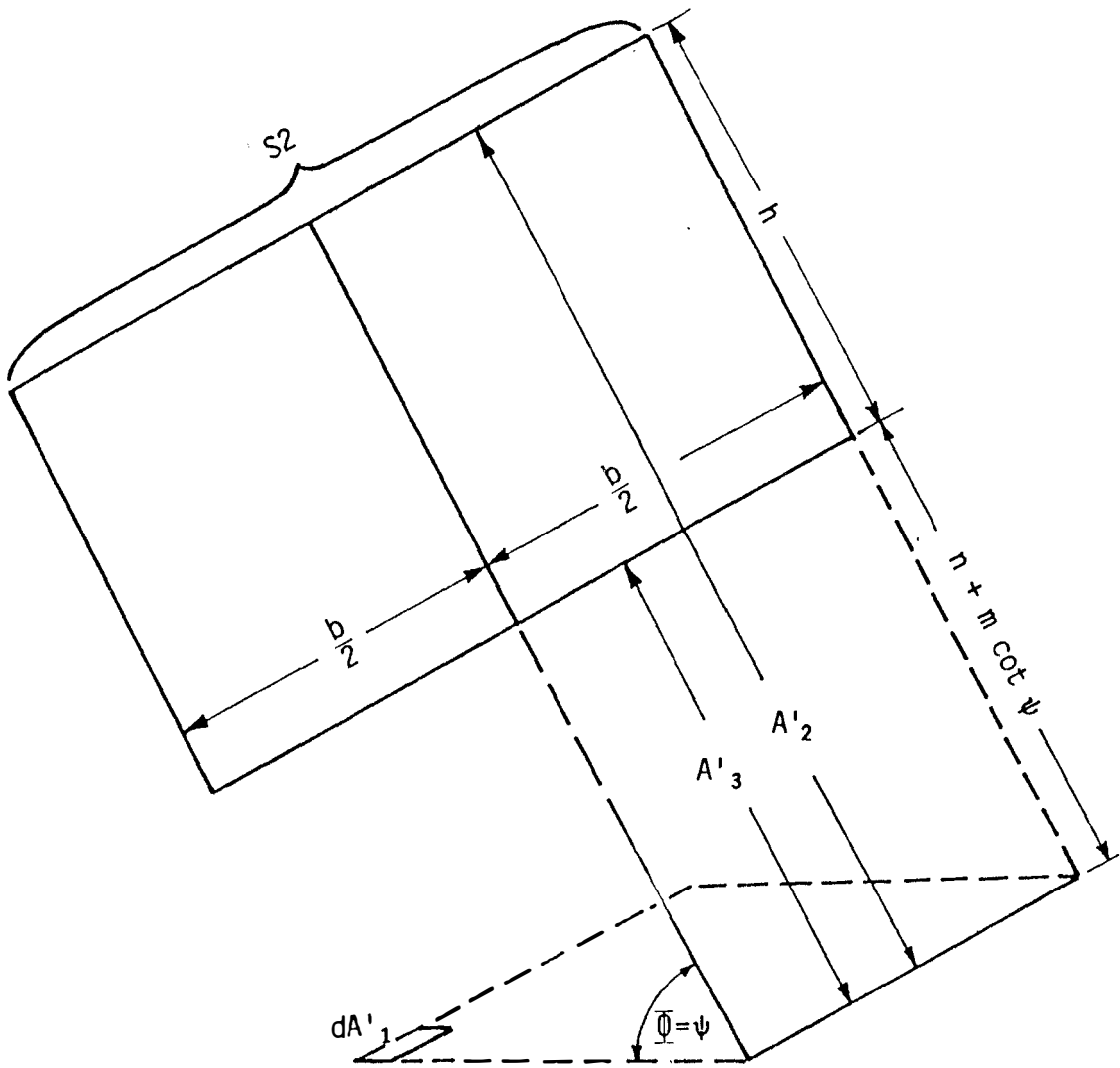


Figure A5.7 Application of configuration # 2 geometry to thermistor \rightarrow S_2 exchange factor.

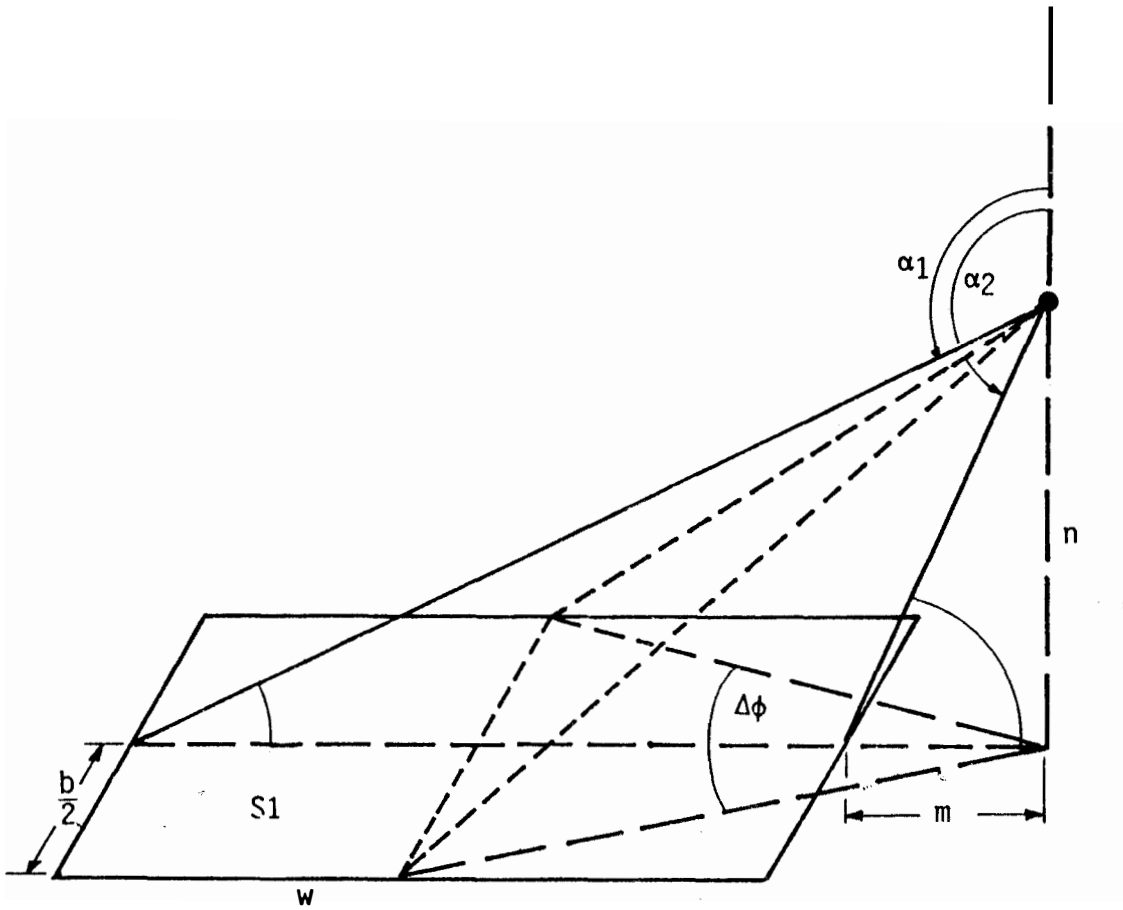


Figure A5.8 Solid angle defining thermistor view of side S1.

Next the exchange factor from the side S1 to the thermistor, considered as an infinitesimal, is derived from reciprocity and from the relationship:

$$F_{S1 \rightarrow th} = F_{S1 \rightarrow dA_1}$$

The reciprocity relationship gives:

$$A_{S1} F_{S1 \rightarrow dA_1} = dA_1 F_{dA_1 \rightarrow S1} \quad (A5.19)$$

$$\text{Thus, } F_{S1 \rightarrow th} = \frac{dA_1}{A_{S1}} F_{dA_1 \rightarrow S1} = \frac{dA_1}{A_{S1}} 2(F_{dA_1 \rightarrow A2} - F_{dA_1 \rightarrow A3})$$

Substituting, $A_{S1} = bw$

$$dA_1 = 2c\ell, \text{ where } c = a \sin\left(\frac{\delta-B}{2}\right)$$

Gives:

$$F_{S1 \rightarrow th} = \frac{2c\ell}{bw} F_{dA_1 \rightarrow S1} = \frac{4c\ell}{bw} (F_{dA_1 \rightarrow A2} - F_{dA_1 \rightarrow A3}) \quad (A5.20)$$

where $F_{dA_1 \rightarrow A2,3}$ is evaluated from Equation A5.18.

The exchange factor from S1 to the thermistor has been numerically evaluated for nominal radiosonde dimensions of:

n = 50 mm
m = 110 mm
b = 125 mm
w = 155 mm
h = 250 mm

The results give the value of $F_{S1 \rightarrow th} = 1.49 \times 10^{-4}$ for the exchange factor from the surface S1 to the thermistor.

A5.3 Exchange Factor for Side S2 with Thermistor

The irradiation of the thermistor from the surface S2 can be considered as that irradiating a flat plate at the location of the thermistor having area equal to that defined by the impingement limits, on the thermistor, of radiation from S2. The flat plate can then be considered as an infinitesimal source and the exchange factor from the source to S2 calculated from textbook configurations. The exchange factor from S2 to the plate is then calculated using reciprocity.

The geometry between the thermistor, infinitesimal flat plate, and side S2 is shown in Figure A5.6.

The exchange factor from the side S2 to the thermistor of finite dimension is the same as that from S2 to the flat plane dA'_1 . The exchange factor from S2 to the flat plate dA'_1 is related to the exchange factor from dA'_1 to S2 by reciprocity. Deriving first the exchange factor from dA'_1 to the side S2 we have from Figure A5.7:

$$F_{dA_1 \rightarrow S2} = 2(F_{dA_1 \rightarrow A_2} - F_{dA_1 \rightarrow A_3}) \quad (A5.21)$$

where for $F_{dA_1 \rightarrow A_2}$

$$\bar{\Phi} = \psi = \frac{\pi}{2} - \frac{\delta' + \beta'}{2}, \quad \delta' = \tan^{-1} \frac{m}{n}, \quad \beta' = \tan^{-1} \frac{m}{n+h}$$

$$a^* = h + n + m \cot \psi$$

$$b^* = \frac{b}{2}$$

$$c^* = m/\sin \psi$$

and for $F_{dA_1 \rightarrow A_3}$

$$\bar{\Phi} = \psi = \frac{\pi}{2} - \frac{\delta' + \beta'}{2}$$

$$a^* = n + m \cot \psi$$

$$b^* = \frac{b}{2}$$

$$c^* = m/\sin \psi$$

The exchange factor is again evaluated from Figure V-2 (Kreith (1962)) or calculated analytically from Equation A5.18.

The exchange factor from the side S2 to the thermistor is derived from reciprocity:

$$A_{S2} F_{S2 \rightarrow th} = A_{S2} F_{S2 \rightarrow dA_1} = dA_1 F_{dA_1 \rightarrow S2} \quad (A5.22)$$

Substituting,

$$A_{S2} = bh$$

$$dA_1 = 2c'l, \text{ where } c' = r \cos \left(\frac{\delta' - \beta'}{\theta} \right)$$

gives,

$$F_{S2 \rightarrow th} = \frac{2c'l}{bh} F_{dA_1 \rightarrow S2} \quad (A5.23)$$

where

$F_{dA_1 \rightarrow S2}$ is evaluated from Equations A5.18 and A5.21.

The exchange factor $F_{S2 \rightarrow th}$ is evaluated for nominal radiosonde dimensions using Equations A5.18, A5.21, and A5.23 as $F_{S2 \rightarrow th} = 2.73 \times 10^{-4}$.

A5.4 Atmospheric Radiation Shielded by Radiosonde

Atmospheric radiation is shielded by the radiosonde from striking the thermistor and being absorbed. The shielded radiation is expressed as:

$$q_{sh/rs} = - 2r\ell \int_{\lambda} \alpha(\lambda) \int_{\Omega_{rs}} I^*(\theta, \phi, \lambda) \cos \theta \sin \theta d\theta d\phi d\lambda \quad (A5.24)$$

This negative term represents the heating rate that would occur from atmospheric radiation that is shielded by the radiosonde, from striking the thermistor. This term is evaluated by establishing the integration limits for the solid angles defining the thermistor view of sides S1 and S2. The geometry of the thermistor with respect to side S1 is shown in Figure A5.8.

As an approximation, we will consider the bisectors of the sides of S1 to define the elevation and azimuth limits, respectively, for the solid angle. The minimum elevation angle is α_1 and the maximum is α_2 where:

$$\tan \left(\alpha_2 - \frac{\pi}{2} \right) = \frac{n}{m}$$

$$\tan \left(\alpha_1 - \frac{\pi}{2} \right) = \frac{n}{m + w}$$

Similarly the azimuth increment is defined by $\Delta\phi$ where:

$$\tan \frac{\Delta\phi}{2} = \frac{b}{2} / \left(\frac{w}{2} + m \right)$$

Because the balloon rotates, the azimuthal variation in radiant intensity is averaged over one revolution and designated as $\bar{I}^*(\lambda, \phi)$. Consequently, only the azimuthal increment, $\Delta\phi$, for the solid angle is required.

Substituting these limits into Equation A5.24 gives the radiant power not absorbed by the thermistor because of shielding by the side S1 as:

$$q_{sh/S1} = - 2r\ell \int_{\lambda} \alpha(\lambda) \int_{\phi=0}^{2\tan^{-1} \left\{ \frac{b}{2(\frac{w}{2} + m)} \right\}} d\phi \int_{\theta=\tan^{-1}(\frac{n}{m+w}) + \frac{\pi}{2}}^{\tan^{-1}(\frac{n}{m}) + \frac{\pi}{2}} \cos \theta \bar{I}^*(\lambda, \theta) \sin \theta d\theta d\lambda \quad (A5.25)$$

Similarly shielding for the side S2 is shown in the Figure A5.9. The bisectors of the side S2 are again chosen to approximate the elevation and azimuthal limits for the solid angle. The elevation angle varies from its minimum value of θ_1 to its maximum value of θ_2 where:

$$\tan \theta_1 = \frac{n}{m}$$

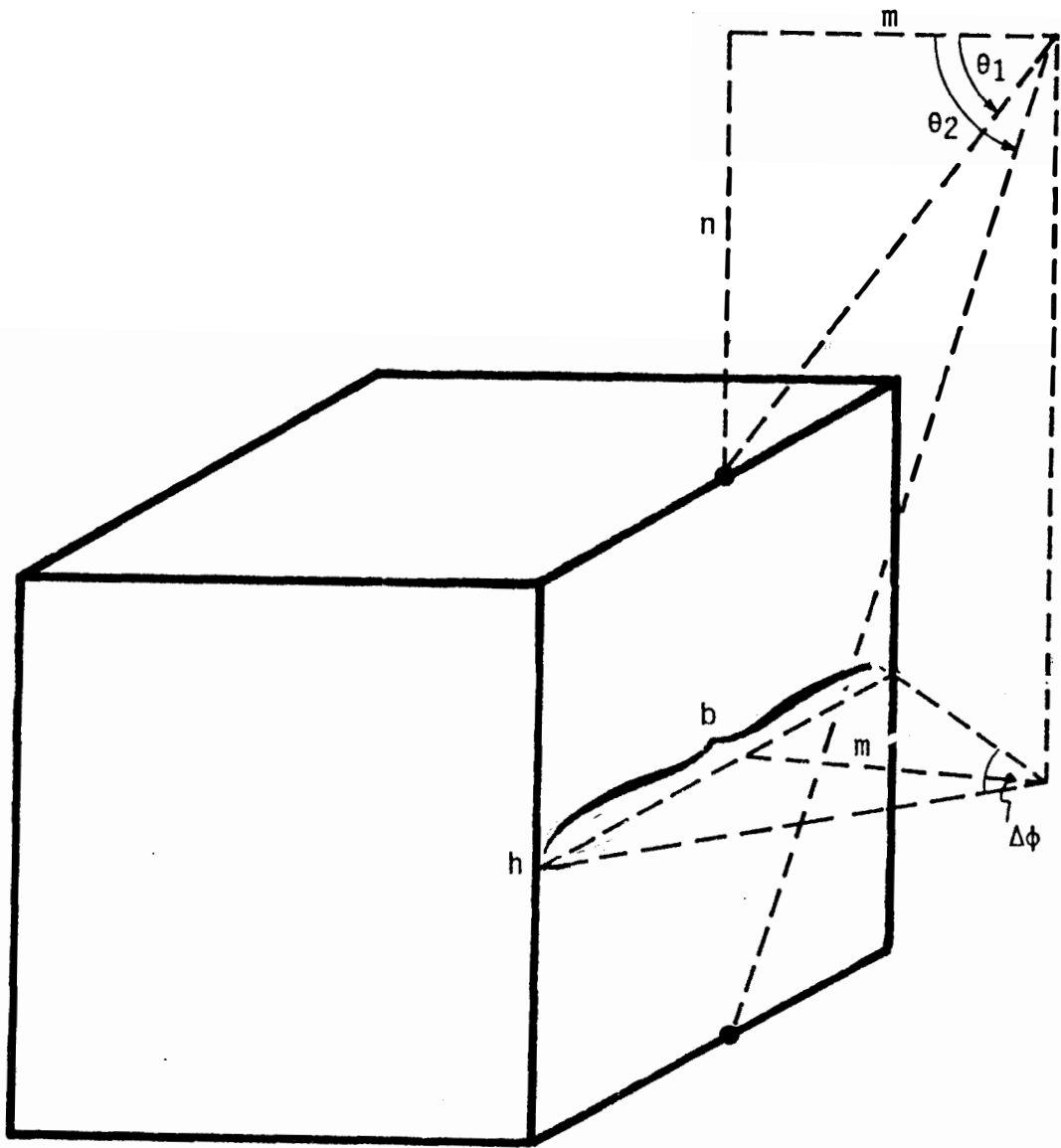


Figure A5.9 Solid angle geometry for thermistor view of side S2.

$$\tan \theta_2 = \frac{n + h}{m}$$

Similarly the azimuth increment is defined by $\Delta\phi$ where:

$$\tan \frac{\Delta\phi}{2} = \left(\frac{b}{2} / m\right)$$

In essence, the bisector of the side approximation defines the limits for the solid angle shown as the filled in area of Figure A5.10 as related to the true solid angle defined by the side S2 boundaries. Thus, a good approximation results.

Combining the shielding from the sides S1 and S2 gives the following as the radiant power due to atmospheric radiation that is shielded by the radiosonde from absorption by the thermistor.

$$q_{sh/rs} = -2r\ell \int_{\lambda} \alpha(\lambda) \left\{ \int_{\phi=0}^{2\tan^{-1}\left\{\frac{b}{2\left(\frac{w}{2} + m\right)}\right\}} d\phi \int_{\theta=\tan^{-1}\left(\frac{n}{m}\right)+\frac{\pi}{2}}^{\tan^{-1}\left(\frac{n}{m}\right)+\frac{\pi}{2}} \cos \theta \bar{I}^*(\lambda, \theta) \sin \theta d\theta d\lambda \right. \\ \left. + \int_{\phi=0}^{2\tan^{-1}\left(\frac{b}{2m}\right)} d\phi \int_{\theta=\tan^{-1}\frac{n}{m}}^{\tan^{-1}\left(\frac{n+h}{m}\right)} \cos \theta \bar{I}^*(\lambda, \theta) \sin \theta d\theta d\lambda \right\} \quad (A5.26)$$

The magnitude of this term is evaluated in the following section along with the magnitude of the terms that denote the absorbed radiation from emissions and reflections off of the radiosonde.

A5.5 Influence of the Radiosonde on Thermistor Temperature

The radiosonde influences the temperature of the thermistor because a) the thermistor receives emitted and reflected radiation from the radiosonde, and b) the radiosonde shields the thermistor from atmospheric radiation from the solid angle defined by the boundaries of the radiosonde. The percent change in radiation absorbed by the thermistor due to the presence of the radiosonde instrument is given by:

$$\frac{\Delta q_{rs}}{q_{abs}} = \frac{|q_{rs} - q_{sh/rs}|}{q_{abs}} \quad (A5.27)$$

To establish the significance of including the radiosonde terms in the heat balance equation, the above equation has been evaluated for an extreme environment in both day and night situations to establish the maximum influence of each term.

Nighttime Radiation

At nighttime the radiosity from the side S1 absorbed by the

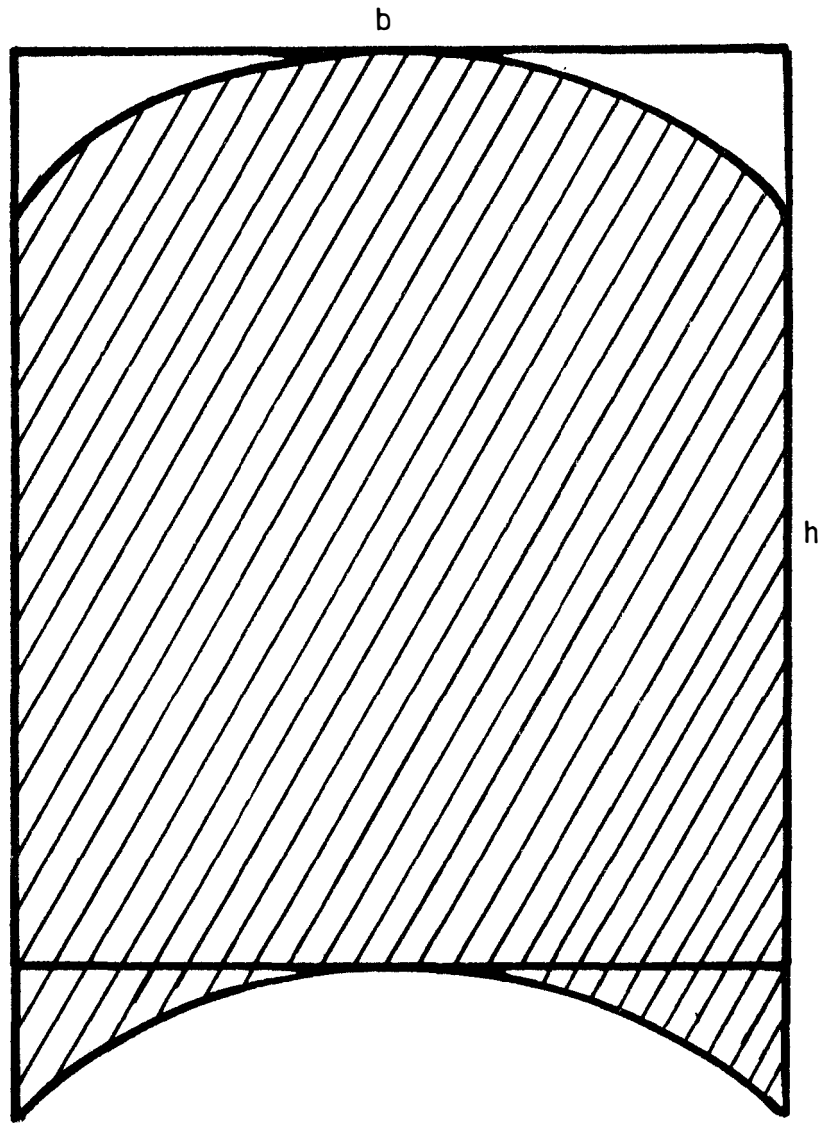


Figure A5.10 Side S2 boundaries of solid angle versus approximation.

thermistor is derived from Equation A5.7 by assuming the downwelling radiation $F_{\downarrow}(\lambda)$ is blackbody radiation at an equivalent sky blackbody temperature of T_d . With this assumption and the absence of solar radiation Equation A5.7 simplifies to:

$$q_{S1} = w_b F_{S1 \rightarrow th} (\sigma T_{S1}^4 \epsilon_{S1} \epsilon + (1 - \epsilon_{S1}) \epsilon \sigma T_d^4) \quad (A5.28)$$

The first term on the right side accounts for the energy emitted by the side S1 at temperature T_{S1} that is absorbed by the thermistor. The second term gives the thermistor heating due to blackbody atmospheric radiation at temperature T_d that is reflected from the side S1 and irradiates the thermistor. The side S1 receives only downwelling radiation from above. To assess the magnitude of q_{S1} values of T_{S1} and T_d are required. The influence of q_{S1} will be greatest when T_{S1} and T_d are large. A reasonable assumption for a warm blackbody sky temperature is $T_d = 200^\circ$ K. The temperature of the surface S1 is probably less than or equal to the air temperature. This conclusion comes from the fact that radiatively S1 is losing energy to a colder sky, while convectively T_{S1} is attempting to approach T_{∞} . Only internal electrical heating from the battery could force T_{S1} greater than T_{∞} . At 30 Km the range of temperatures for the side S1 is approximated as:

$$190^\circ \leq T_{S1} \leq 220^\circ$$

Substituting these values and a representative values of $\epsilon_{S1} = 0.9$ for the emissivity of S1 into Equation A5.28 gives:

$$q_{S1} = 7.67 \times 10^{-5} \text{ cal/sec}$$

Similarly for nighttime conditions the thermistor heating rate Equation A5.16 for interaction with side S2 can be simplified to:

$$q_{S2} = b_h F_{S2 \rightarrow th} (\sigma T_{S2}^4 \epsilon_{S2} \epsilon + (1 - \epsilon_{S2}) \epsilon \int_{25}^{40} \bar{Q}_D(\lambda) d\lambda) \quad (A5.29)$$

where $\bar{Q}_D(\lambda)$ is the average diffuse power irradiating the side S2 during one revolution. Since the side S2 is vertically oriented it provides partial exposure to both upwelling and downwelling radiation. Thus, an upper limit for an equivalent blackbody exposure temperature for the side S2 is on the order of $T_E = 250^\circ$ K. This temperature is used to approximate the \bar{Q}_D integral as σT_E^4 . The temperature of the vertical side S2 can be estimated for its maximum value to be slightly warmer than the air temperature. Thus, at 30 Km, a maximum value of 245° K might be assumed. Evaluating the emission and reflected infrared radiation terms for the side S2 gives:

$$q_{S2} = 3.62 \times 10^{-4} \text{ cal/sec}$$

Summing the nighttime heating terms for both sides S1 and S2 gives the total thermistor heating rate of

$$q_{rs} = 4.39 \times 10^{-4} \text{ cal/sec}$$

This can be compared with the range of total thermistor absorbed atmospheric radiation for representative mid-latitude conditions obtained from LOWTRAN 6 of:

$$2.0 \times 10^{-3} \leq q_{\text{abs}} \leq 4.0 \times 10^{-3} \text{ cal/sec}$$

Initially this comparison indicates that under the extreme ranges considered the emission from the sides S1 and S2 could account for up to 22% of the thermistor heating. Up to this point, however, we have ignored subtracting the atmospheric radiation shielded by the sides S1 and S2 that would otherwise have impinged upon and been partially absorbed by the thermistor. Using the same type assumptions for the blackbody temperatures of the sky the shielded radiation Equation A5.26 can also be simplified. In this formulation the blackbody temperature shielded from view by the thermistor because of the sides S1 and S2 is the upwelling blackbody temperature which may vary from $240 \leq T \leq 300^\circ$. Depending on the season, clouds, etc. Substituting these values of temperature into Equation A5.26 gives:

$$q_{\text{sh}/r_w = -2r\ell \epsilon \frac{\sigma T_U^4}{\pi} \left[\int_{\phi=0}^{2\tan^{-1}\left(\frac{b}{2\left(\frac{w}{2} + m\right)}\right)} d\phi \int_{\theta=\tan^{-1}\left(\frac{n}{m+b}\right) + \frac{\pi}{2}}^{\tan^{-1}\left(\frac{n}{m}\right) + \frac{\pi}{2}} \cos \theta \sin \theta d\theta \right. \\ \left. + \int_{\phi=0}^{2\tan^{-1}\left(\frac{b}{2m}\right)} d\phi \int_{\theta=\tan^{-1}\left(\frac{n}{m}\right)}^{\tan^{-1}\left(\frac{n+h}{m}\right)} \cos \theta \sin \theta d\theta \right] \quad (\text{A5.30})$$

Evaluation of the above yields

$$q_{\text{sh}/r_w = -6.85 \times 10^{-5} - 3.72 \times 10^{-4} = -4.40 \times 10^{-4}$$

Thus, the infrared radiation shielded by the sides S1 and S2 is nearly of identical magnitude as the radiosity from these surface. Consequently for a nighttime flight a negligibly small error (less than a few percent), will result if the thermistor is assumed exposed only to atmospheric radiation in all surrounding spherical directions and the radiational interactions with the radiosonde instrument ignored.

Daytime Radiation

During the day the infrared exchange between the thermistor and the radiosonde instrument is essentially the same as at night. During the day both direct and diffuse solar radiation are reflected from the sides S1 and S2 and irradiates the thermistor. These terms are evaluated individually.

The direct solar irradiation of the (top) side S1 of the radiosonde reaches a maximum as the solar elevation angle approaches 90° . The direct solar energy diffusely reflected by S1 that is absorbed by the thermistor has been given by Equation A5.6 as:

$$q_{SS1} = wb \sin Z_e F_{S1 \rightarrow th} \int_{\lambda=0.25}^{2.5} \alpha(\lambda) \rho_{S1}(\lambda) d\lambda I_0(\lambda) \quad (A5.31)$$

Assuming a wavelength integrated value of solar power, and solar spectrum weighted values of absorption and reflection coefficients ($\rho_{S1}(\lambda) = 0.8$, $\alpha(\lambda) = 0.15$) the above equation is evaluated as:

$$\begin{aligned} q_{SS1} &= 1.32 \times 10^{-4} \text{ cal/sec at } Z_E = 90^\circ \\ &= 0.66 \times 10^{-4} \text{ cal/sec at } Z_E = 30^\circ \\ &= 0 \text{ at } Z_E = 0^\circ \end{aligned}$$

Consider next the side S2. The direct solar radiation reflected from the vertical side, S2, that irradiates the sensor was derived (Equation A5.12) as:

$$q_{SS2} = \frac{bh \cos Z_E F_{S2 \rightarrow th}}{\pi} \int_{\lambda} \rho_{S2}(\lambda) \alpha(\lambda) I_0(\lambda) d\lambda \quad (A5.32)$$

Evaluating Equation A5.2 under the same assumptions gives:

$$\begin{aligned} q_{SS2} &= 1.23 \times 10^{-4} \text{ cal/sec at } Z_E = 0^\circ \\ &= 1.06 \times 10^{-4} \text{ cal/sec at } Z_E = 30^\circ \\ &= 0 \text{ at } Z_E = 90^\circ \end{aligned}$$

Consider next the reflected diffuse solar radiation from the sides S1 and S2. The reflected diffuse solar radiation from the side S1 that irradiates the thermistor comes from scattering that occurs at altitudes above 30 Km and scatters downward irradiating the upper radiosonde surface S1. Using LOWTRAN 6 runs with typical stratospheric aerosol profiles, the hemispheric irradiance from downwelling scattered solar radiation at 30 Km altitude is of order of magnitude

$$q \sim 1 \times 10^{-7} \text{ cal/sec cm}^2$$

The resulting thermistor heating is

$$q_{sdS1} = 2r\ell \alpha(\lambda) \rho(\lambda) F_{S1 \rightarrow th}$$

This term is of order 1×10^{-11} and clearly insignificant.

The reflected diffuse radiation from the side S2 that irradiates the thermistor comes from the hemisphere vertically oriented with the side S2. Utilizing the diffuse solar term in Equation A5.15 the reflected solar radiation absorbed by the thermistor can be written as:

$$q_{sdS2} = \bar{q}_d F_{S2 \rightarrow th} \alpha \rho_{S2}$$

where the usual assumptions are made and \bar{q}_d is the wavelength integrated average diffuse solar power irradiating the side S2 over one revolution. Utilizing LOWTRAN 6 with a range of mid-latitude environmental conditions a range of values for \bar{q}_d has been derived and used in the equation above to derive:

$$0.5 \times 10^{-5} \leq q_{sdS2} \leq 0.2 \times 10^{-4}$$

In contrast, calculations using LOWTRAN 6 for the total direct and diffuse solar radiation absorbed by the thermistor under differing environmental conditions for a mid-latitude site give a range of:

$$2 \times 10^{-3} \leq q_{abs} \leq 4.0 \times 10^{-3} \text{ cal/sec}$$

Thus the combined influences of reflected direct and diffuse radiation from both surfaces S1 and S2 are less than 10% (2×10^{-4}) of the minimum value. Furthermore, this calculation does not include compensation for the heating of diffuse solar radiation that otherwise would have occurred had it been shielded by the sides S1 and S2.

In conclusion, it has shown that during both day and night conditions, the heating rate of the thermistor as a result of radiation exchange with the radiosonde instrument and the balloon, is not significantly different than if these heating rates were ignored and the thermistor temperature were calculated assuming its exposure only to atmospheric radiation in all spherical conditions.

VITA

James Koenig Luers was born on the 4th of July, 1940 in Cincinnati, Ohio. He attended St. Peter and Paul Grade School and graduated from Roger Bacon High School in 1958. Enrollment at Xavier University began in the fall of that year and culminated in the award of a B.S. degree in Mathematics (June 1962) and a M.S. degree in Mathematics (August 1963). He then accepted a teaching position as instructor in mathematics at Chaminade College of Honolulu, Hawaii. Returning the following year to the contiguous United States, Jim began work as a research scientist at the University of Dayton Research Institute (UDRI), his present employer. During his twenty-five years of employment with UDRI, he has addressed problems related to meteorological instrumentation and data analysis, aviation meteorology, the reconstruction of weather-related airplane accidents, and atmospheric sound propagation. Jim is a member of the American Meteorological Society and the American Institute of Aeronautics and Astronautics (AIAA). He has served as National Committee member for the AIAA, and has consulted privately on problems related to aviation meteorology.

Married to Tara (nee Chenoweth) for precisely half of his lifetime, they are the proud parents of six "outstanding" boys, four of which attended the University of Dayton this past year. Living on a min-farm in Lebanon, Ohio, the family jointly tends to raising Christmas trees, Chinese chestnuts, a few grapes, and an occasional cow or two. Jim looks forward toward an opportunity to teach an engineering course at U.D. while striving to spend more leisure time on the farm.